STARS

University of Central Florida
STARS

Electronic Theses and Dissertations, 2004-2019

2019

Experimental and Numerical Investigation of a Novel Adsorption Bed Design for Cooling Applications

Ramy H. Mohammed
University of Central Florida, rhamdy@knights.ucf.edu

Part of the Mechanical Engineering Commons
Find similar works at: https://stars.library.ucf.edu/etd
University of Central Florida Libraries http://library.ucf.edu

This Doctoral Dissertation (Open Access) is brought to you for free and open access by STARS. It has been accepted for inclusion in Electronic Theses and Dissertations, 2004-2019 by an authorized administrator of STARS. For more information, please contact STARS@ucf.edu.

STARS Citation
Mohammed, Ramy H., "Experimental and Numerical Investigation of a Novel Adsorption Bed Design for Cooling Applications" (2019). *Electronic Theses and Dissertations, 2004-2019*. 6335.
https://stars.library.ucf.edu/etd/6335

EXPERIMENTAL AND NUMERICAL INVESTIGATION OF A NOVEL ADSORPTION BED DESIGN FOR COOLING APPLICATIONS

by

RAMY HAMDY MOHAMMED ABDELHADY

B.S. Zagazig University, Egypt, 2008
M.S. Zagazig University, Egypt, 2013
M.S. University of Central Florida, 2017

A dissertation submitted in partial fulfillment of the requirements
for the degree of Doctor of Philosophy
in the Department of Mechanical and Aerospace Engineering
in the College of Engineering and Computer Science
at the University of Central Florida
Orlando, Florida

Spring Term

2019

Major Professor: Louis Chow

© 2019 Ramy Abdelhady

ABSTRACT

A global challenge is to develop environmentally friendly, affordable, compact and sustainable technologies to provide heating and cooling power. Adsorption cooling (AC) technology is one of the most promising ways to solve the environmental issues and cut down the energy consumption related to the traditional air conditioning and refrigeration systems. However, AC systems still suffer from poor heat and mass transfer inside the adsorption bed, which is the main obstacle to commercialization of adsorption cooling units. The main goal of this study is designing an efficient adsorption cooling cycle. In this research work, an in-depth scaling analysis of heat and mass transfer in an adsorption packed bed has been performed to identify and quantify how the effective thermal diffusivity of an adsorption bed and the surface diffusion rate of an adsorbate in a nanoporous adsorbent affect the specific cooling power of an adsorption cooling system. The main goal of this study is to derive new scaling parameters that can be used to specify the optimal bed dimensions and select the appropriate adsorbate/adsorbent pair to achieve the maximum cooling power. As the choice of a suitable working pair is critical for an adsorption cooling cycle, an experimental setup is designed and built to measure the adsorption kinetics and isotherms of any working pair accurately. This setup is also able to measure the dynamic performance of an adsorption bed. The equilibrium uptakes of Fuji silica-gels Type-RD and RD-2060 (manufactured by Fuji Silysia, Japan), which are commonly used in adsorption cooling systems, are measured experimentally. Based on the adsorption rate and the adsorbent temperature measured simultaneously, a new approach is proposed to measure the surface diffusivity in the temperature and pressure ranges typical of those during the operating conditions of adsorption cooling systems. In addition, the experimental measurements from the lab-scale adsorption bed

are used to validate the numerical models that are commonly used for estimating the SCP of AC cycle. By using the scaling parameters driven from the scaling analysis, a newly designed packed bed for use in AC systems is proposed and evaluated in this research. The proposed design consists of repeated packed bed cells (modules). Each module is an open-cell aluminum foam packed with silica gel to enhance the overall thermal conductivity of the bed from 0.198 to 5.8 W/m.K. the experimental test rig is used to evaluate the performance on the new adsorption bed. The effect of pores per inch (PPI) of the foam, silica-gel particle size, bed height and adsorption isotherm of different types of silica gel on the bed performance are investigated.

Dedication

To my beloved parents, wife, brother, sisters and daughters.

ACKNOWLEDGMENTS

First, thanks and all praise be to Allah Almighty who gives me ideas and strengths to accomplish this work.

I would like to express my sincere gratitude to my Ph.D. supervisor, Professor Louis Chow, for his invaluable academic guidance, research techniques and inspiration to accomplish this work. He generously supported me during my graduate school and constantly urges me to do my best and push the boundaries. I am really indebted to him in the preparation and finishing this work. I extend my appreciation and thanks to Prof. Osama Mesalhy for his technical advices, and my classmate Mr. Mohamed Abdelkareem for his help.

I would like to express appreciation to my Ph.D. committee members, Professor Steven Duranceau, Associate Professor Hansen Mansy and Associate Professor Tuhin Das, for their kind advices for manuscript of my dissertation. My warm thanks to Mr. Abdulbaset Benwali for his help.

I cannot imagine accomplishing this dissertation work without my family's support. My parents have been a constant source of support and always provided motivation to stay focused on my goal. I am greatly indebted to my wife for her patience, strength and kindness. Her unconditional love and determined faith in my capabilities always supported me during challenging moments.

I also acknowledge the Department of Mechanical and Aerospace Engineering (MAE) at the University of Central Florida (UCF) as well as the all faculties who taught and helped me.

Finally, I acknowledge the Egyptian Ministry of Research and Higher Education for providing me Ph.D. scholarship.

TABLE OF CONTENTS

LIST OF FIGURES xiii

LIST OF TABLES xviii

NOMENCLATURE xix

LIST OF PUBLICATIONS xxi

CHAPTER 1 INTRODUCTION 1

1.1 Introductory Background 1

1.2 Problem Statement 2

1.3 Objective and Scope 3

1.4 Research Methodology 4

1.5 Thesis Outline 4

CHAPTER 2 ADSORPTION KINETICS 6

2.1 Adsorption Phenomenon 6

2.2 Diffusion in Porous Material 7

2.3 Adsorption Isotherm 9

2.3.1 Freundlich isotherm model 11

2.3.2 Langmuir model 11

2.3.3 Brunauer-Emmett-Teller (BET) isotherm 12

2.3.4 Modified Freundlich model 13

2.3.5 Dubinin models 13

2.3.6 Tòth equation 15

2.4 Adsorption Cycle Description 15

CHAPTER 3 LITERATURE REVIEW 18

3.1 Adsorption Working Pairs Studies 18

3.1.1 Classical adsorbents 20

3.1.2 Composite and consolidated adsorbents 22

3.2 Adsorption Kinetics Studies-Grain Level 25

3.3 System Performance Studies 29

3.4 Conclusion of Previous Studies 32

CHAPTER 4 EXPERIMENTAL WORK 33

4.1 Introduction 33

4.2 Experimental Setup Description 33

4.2.1 Measuring unit chamber 36

4.2.2 Evaporator/condenser vessel 38

4.2.3 Sealing method 39

4.2.4 Temperature measurements 40

4.2.5 Pressure measurements 41

4.3 Test Procedure 42

4.3.1 Measuring of adsorption isotherm and kinetics 43

4.4 Measurements Repeatability 44

4.5 Error Analyses 45

CHAPTER 5 MEASUREMENTS OF ADSORPTION ISOTHERM AND KINETICS 47

5.1 Introduction 47

5.2 Inconsistencies in Adsorption Models of Silica-Gel/Water 47

5.3 Experimental Work 51

5.3.1 Physical properties measurements 51

5.3.2 Testing procedure of adsorption isotherm and kinetics 53

5.4 Results and Discussion 54

5.4.1 Adsorption equilibrium 54

5.4.2 Data analysis and regression 57

5.4.3 Adsorption kinetics 60

5.5 Conclusions 66

CHAPTER 6 ASSESSMENT OF THE NUMERICAL MODELS 68

6.1 Introduction 68

6.2 Experimental Work 69

6.2.1 Measurements procedure 69

6.3 Numerical Modeling 70

6.3.1 Coupled heat and mass transfer (CHMT) model 70
6.3.2 Lumped parameter (LP) model 73
6.4 Validation of Numerical Models 75
6.5 Results and Discussion 77
6.5.1 CHMT model 77
6.5.2 Modified CHMT model 81
6.5.3 LP model 82
6.6 Conclusions 85
CHAPTER 7 SCALING ANALYSIS 87
7.1 Introduction 87
7.2 Theory of Heat and Mass Transfer in an Adsorption Packed Bed 87
7.3 Scaling/Order-of-Magnitude Analysis 88
7.4 Numerical Work 93
7.4.1 Computational domain and initial and boundary conditions 94
7.4.2 Mesh sensitivity and Code validation 94
7.5 Results and Discussion 95
7.5.1 Vapor penetration depth 96
7.5.2 Apparent heat capacity 97
7.5.3 Fourier number 99

7.5.4 Dimensionless temperature ratio 102

7.5.5 Design criteria for an efficient silica gel/water adsorption bed 103

7.6 Conclusion 104

CHAPTER 8 PERFORMANCE EVALUATION OF NEW BED DESIGN 105

8.1 Introduction 105

8.2 Description of the New Modular Packed Bed Design 106

8.3 Heat and Mass Transfer Mechanisms in Silica-Gel/AL Foam Bed 107

8.4 Testing Methodology 108

8.5 Numerical Study 110

8.5.1 Computational domain description 110

8.5.2 Assumptions 111

8.5.3 Mathematical Equations 111

8.5.4 Initial and boundary conditions 115

8.5.5 Mesh sensitivity and code validation 116

8.6 Results and Discussion 118

8.6.1 Effect of using AL foam 118

8.6.2 Effect of particle size 121

8.6.3 Effect of bed height 124

8.6.4 Effect of silica gel/water adsorption isotherm 126

8.6.5 Bed performance 128

8.7 Conclusion 129

CHAPTER 9 SUMMARY AND FUTURE WORK 131

9.1 Summary and Conclusions 131

9.2 Future Work 134

LIST OF REFERENCES 135

LIST OF FIGURES

Figure 2-1 The IUPAC classification of adsorption isotherms for gas 10

Figure 2-2 Schematic of the solar adsorption cooling system 17

Figure 2-3 Schematic and thermodynamic illustration of the four stages in adsorption system on a P-T diagram 17

Figure 4-1 Experimental test rig 35

Figure 4-2 Pictorial view of the entire test rig 35

Figure 4-3 Pictorial view of the load cell used in this study 36

Figure 4-4 Load cell arrangement 37

Figure 4-5 Load cell calibration curve 38

Figure 4-6 Pictorial inside view of the evaporator/condenser chamber 39

Figure 4-7 Sealing method used for the two vacuumed chambers 40

Figure 4-8 Thermocouple feedthrough used in evaporator/condenser chamber 41

Figure 4-9 Calibrations of the pressure transducers 42

Figure 4-10 Average adsorbent temperature and fractional uptake for different tests at the same conditions 45

Figure 5-1 Comparison between the measured isotherm of silica-gel/water and the predicated one using D-A model. 49

Figure 5-2 Surface mass diffusivity of water vapor onto silica gel obtained from previous studies 51

Figure 5-3 N_2 uptake by two types of porous silica-gel beads 52

Figure 5-4 Optical images of (A) type-RD and (B) RD-2060 porous silica beads with computer-aided statistical analysis; particle size distribution of (C) RD and (D) RD-2060 porous silica beads. 53

Figure 5-5 Equilibrium uptake of RD-2060 at different pressures and temperatures..... 55

Figure 5-6 Equilibrium uptake of Type-RD at different pressures and temperatures 56

Figure 5-7 Isosteres of Type-RD silica-gel/water..... 56

Figure 5-8 Data fitting of the experimental water sorption isotherm of silica-gel Type-RD 59

Figure 5-9 Data fitting of the experimental water sorption isotherm of silica-gel RD-2060 59

Figure 5-10 Load cell response and silica gel RD temperature during adsorption process..... 62

Figure 5-11 Procedure of calculating the activation energy and pre-exponential factor..... 65

Figure 5-12 Experimental and predicted adsorption rates for 5 g silica-gel RD-2060 with particles sizes of 0.3-0.79 mm..... 66

Figure 5-13 Experimental and predicted adsorption rates for 20 g silica-gel RD with particles sizes of 0.7-2.0 mm..... 66

Figure 6-1 Schematic diagram of (A) experimental test rig, (B) pictorial view of the tested bed, and (C) computational domain..... 70

Figure 6-2 Comparison of temperature and uptake profiles obtained from experiments and LP model..... 76

Figure 6-3 Comparison of temperature and uptake profiles obtained from experiments and CHMT model..... 77

Figure 6-4 SCP of the tested bed at various evaporation temperatures estimated from experimental measurements and CHMT model 78

Figure 6-5 Deviation between SCP obtained from experimental results and CHMT model 78

Figure 6-6 SCP of adsorption system at various chilled water flow rates and cycle times 79
Figure 6-7 Deviation between SCP_{Exp} and SCP_{CHMT} at various chilled water flow rates and cycle times 80
Figure 6-8 Temporal variation of the evaporator pressure during the adsorption period at different chilled water flow rates 80
Figure 6-9 Deviation between SCP calculated from Exp. data and modified CHMT model at different cycle times 82
Figure 6-10 SCP of the tested bed at various overall heat transfer coefficient of evaporator 83
Figure 6-11 SCP of the tested bed at various heat capacities and cycle times estimated from CHMT (red line) and LP model (black lines) 84
Figure 6-12 Deviation between SCP_{LP} and SCP_{CHMT} at various heat capacities and cycle times 85
Figure 7-1 Schematic representation of (a) an adsorbent embedded heat exchanger, (b) mass transfer resistances, and (c) thermal resistances of a bed 88
Figure 7-2 Comparison between the experimental measurements and the numerical results 95
Figure 7-3 Comparison between the pressure drop calculated from numerical simulation and scaling analysis at various particle diameter to bed thickness ratios 97
Figure 7-4 Comparison of bed temperature variation obtained from numerical simulation (black lines) and exact solution (red lines) at various adsorption times 98
Figure 7-5 Comparison of average bed temperature and uptake calculated of exact solution and numerical simulation 99
Figure 7-6 Temporal variation of average bed temperature and uptake at various bed thermal conductivity 100

Figure 7-7 Effect of Fourier number of the adsorbent-adsorbate layer (F_o) on SCP for various bed thicknesses 100
Figure 7-8 SCP produced after 600 s by silica gel bed at various particle sizes. 101
Figure 7-9 Temporal average silica gel bed temperature and uptake of bed thickness of 7 mm at various convective heat transfer coefficient 102
Figure 7-10 Effect of dimensionless temperature ratio parameter (Θ) on SCP produced at 300 s (solid lines) and 600 s (dashed lines)..... 103
Figure 8-1 (A) schematic drawing for the proposed bed and (B) pictorial views of 10 and 20 PPI foams with/without silica-gel..... 107
Figure 8-2 Schematic drawing of an AL foam filled with adsorbent beads 108
Figure 8-3 Pictorial view of the tested module arrangement..... 109
Figure 8-4 Computational domain of the silica gel/AL foam bed 111
Figure 8-5 Experimental and fitted inlet cooling water temperature profile. 116
Figure 8-6 Average temperature and uptake of AL foam bed with a height of 10 mm during adsorption process..... 117
Figure 8-7Average temperature and uptake of AL foam bed with a height of 10 mm during the desorption process..... 117
Figure 8-8 Temperature contours at different times for (A) silica gel layer and (B) silica gel/AL foam bed..... 119
Figure 8-9 Temporal variation of the average bed temperature with and without foam. 120
Figure 8-10 Temporal variation of the average beds uptake with and without foam 121
Figure 8-11 Percentage of the pressure drop across the beds for different particle sizes..... 122
Figure 8-12 Average bed temperature for different particle sizes 123

Figure 8-13 Average bed uptake for 0.35 mm and 0.70 mm particle sizes 124

Figure 8-14 Temporal average temperature of beds with different heights using 0.35 mm particle size 125

Figure 8-15 Temporal average uptake of beds with different heights using 0.35 mm particle size 125

Figure 8-16 Adsorption isotherm of various silica gel types 126

Figure 8-17 Temporal temperature of beds using various silica gel types 127

Figure 8-18 Dynamic adsorption characteristics for various silica gel 128

LIST OF TABLES

Table 3-1 Thermo-physical properties of common adsorption working pairs 24

Table 5-1 The physical properties of type-RD and RD-2060 silica-gel beads. 52

Table 5-2 Isosteric heat of adsorption of Fuji RD silica-gels 56

Table 5-3 Coefficients of D-A and Tòth model for the tested silica-gels..... 60

Table 5-4 Tested silica-gels samples 64

Table 6-1 Input parameters and operating conditions for CHMT model [41]..... 73

Table 6-2 LP model input parameters..... 75

Table 7-1 Thermo-physical properties of common working pairs [74, 137-139] 90

Table 7-2 Boundary conditions used in this study..... 94

Table 7-3 Summary of the scales discussed in this study and their physical meanings 96

Table 8-1 Physical characteristics of the aluminum foams used in this study [141]..... 106

Table 8-2 Numerical values of the parameters used in this study 114

Table 8-3 Coefficients of adsorption isotherm equation (Eq. 4) for different silica-gels..... 126

Table 8-4 SCP and COP for beds with a height of 10 mm using 0.35 mm silica gel at T_e=10ºC, T_c=30ºC and T_d=85ºC..... 129

NOMENCLATURE

a_{sv}	:	area of gas-solid interface per unit volume	1/m
CP_v	:	Cooling capacity per unit volume	kW/m^3
C_f	:	drag coefficient of the Forchheimer term	---
C_p	:	specific heat	J/kg.K
d_p	:	particle diameter	m
D	:	Mass diffusivity	m^2/sec
$g^{'}$	:	derivative of equilibrium isotherm	---
H_{ads}	:	heat of adsorption	J/kg,
H	:	bed height	m
h	:	heat transfer coefficient	$W/m^2.K$
K	:	permeability	m^2
k	:	thermal conductivity	W/m.K
Nu	:	Nusselt number	---
p	:	pressure	Pa
Pr	:	Prandtl number	---
r	:	radius	m
R	:	universal gas constant, 8314	J/kmol.K
Re	:	Reynolds number	---
S	:	source term	---
SCP	:	specific cooling power	kW/kg of adsorbent
t	:	time	sec
T	:	temperature	K
t_1	:	bed thickness	m
t_2	:	vapor passage	m
U	:	velocity vector	m/sec
W	:	bed width	m
X	:	water uptake	kg_w/kg of adsorbent
X_∞	:	equilibrium adsorption capacity	kg_w/kg of adsorbent

Greek symbols

α	:	thermal diffusivity	m^2/sec
ε	:	porosity	---
μ	:	dynamic viscosity	Pa.sec
ρ	:	density	kg/m^3
τ	:	tortuosity	---

Subscripts

bed	:	bed
c	:	cooling, condenser
e	:	evaporator
eff	:	effective
i	:	initial
K	:	Knudsen
m	:	mass
M	:	molecular weight
max	:	maximum
mo	:	momentum
ord	:	ordinary
p	:	particle
s	:	solid phase, surface
sat	:	saturation
t	:	total
th	:	thermal
v	:	vapor phase
w	:	water

LIST OF PUBLICATIONS

1. R. H. Mohammed, O. Mesalhy, M. L. Elsayed, L. C. Chow, Performance enhancement of adsorption beds with silica-gel particles packed in aluminium foams, International Journal of Refrigeration, 2019. (Accepted).
2. R. H. Mohammed, O. Mesalhy, M. L. Elsayed, L. C. Chow, Assessment of numerical models in the evaluation of adsorption cooling system performance, International Journal of Refrigeration, 99, 166-175, 2019.
3. R. H. Mohammed, O. Mesalhy, M. L. Elsayed, L. C. Chow, Scaling analysis of heat and mass transfer processes in an adsorption packed bed, International Journal of Thermal Sciences 133, 82-89, 2018.
4. R. H. Mohammed, O. Mesalhy, M. L. Elsayed, S. Hou, M. Su, L. C. Chow, Physical properties and adsorption kinetics of silica-gel/water for adsorption chillers, Applied Thermal Engineering 137, 368-376, 2018.
5. R. H. Mohammed, O. Mesalhy, M. L. Elsayed, L. C. Chow, Performance evaluation of a new modular packed bed for adsorption cooling systems, Applied Thermal Engineering 136, 293-300, 2018.
6. R. H. Mohammed, O. Mesalhy, M. L. Elsayed, M Su, L. C. Chow, Revisiting the adsorption equilibrium equations of silica gel/water for adsorption cooling applications, International Journal of Refrigeration 86, 40-47, 2018.
7. R. H. Mohammed, O. Mesalhy, M. L. Elsayed, L.C. Chow, Experimental and numerical investigation of a new silica-gel/water packed bed for adsorption cooling applications, 3rd Thermal and Fluids Engineering Conference (TFEC), March 4-7, 2018, Fort Lauderdale, FL, USA.
8. R. H. Mohammed, A novel silica-gel/foam packed bed for adsorption cooling applications, ASME's International Mechanical Engineering Congress and Exposition (IMECE), Nov. 9-15, 2018, Pittsburgh, PA, USA.
9. R. H. Mohammed, O. Mesalhy, M. L. Elsayed, L. C. Chow, Novel compact bed design for adsorption cooling systems: Parametric numerical study, International Journal of Refrigeration 80, 238-251, 2017.

CHAPTER 1 INTRODUCTION

1.1 Introductory Background

Demands for heating, refrigeration and air conditioning are increasing in a rapid pace because of the ever increasing in population as well as the dramatical growth of industries. During the last century, numerous refrigeration and cooling technologies were developed and the Vapor Compression Refrigeration (VCR) systems broadly dominate the human use for satisfying the thermal comfort conditions, ice making food preservation and vaccine storage. Although these traditional vapor compression refrigeration systems have improved the indoor environment and human thermal comfort levels, they are affecting the environment in two ways. The first one is due to the emissions of chlorofluorocarbons (CFCs) and hydrochlorofluorocarbons (HCFCs) that are used as refrigerants in these systems. These refrigerants are causing the breakdown of the ozone layer which shields the earth from cancer-causing ultraviolet solar radiation. The second way is its impact on the global warming. Most of the commonly used refrigerants in vapor compression refrigeration cycles have high Global Warming Potential (GWP) [3]. For instance, R-134 a, one of the most widely used refrigerant, has a GWP equivalent to 1320 times that of CO_2. Besides the environmental effects, the conventional cooling cycles consume approximately 15% of all the electricity produced in the world and 45% of the whole households and commercial buildings [4].

Adsorption cooling technology is one of the most promising ways to solve the environmental issues and cut down the energy consumption related to the traditional air conditioning and refrigeration systems. It can be powered by solar energy or low-grade heat, so it reduces the fossil fuel burning and hence reducing greenhouse gases in the atmosphere. It can use environmentally friendly refrigerants such as water. Compressors, the main electricity consuming component in VCR, are not required and solid adsorbents are used instead. Moreover, it does not

have moving parts, such as compressors or pumps, for circulation of working fluids and hence can operate without vibration and noise. Despite these advantages, adsorption cooling cycle has not been competitive as mechanical vapor compression system due to the high thermal and mass resistances within the adsorption bed. These large resistances directly lead to low coefficient of performance (COP), low specific cooling power (SCP) and large volume and high capital cost [5].

The concept of adsorption cooling (AC) system is based on the reversible physical adsorption of vapor (adsorbate) on the surface of a porous solid material (adsorbent). This attractive system is simply composed from adsorption bed (adsorptive reactor) integrated into a solar collector for desorption period during the daytime. During the night-time, the adsorbent is cooled and adsorbs the refrigerant comes from the evaporator, in which the cooling effect is obtained.

1.2 Problem Statement

Although performance of adsorption cooling (AC) systems with different design configurations and operating conditions was investigated, AC systems still suffer from poor heat and mass transfer inside the adsorption bed, which is the main obstacle to commercialization of adsorption cooling units. Therefore, fundamental study should be performed to identify and quantify how the thermal resistance of an adsorption bed and the surface diffusion rate of an adsorbate in a nanoporous adsorbent affect the specific cooling power of an adsorption cooling system. Also, significant efforts towards the enhancement of adsorption cooling system performance are required to increase the specific cooling power (SCP) of AC systems. Improvements should be made to obtain more efficient and more compact units.

1.3 Objective and Scope

The main objective of this work is to provide a fundamental understanding of the heat and mass transport processes in packed bed using order of magnitude analysis of governing equations. Therefore, importance of each term of the governing equations is identified. Based on the scaling analysis, a new modular adsorption bed design with different configurations are proposed. Moreover, a radically different and potentially transformative air-conditioning system based on adsorption cooling using aluminum foam is developed. These novel adsorption bed designs achieve several folds increase in specific cooling power (SCP) of AC system. Accordingly, this work contributes in enhancing the overall system performance and facilitating the commercialization of this technology. The scopes of the present work are summarized as follows:

1. Design and build an experimental test rig to measure the adsorption isotherm and kinetics of any working pairs, and study the performance of an adsorption cooling bed under typical operating conditions of adsorption cooling cycle.
2. Determine the thermo-physical properties and adsorption characteristics of the two different types of silica gel; RD-2060 and RD to be used as an adsorbent.
3. Measure the adsorption isotherms of water vapor onto granular Fuji silica gel of type RD-2060 and RD.
4. Investigate heat and mass transport processes in adsorption cooling bed using scaling analysis and order of magnitude approach.
5. Propose a new design of adsorption bed to be employed in adsorption cooling system.
6. Study experimentally and numerically the transient behavior of the proposed bed, and investigate the effect of operating conditions on SCP and COP produced by this bed.

1.4 Research Methodology

The methodology of the present study to achieve the above-mentioned objectives are set out as following:

1. Review the features of the current adsorption beds and identify their advantages and disadvantages. Pervious research studies on silica gel packed beds are also reviewed.
2. Investigate the adsorption kinetics and isotherm of various silica gel types and select the appropriate one, in terms of SCP, to be utilized in AC applications.
3. Develop a coupled heat and mass transfer (CHMT) mathematical models to simulate and study the transient behavior of a new adsorption packed bed, and hence evaluate its performance.
4. Develop a lumped-parameter (LP) mathematical model to simulate the whole AC system. This model is implemented to allocate the operating conditions to achieve the maximal SCP of system.
5. Design and construct an experimental set-up to measure and evaluate performance of adsorption beds with various arrangements. In addition, the experimental facility is used to validate the numerical models and study the effect of operating conditions on AC performance.

1.5 Thesis Outline

The results and findings of this research work have been presented in international journal papers and conference articles as shown in the list of publications. These published papers are incorporated and organized in a thesis form. The thesis consists of nine chapters. Chapter 1, the present chapter, discusses the background of the adsorption cooling technology and highlights its importance. It outlines the objectives and scope of this study. It also summarizes the research

methodology that is used to achieve the goals of this research work. Chapter 2 discusses the adsorption phenomenon and the vapor diffusion inside the porous adsorbents. It presents the various types of adsorption isotherms. It also describes the adsorption cycle and how it works. In chapter 3, previous studies have been reviewed and the main findings have been presented. The literature review is divided into adsorption working pairs studies, adsorption kinetics studies and system performance studies. Also, summary and comments on the previous studies have been presented at the end of this chapter. Chapter 4 provides details information about the experimental work. It discusses the experimental test rig and its facilities, the testing procedure and uncertainty in the measurements. In chapter 5, experimental measurements and results from a Lumped Parameter (LP) model or a Coupled Heat and Mass Transfer (CHMT) model are compared to evaluate the validity of the CHMT model and the LP model in estimating the SCP of adsorption cooling systems. This chapter also presented a modified version of CHMT model is proposed to reduce this deviation and provide a more accurate value for the SCP of the adsorption bed. Chapter 6 provided new scaling parameters that can be used to specify the optimal bed dimensions and select the appropriate working pair to achieve the maximum cooling power. Also, a numerical study is performed in this chapter to illustrate the roles played by the newly derived scaling parameters. Chapter 7 presents the sorption kinetics and equilibrium uptake of two different types of silica gel: silica gel RD-2060 and silica gel RD. it also proposes a new approach to measure the surface diffusivity in the temperature and pressure ranges typical of those during the operating conditions of adsorption cooling systems. a newly designed packed bed for use in AC systems is proposed and evaluated in chapter 8. The thermal response and adsorption kinetics of the proposed bed are investigated experimentally and numerically at various operating conditions in this chapter. The summary and conclusion of this research work are presented in chapter 9. Also, the future work in included in this chapter.

CHAPTER 2 ADSORPTION KINETICS

2.1 Adsorption Phenomenon

The ability of porous solid materials to reversibly adsorb vapor has been recognized in the eighteenth century and early experiments have been carried out to study the separation and purification process [6]. Adsorption is a surface phenomenon where gas molecules stick to a surface. This process creates a film of adsorbate on the surface of adsorbent. It differs from absorption, in which a fluid is dissolved by a liquid or permeates a solid. Adsorption is a surface-based process, while absorption involves the entire volume of the material. In general, the adsorption phenomenon could be classified in different ways. It can be classified as mobile or immobile adsorption from molecular mobility point of view. Adsorption can also be classified as physical or chemical adsorption based on the type of bond between adsorbate and adsorbent and the magnitude of the heat of adsorption. This classification is widely used because of its convenience but it is not precise enough. Alternatively, it can be classified as monolayer or multilayer depending on the relative pressure magnitude and the adsorbed layers number [7].

In the case of immobile adsorption, a molecule does not leave its location until it desorbs and returns to the fluid phase. For mobile adsorption, molecule remains in the adsorbed state all the time but it can freely move from position to another. As the adsorption happens due to interactions between a solid (adsorbent) and vapor molecules (adsorbate), it is important to differentiate between physical and chemical adsorption. In physical adsorption, there is no direct chemical bond between the surface and the adsorbate and the adsorbate is held by physical forces (i.e., van der Waals and electrostatic), whereas in chemical adsorption, a direct chemical bond is formed and monolayer is created on the surface. Since the physical sorption is due to attraction forces, heat is released due to the change in energy level of the adsorbate molecules between

gaseous and adsorbed phases; therefore, physical adsorption is an exothermic process. In physical adsorption, gas molecules are captured in the pores of an adsorbent due to van der Waals force and forming a monolayer. Each molecule in the monolayer provides one "site" for the second and subsequent layers. The molecules in the second and subsequent layers are considered to behave as a saturated liquid. The physical adsorption involves relatively weak intermolecular forces. This phenomenon is similar to the condensation process and for most adsorbents the heat required to release the adsorbate (i.e. heat of adsorption) is similar to its latent heat [8]. The amount of physically adsorbed gas molecules always decreases monotonically as temperature increases. The amount is usually associated with the relative pressure (RP), P/P_o, where P and P_o are the partial vapor pressure of a component in the system and the saturation vapor pressure at the same temperature, respectively. For RP ≈ 0.1, the amount adsorbed corresponds to a monolayer. The monolayer capacity is usually defined as the amount required to cover the surface. As the pressure increases progressively, multilayer adsorption occurs at pressure ratio range from 0.1 to 0.3 [7], beyond which pores are filled with a liquid like phase. This is possible because the equilibrium vapor pressure inside the pores is decreased significantly due to the curvature and surface tension in accordance with the Kelvin equation. This phase transition is known as capillary condensation.

2.2 Diffusion in Porous Material

Diffusion is a random migration of molecules along concentration gradient. It is a general property of matter related to the tendency of molecules to occupy all the accessible sites. The diffusion of adsorbed molecules in solid porous materials has long been considered one of the most interesting subjects, since the surface diffusion participates significantly to the mass transport in the porous materials, especially in the adsorption, separation, and many other industrial applications.

Although the mechanism of surface diffusion is rather complicated, two well-known models have been developed to describe the dependence of the surface diffusivity on the surface operating temperature and the surface coverage. These two models are the hydrodynamic model [9] and the hopping model [10]. Gilliland et al. [9] derived an equation for adsorbed-layer movement based on thermodynamic principles. It was assumed that the shear stress between the adsorbed layer and the solid is proportional to the average rate of movement of adsorbed molecules past the surface. The resulting equation has just one empirical constant and its application requires adsorption-isotherm data. Although the equation correlates their experimental measurements well with the surface flow rates for the range of the studied variables, it is in integral form which can be solved for special isotherm cases only. On the other hand, the hopping or jumping mechanism is conceptually the most basic mechanism for diffusion of adsorbate molecules. It assumes that the gas molecules move over the surface from one site to another by hopping with a certain velocity [5, 10].

Many experimental measurements have been carried out to investigate the diffusion process inside porous materials. The Isothermal Differential Step (IDS) method was considered to be the most reliable method for identification of the kinetic parameters such as the diffusion constant and the adsorbate diffusivity [1, 11]. In this method, the pressure and temperature are controlled, and a small amount of pure liquid adsorbate is set inside the evaporator. The dry sample is exposed to the evaporator and the decrease in the liquid indicates the adsorption uptake of this adsorbent. This approach has some drawbacks like the testing conditions are far away from the real operating conditions of adsorption cooling cycle as well as the difficulty to keep the adsorbent at constant temperature during the adsorption process to be able to use the Arrhenius equation for calculating the surface diffusivity. To overcome the last limitation, the amount of tested material

should be small (7-10 mg) to reduce the thermal effects on the adsorption kinetics [12]. For further reduction of the thermal effects, the particles of the tested material are mixed with copper wires to keep the sample more isothermal. Still, it is difficult to achieve isothermal condition.

Strauss et al. [13] proposed an non-isothermal approach for adsorption kinetic characterization to overcome the isothermal limitation. In this case, a sample is placed inside an evacuated closed chamber and subjected to temperature change. The adsorption rate is monitored by recording the pressure evolution inside the system. As this methodology cannot be considered isothermal, a complicated model based on solving partial differential equations of energy and mass inside the adsorbent material is used to fit the experimental data. Furthermore, this experimental approach cannot be considered satisfactory, because the adsorption uptake is measured based on the change in the pressure and these conditions are far from the actual operating condition of the adsorption cooling system, where both adsorption and desorption process are isobaric.

2.3 Adsorption Isotherm

Adsorption isotherm model describes the equilibrium amount of adsorbate molecules at certain pressure and temperature. Adsorption isotherm depends on the pore structure of the solid adsorbent. The pore structure includes surface area, pore volume and pore size distribution and these parameters are extracted from the adsorption isotherms for a gas. Adsorption isotherms are classified by their shapes into six types, as shown in Fig. 2-1, which has been proposed by the International Union for Pure and Applied Chemistry (IUPAC) [6]. Type 1 corresponds to the Langmuir equation which describes a complete monolayer surface coverage by a monolayer of adsorbed molecules. Type 2 corresponds to the case when first, a monolayer surface coverage is formed, and then followed by multilayer adsorption at higher P/P_o. Types I and II isotherms are

frequently observed on carbon. Isotherm of Type 3 is relatively uncommon in porous materials and occurs when the cohesive force between adsorbate molecules is greater than the adhesive force between adsorbate molecules and adsorbent. On the other words, it corresponds to the formation of multilayers when heat of adsorption is less than or equal to adsorbate heat of condensation. Type 4 is called a staged adsorption where additional layers are adsorbed after monolayer. Type 5 is noticeable when the cohesive force between adsorbate molecules is smaller than the adhesive force between adsorbate molecules and adsorbent. Isotherms of Types 4 and 5 are characteristic of capillary condensation in porous solids.

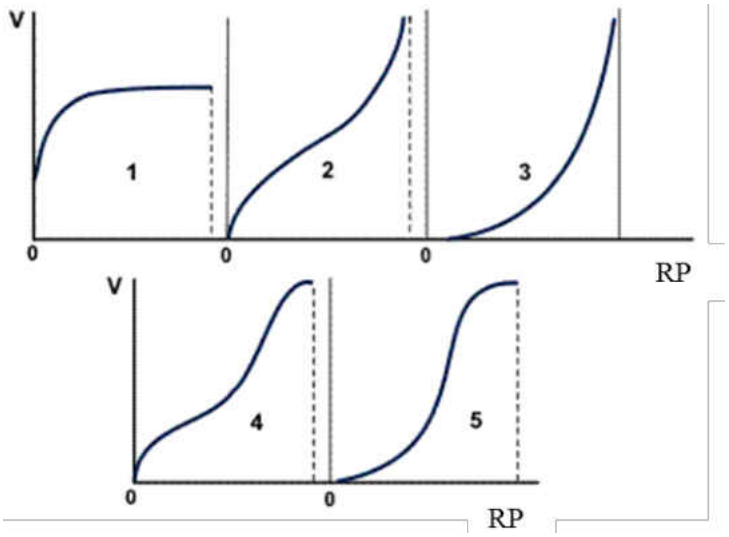

Figure 2-1 The IUPAC classification of adsorption isotherms for gas

Equilibrium state is achieved after a long time when molecules of refrigerant are captured onto adsorbent surfaces at a given pressure and temperature and this amount adsorbed is called the equilibrium concentration/uptake. When the adsorbent temperature is kept constant (isothermal process), the change in equilibrium uptake (X) against the equilibrium pressure (P) is called the adsorption isotherm. Several adsorption equilibrium equations have been proposed to describe the adsorption isotherm of different working pairs based on different approach and to correlate the experimental adsorption uptake measurements. These adsorption equilibrium models are:

2.3.1 Freundlich isotherm model

In 1909, Herbert Freundlich proposed a relationship between the isothermal variation of adsorption of a quantity of gas adsorbed by unit mass of solid adsorbent with pressure [14]. Freundlich equation is an empirical equation that is valid only when the adsorption isotherm is linear, and it is written as [1]:

$$X = X_o \left(\frac{P_v}{P_s}\right)^{1/n} \quad (1)$$

where X is the uptake (kg of adsorbate per kg of adsorbent), X_o is the maximum uptake (adsorbent capacity), 1/n describes the surface heterogeneity of the adsorbent and it varies from 0 to 1, and P_s is the saturation vapor pressure at the adsorbent temperature (T_s).

2.3.2 Langmuir model

The Langmuir model is the simplest one for monolayer adsorption [7, 15]. This model was originally developed because Freundlich model agrees very poorly with experiment when the range of pressures is large [15]. The Langmuir model represents chemisorption and its basic assumptions are given in [6, 16]:

a. Adsorbed molecules are stationary (immobile).
b. Each site can hold one adsorbed molecule.
c. No interaction between the adsorbed molecules at neighboring sites.
d. All sites are energetically equivalent.

Based on these assumptions, the following equation is proposed:

$$y = \frac{bP_v}{1+bP_v} \quad (2)$$

where y is the fractional surface coverage, P_v is the vapor pressure, and b is the adsorption equilibrium constant that follows the van't Hoof equation [8].

$$b = b_o \, exp\left(-\frac{\Delta H}{RT_s}\right) \quad (3)$$

where ΔH is the heat of adsorption (kJ/mol), R is the universal gas constant, and T_s is the adsorbent temperature (K).

As Langmuir model is valid for monolayer adsorption, it is good for very low pressure close to vacuum, and it has limitations to fit the uptake at pressures above 10 kPa for heterogeneous adsorbents [17]. As a result, this model is not suitable to fit the experimental data for multilayer adsorption.

2.3.3 Brunauer-Emmett-Teller (BET) isotherm

Brunauer–Emmett–Teller (BET) theory was proposed to extend the Langmuir model to multilayer adsorption as [6, 16]:

$$\frac{P_v}{(P_s - P_v)W} = \frac{1}{W_m e^{\frac{E_1 - E_L}{RT_s}}} + \frac{\left(e^{\frac{E_1 - E_L}{RT_s}} - 1\right)P_v}{W_m e^{\frac{E_1 - E_L}{RT_s}} P_s} \quad (4)$$

where W is the concentration of adsorbate at certain pressure and temperature per unit mass of the solid adsorbent (m^3/kg), P_s is the saturation vapor pressure at adsorbent temperature T_s, E_1 is the heat of adsorption for the first layer, E_L is the heat of adsorption for the second and higher layers and W_m is the monolayer capacity.

The BET model is mainly used for the measurement of the specific surface area and pore volume of porous materials, and is not used to fit the experimental data of physical adsorption.

2.3.4 Modified Freundlich model

The original form of Freundlich model is not valid at low and high relative pressure. So, Saha, Boelman and Kashiwagi (S-B-K) equation is a modified version of the Freundlich equation that gives better fitting of the experimental data. The S-B-K equation is given by [18]:

$$X = A(T_s)\left(\frac{p_v}{p_s}\right)^{B(T_s)} \qquad (5)$$

where $A(T_s) = \sum_{i=0}^{i=3} A_i T^i$ and $B(T_s) = \sum_{i=0}^{i=3} B_i T^i$. Both the coefficients A(T_s) and B(T_s) are calculated based on fitting of experimental data.

2.3.5 Dubinin models

The description of adsorption equilibria for microporous adsorbents is based on the theory of volume filling of micropores. This theory is based on the concept of temperature invariance of the characteristic curve expressing the distribution of the degree of filling (θ). The Polanyi theory was originally developed to study the adsorption of gas molecules onto porous materials [19]. Based on Polanyi adsorption theory, the degree of filling of adsorption space can be written as:

$$\theta = \frac{W}{W_o} = exp\left\{-\left(\frac{RT_s}{E} ln\left(\frac{P_s}{P_v}\right)\right)^n\right\} \qquad (6)$$

where θ is the degree of filling, W is the adsorbate concentration at certain pressure and temperature per unit mass of the adsorbent solid (m^3/kg), W_o is the maximum adsorption concentration which is the micropore volume of the adsorbent per unit mass of adsorbent (m^3/kg), $RT_s \ln\left(\frac{P_s}{P_v}\right)$ is the differential work of adsorption, T_s is the adsorbent temperature, R is the universal gas constant, and E is the characteristic energy of adsorption (J/mol) and is obtained from adsorption potential at $\theta = e^{-1} = 0.368$.

When n equals 2, Eq. 6 is known as the Dubinin–Raduschkevich equation (D-R) [16]. The D-R equation has been widely used to calculate the equilibrium concentration of hydrocarbons and other organics onto activated carbon adsorbents. It was found that Eq. 6 with n from 3 to 6 satisfactorily describes the experimental data of zeolites over the range of fillings, θ, from ≈ 0.1 to 1.0, while n of 2.0 is applicable only to the region of high filling from 0.8 to 1.0 [20]. In addition, it was pointed out that this equation is not thermodynamically consistent with Henry's law [21].

Converting the fractional concentration (W/W_o) to the uploading ratio (X/X_o) requires the knowledge of W_o which is usually not known because the molecular volume of the adsorbed fluid is not known. As a result, this equation was modified with the assumption that the density of the adsorbed phase is constant. The D-A equation is rewritten in terms of mass capacity as follows [22, 23]:

$$X = X_o \, exp\left\{-D\left(ln\left(\frac{P_s}{P_v}\right)\right)^n\right\} \qquad (7)$$

where D is the coefficient of affinity that is a function of the adsorbent microstructure. Both D and n depend not only on the adsorbate–adsorbent pair but also on the brand and type of the adsorbent.

Trouton's rule assumes that the isosteres on the ln P_v vs. 1/T plot are indeed linear:

$$ln\frac{P_v}{P_b} = a\left(1 - \frac{T_b}{T_v}\right) \qquad (8)$$

where a is a constant which depends on the adsorbate type and T_b is the saturation temperature at atmospheric pressure (P_b).

Based on the Trouton's rule, a simple equation of adsorption state has been proposed as follows [24]:

$$X = X_o \, exp\left\{-k\left(\frac{T_s}{T_v} - 1\right)^n\right\} \qquad (9)$$

2.3.6 Tòth equation

The D-A model sometimes does not represent the adsorption isotherm correctly at low relative pressure. This is due to the zero slope at zero loading [17]. Tòth [25, 26] proposed an equation that is based on the state equation of multilayers. It could satisfy the monolayer coverage and the multilayer adsorption. It corrects the wrong behavior at both the low and high pressure ends of adsorbate concentration that the Langmuir and Freundlich models cannot describe accurately [17]. It is also the first choice for fitting the experimental data to get the isotherm equation of several heterogeneous solid adsorbents [17]. This equation is given as [27-29]:

$$X = \frac{b_o P_v \exp\left(\frac{\Delta H}{RT_s}\right)}{\left\{1+\left[\frac{b_o P_v}{X_o}\exp\left(\frac{\Delta H}{RT_s}\right)\right]^t\right\}^{\frac{1}{t}}} \qquad (10)$$

where t is the adsorbent structural heterogeneity parameter and b_o is the equilibrium constant based on the working pair. Both t and b_o can be calculated from the experimental data.

2.4 Adsorption Cycle Description

Intermittent adsorption cooling systems usually have a single bed, where adsorption bed is charged with refrigerant at low temperature and pressure. When adsorption process ends, the adsorption bed is heated up and vapor with high temperature and pressure is released from the bed. To obtain a continuous cooling effect, two or more adsorption beds are used as shown in Fig. 2-2. If switching between the adsorption and desorption phase is not well controlled, cooling production and cycle efficiency will be reduced due to wasting a large amount of energy.

Adsorption cooling cycle normally consists of three main parts: adsorption bed where a porous solid material is placed, condenser and evaporator as shown in Fig. 2-2. A basic adsorption cycle consists of four thermodynamic processes which are illustrated in the schematic and

Clapeyron diagram in Fig. 2-3. The processes of adsorption cooling cycle are described as follows [30]:

1. Isosteric pre-heating process (1-2): At starting of this process, the adsorption bed is cold and saturated with the maximum refrigerant capacity (X_{max}) and this state is represented as point 1. When heat is supplied, the adsorbent is heated up which results in increasing in pressure from evaporator pressure (P_e) to condenser pressure (P_c), without changing the refrigerant uptake and this process continues until the minimum desorption temperature is reached and the bed pressure reaches to the condenser pressure at state point 2. This process is like the compression in the vapor compression refrigeration cycle.
2. Isobaric heating desorption process (2-3): While the adsorber continues receiving heat and the pressure inside the adsorption bed reaches to the condenser pressure, desorption process starts from the point 2 and the refrigerant vapor flows into the condenser and is condensed at a constant pressure. Desorption process proceeds until the adsorbent temperature reaches the desorption temperature and the refrigerant uptake reaches the cycle minimum uptake (X_{min}) and the end of this process is represented by point 3. This process is similar to condensation in vapor compression refrigeration system.
3. Isosteric pre-cooling process (3-4): Consequently, the adsorption bed is cooled down and this results in decreasing the bed pressure from the condenser pressure to the evaporator one without changing the adsorption capacity of the bed. This results in decreasing the refrigerant temperature from state point 3 to state point 4 which allows the adsorbent to be able to adsorb refrigerant vapor. This process is like expansion in vapor compression refrigeration system.

4. Isobaric cooling adsorption process (4-1): The adsorption bed is connected to evaporator while continuous releasing heat. The adsorbent temperature continues decreasing, which induces adsorption of vapor. Refrigerant vapor exiting from the evaporator is adsorbed by the adsorbent until reaching the maximum uptake (X_{max}) at point 1 again. The refrigerant, evaporates in the evaporator, produces the cooling effect.

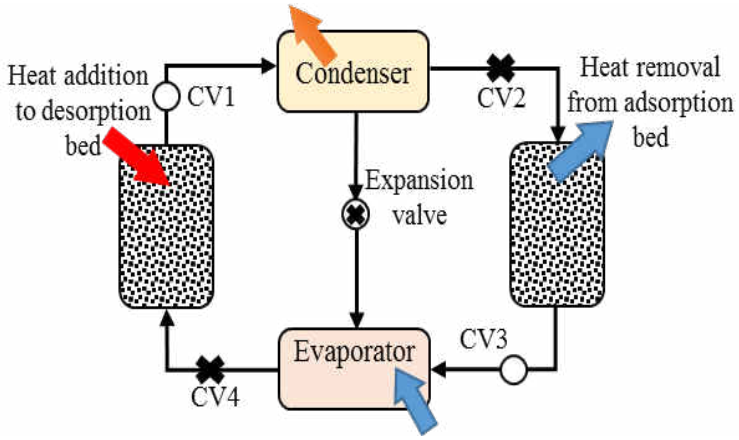

Figure 2-2 Schematic of the solar adsorption cooling system

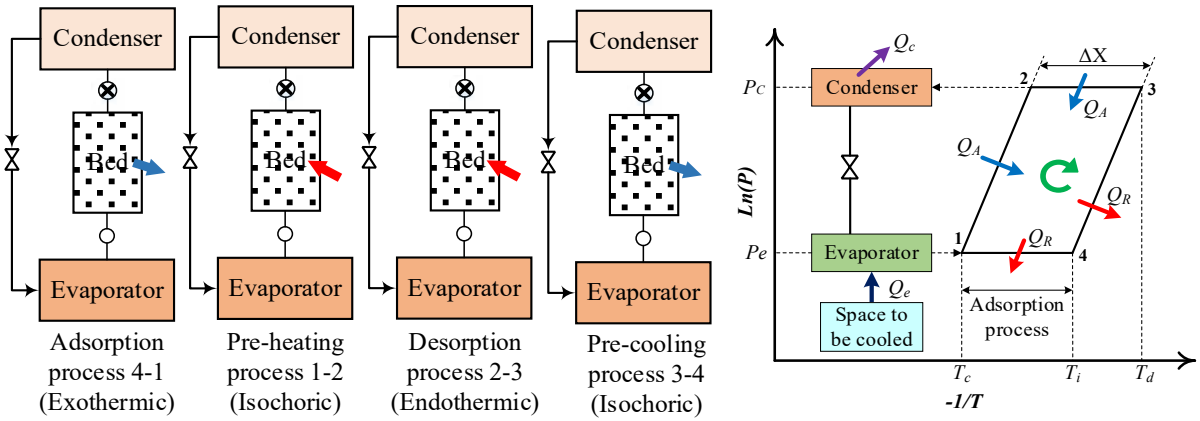

Figure 2-3 Schematic and thermodynamic illustration of the four stages in adsorption system on a P-T diagram

CHAPTER 3 LITERATURE REVIEW

A vast majority of global cooling and heating demands is covered by traditional vapor compression systems, employing refrigerants which have high Global Warming Potential (GWP) [31, 32]. The abundant renewable energy resources such as low-grade waste energy or solar energy can be converted into beneficial cooling and electricity using promising clean energy technologies like adsorption, absorption and Organic Rankine Cycle (ORC). Therefore, adsorption cooling/heat pump technology, which has received much attention in the recent years, is a favorable alternative for conventional refrigeration and air conditioning systems that converts low-grade heat source into useful cooling/heating power and utilizes refrigerants with zero Ozone Depletion Potential (ODP) and Global Warming Potential (GWP) [33-35].

Over the years, comprehensive studies have been reported in the field of adsorption cooling technology. These studies could be classified as [**]:

1. thermo-physical characteristics of adsorption working pairs [36-41];
2. grain level studies to investigate the effect of adsorption kinetics, operating conditions and grain size of adsorbent on adsorption cycle performance [42-46];
3. system level studies of different beds configurations to study the overall system performance and optimize the operating conditions [47-51].

3.1 Adsorption Working Pairs Studies

Performance of adsorption cooling systems critically depends on the capacity of the adsorbent to adsorb vapor as well as on the rate at which the bed can adsorb/desorb the working

[**] This literature review has been quoted from the Author's publications shown in the List of Publications.

fluid. Therefore, solid adsorbent with large specific surface area is preferable to provide a large adsorption capacity. Surface area, pore volume and pore size of porous adsorbent are usually measured by using the Brunauer-Emmett-Teller (BET) method [52]. Adsorbent capacity is traditionally measured by either volumetric or gravimetric method [53]. The volumetric approach depends on monitoring the pressure change during the adsorption, which indicates the adsorption rate. The tested adsorbent should be in a small amount for the pressure change to be small, so the process could be assumed to be isobaric. The main disadvantage of this method is the testing conditions are far away from the real operating conditions of the adsorption cooling unit. On the other hand, the gravimetric method measures directly the adsorbent capacity by means of mass balances at specific operating conditions. This makes this method more suitable to measure the adsorption isotherms of working pairs.

Working pairs can be classified based on the operating pressure as follows:

Low pressure: silica gel/water, zeolite/water and activated carbon/methanol.

High pressure: silica gel/sulfur dioxide, zeolite/fluorocarbon, activated carbon/ammonia and activated carbon/fluorocarbon.

In low pressure systems, good manufacturing is required to avoid leakage which significantly affects the performance. Whereas, the high-pressure adsorption cooling systems require higher generation (desorption) temperature.

Adsorbents for adsorption cooling applications can also be classified into two main categories; classical and composite adsorbent.

3.1.1 Classical adsorbents

Classical adsorbents are zeolite, silica-gel, activated carbon and activated carbon fiber (ACF). Thu et al. [36] investigated three types of commercially available silica gels (Type-RD 2560,Type-A5BW and Type-A^{++}) using a surface characteristic analyzer and evaluated their thermo-physical properties using several analysis methods. The surface area of each adsorbent was studied using Brunauer-Emmett-Teller (BET) method whilst the pore size distribution (PSD) analysis was conducted with the Non-Local Density Functional Theory (NLDFT). It was observed that the Type-A^{++} silica gel (granular type) possesses the highest surface area of 863.6 m^2/g amongst the three parent silica gels studied. In addition, water vapor concentration capacity of silica gels were studied and the results showed that the Type-A^{++} silica gel exhibits a highest equilibrium concentration at 537 cm^3/g. El-Sharkawy et al. [54] measured the adsorption equilibrium of ethanol onto activated carbon fiber (ACF) of types (A-20) and (A-15) and Dubinin-Radushkevich (D-R) equation was used to fit the experimental data. It was concluded that the adsorption capacity of (A-20)/ethanol and (A-15)/ethanol are from 0.5 to 0.65 and 0.4 to 0.45 kg/kg, respectively. Therefore, ACF (A-20) seems to be a promising adsorbent as it has large affinity to adsorb ethanol vapor however, the main challenge is to develop a compact heat exchanger suitable for the densely fiber packing. Saha et al. [55] measured experimentally the adsorption equilibrium of R134a onto granular activated carbon (AC) and Unitika activated carbon fiber (ACF) of type (A-20) within evaporation temperatures range between -20 and 40 ℃ and adsorption temperatures range from 30 to 80 ℃. Adsorption isotherms were predicted using the D-A equation with and without volume correction factor. The experimental measurements showed that the adsorption capacity of R134a onto AC and ACF is 0.926 and 1.256 kg/kg, respectively.

San et al. [56] carried out a comparison among the three classical adsorption pairs; activated carbon-methanol, silica gel-water and zeolite 13X molecular sieves-water. Analysis of the results showed that the capacity of the silica gel-water pair is approximately a half of that of the activated carbon-methanol pair, but the latent heat of water is almost twice of that of methanol. Due to the high heat of adsorption of silica gel-water, silica gel temperature increases significantly during the adsorption and leads to a decrease in the equilibrium uptake. Consequently, it slows down the adsorption process, and the system performance is deteriorated. A review study was devoted to present the adsorption characteristics of activated carbon with ammonia, methanol, ethanol, hydrogen, nitrogen and diethyl ether, R134a, R507a, n-butane and CO_2 [57]. It was shown that the activated carbon has the affinity to R134a followed by R507a. The measured adsorption capacity of activated carbon/R134a and activated carbon/R507a was 2 kg/kg and 1.3 kg/kg, respectively.

Bentonite was introduced as a cheap adsorbent with high potential for use in heat pumps or chillers driven by renewable energy [58]. A simple acid activation procedure increased the surface area of the bentonite from 64 m^2/g to 500 m^2/g. The results showed that the maximum uptake of the bentonite is about 0.27 kg/kg. Ghazy et al. [59] developed a new working pair to be used in adsorption cooling applications. Adsorption isotherms and kinetics of Difluoroethane (HFC-152a) onto highly porous activated carbon Maxsorb III at temperatures ranging from 25 to 75 ℃ were investigated. Experimental results showed that Maxsorb III adsorbs up to 1.3 kg of HFC-152a per kg of adsorbent. In addition, adsorption characteristics of granular activated carbon/HFC-404A was investigated in terms of adsorption isotherms and kinetics [60]. It was reported that the maximum adsorption capacity is about 0.52 kg/kg.

Among the classical working pairs, silica gel/water is preferred due to its safety, reliability, repeatability and inexpensiveness as compared to other working pairs. However, silica gel/water has a low adsorption capacity and cannot produce evaporation temperatures below 0 ℃. Moreover, the system works under a low vacuum pressure and sealing could be a problem. Silica gel has the ability to adsorb water with good stability. Desorption temperature can be lower than 90 ℃, and such a low desorption temperature is very suitable for solar energy and waste heat energy utilization.

3.1.2 Composite and consolidated adsorbents

Because the adsorption ability of the classical adsorbents is low, composite and consolidated solid desiccant materials are formed and developed to increase the adsorption quantity and improve heat and mass transfer due to the swelling and agglomeration phenomena [61, 62]. One way to improve the adsorbent capacity is to impregnate adsorbent with hygroscopic salt to form a composite adsorbent. Salt swelling reduces the heat transfer, and salt agglomeration reduces the mass transfer [38]. Impregnation method is generally used to prepare composite adsorbents based on silica gel as a matrix [63-65], for which silica gel is soaked in salt solutions (such as $CaCl_2$) with a fixed solubility, and then the silica gel is dried to obtain a composite adsorbent with a strong adsorption [53]. This new adsorbent is called selective water sorbent (SWS) and its adsorption capacity is about 0.7 grams of water per gram of adsorbent.

Cacciola et al. [66] developed brick shaped adsorbent materials based on activated carbons and PTFE (poly-tetra-fluoroethylenes) as a binder. It was reported that the adsorption capacity of methanol onto the developed adsorbents increased by 40%. Jin et al. [67] tested thermal conductivity and permeability of granular activated carbon (AC), consolidated AC with chemical

binder and consolidated AC with expanded natural graphite. It was reported that thermal conductivity of granular activated carbon and consolidated activated carbon with chemical binder are about 0.36 W/m.K and 0.4 W/m.K, respectively. Thermal conductivity of consolidated activated carbon with expanded natural graphite ranges from 2.08 W/m.K to 2.61 W/m.K, however, its permeability is lower than that of the granular AC and consolidated AC with chemical binder. Tamainot-Telto et al. [68] measured the thermo-physical properties of two types of monolithic activated carbons. The authors reported that the thermal conductivity of the tested samples is 0.44 W/m.K and the adsorption capacity for ammonia is 0.36 kg/kg. Wang et al. [69] developed composite adsorbents which are combinations of activated carbon and expanded natural graphite. Thermal conductivity and permeability have been experimentally investigated. It was reported that the best values of measured thermal conductivity and permeability are 2.47 W/m.K and 4.378×10^{-12} m^2, respectively. Wang et al. [70] developed consolidated composite activated carbon (AC) with a host matrix of expanded natural graphite treated with sulfuric acid (ENGTSA). It was shown that the highest effective thermal conductivity of consolidated composite AC is 34.2 W/m.K which is 150 times higher than ordinary granular activated carbon. Zheng et al. [62] proposed composite desiccant adsorbent that comprises silica gel with expanded natural graphite treated with sulfuric acid (ENG-TSA) as a host matrix. It is reported that the highest thermal conductivity of consolidated composite adsorbents increased more than 270 times as compared to that of pure silica gel.

El-Sharkawy et al. [71] developed and characterized a consolidated composite adsorbents which are combinations of a highly porous activated carbon powder (Maxsorb III), expanded graphite (EG) and binder. Porous properties of the developed composite adsorbents were investigated experimentally using Nitrogen adsorption. Adsorption isotherm of ethanol onto

composite adsorbents was measured and fitted using suitable adsorption isotherm models. Thermal conductivity of the adsorbents was also measured. The experimental results showed that the adsorption equilibrium capacity of ethanol onto consolidated composite (70% Maxsorb III, 20% EG, 10% binder) is 0.89 kg/kg, which is about 74% of the maximum adsorption uptake of Maxsorb III/ethanol pair. This means that the binder did not sacrifice the adsorption capacity of Maxsorb III of consolidated composites. It was also found that the thermal conductivity of the developed consolidated adsorbents increased by 11 times compared to Maxsorb III powder.

The maximum equilibrium uptake and the thermo-physical properties of different working pairs are shown in Table 3-1.

Table 3-1 Thermo-physical properties of common adsorption working pairs

Working pair	Pore diameter [nm]	Pore volume [m^3/kg]	Surface area [m^2/g]	Max. capacity [kg/kg of solid]
Silica gel RD/water [72]	2.20	$4.0x10^{-4}$	838	0.30
Fuji silica gel RD/water [41]	2.24	$4.4x10^{-4}$	780	0.48
Fuji silica gel 2060/water [41]	1.92	$3.4x10^{-4}$	707	0.37
Silica gel 2560/water [36]	1.32	$3.27x10^{-4}$	636.4	0.32
Silica gel A^{++}/water [36]	1.38	$4.89x10^{-4}$	863.6	0.48
Zeolite/water [73]	1.78	$3.1x10^{-4}$	643	0.25
AQSOA-Z01/water [74]	1.178	0.712×10^{-4}	189.6	0.215
AQSOA-Z02/Water [74]	1.184	2.69×10^{-4}	717.8	0.29
AQSOA-Z05/water [74]	1.176	0.7×10^{-4}	187.1	0.22
ACF (A-20)/ethanol [54]	2.16	$10.28x10^{-4}$	1900	0.80
ACF (A-15)/ethanol [54]	2.18	$7.65x10^{-4}$	1400	0.60
AC-35/methanol [75]	2.23	$6.9x10^{-4}$	1200	0.38
AC/ammonia [76, 77]	2.00	$6.2x10^{-4}$	1843	0.29
Maxsorb III/ethanol [78]	1.12	$1.7x10^{-4}$	3045	1.20
Maxsorb III/R134a [76]	1.12	$1.7x10^{-4}$	3045	2.0
Maxsorb III/R507[76]	1.12	$1.7x10^{-4}$	3045	1.3
Maxsorb III/n-Butane[76]	1.12	$1.7x10^{-4}$	3045	0.8
KOH4-PR/ethanol [79]	1.25	$19x10^{-4}$	3060	1.43
KOH6-PR/ethanol [79]	1.78	$25.3x10^{-4}$	2910	2.00

3.2 Adsorption Kinetics Studies-Grain Level

Performance of adsorption heat pumps and chillers depends on the heat and mass transfer in the adsorption bed. Intra-particle mass diffusion resistance is shown to present a significant mass transfer resistance compared with inter-particle mass diffusion resistance. Therefore, accurate modeling of intra-particle mass transfer is essential for the accurate prediction of overall system performance. Fickian diffusion (FD) equation and linear driving force (LDF) approximation are used to model the intra-particle mass transfer. Glueckauf [80] derived the LDF approximation by assuming a parabolic concentration profile for adsorbed phase inside particle. Later, it was shown that the general profiles, $X(t) = A(t) + B(t)r^n$ where n is an integer > 2, led directly to the LDF model and that the parabolic profile is only one specific solution [81]. The LDF model assumes that the adsorbent particle temperature is uniform and its thermal conductivity is infinity, which means that the heat transfer effect is neglected. By using the LDF approximation, the mass balance equation is eliminated from the model, leaving only the mass balance equation in the fluid phase to be dealt with. This results in a tremendous simplification of the model that is to be solved either analytically or numerically. Because of its simplicity that significantly saves the computational time, the LDF model is widely used to simulate the dynamic behavior of adsorption chillers and predict the system performance. However, it has limitations especially at short cycle times where it underestimates the adsorption uptake which affects the estimated SCP and COP of the system. The underestimation of adsorption uptake at relatively shorter adsorption times might be because the adsorption uptake difference is quite large at earlier period of adsorption.

An experimental and theoretical study were conducted on the adsorption kinetics of ethanol onto ACF of type (A-20) [82]. Thermal-gravimetric analyzer (TGA) was used to measure the

adsorption kinetic, then the diffusion time constant and the overall mass transfer coefficient were evaluated. A concentration profile, with an exponent parameter that accounts for the effect of mesopores and micropores structures, was proposed to better describe the adsorption kinetics. Based on the measured kinetics, the numerical value of k was evaluated, leading to a new form of the linear driving force (LDF) model. EL-Sharkawy [83] addressed effect of using the classical Linear Driving Force (LDF) model on the performance of adsorption chillers. A comparative study between the LDF model and the Fickian diffusion (FD) model was conducted. Relative and absolute errors between adsorption uptakes estimated by both models were reported. The LDF model was found to have numerous errors at relatively shorter adsorption times, which imply that using LDF model leads to incorrect evaluation of the performance of adsorption chiller especially at short cycle times. Accordingly, an improved form of LDF model considering the dependency of the particle mass transfer coefficient on the dimensionless time was proposed. Calculations showed a good agreement between the improved LDF approximation and the FD model. Raymond and Garimella [84] conducted a comparison between the LDF approximation and the Fickian diffusion equation. It was shown that the LDF can result in considerable errors if used to model adsorption cooling systems with short cycle times. Sun and Chakraborty [85] investigated the dynamic uptakes of water vapor on various sizes and layers of silica gels for adsorption cooling applications. A thermodynamically consistent adsorption kinetics equation was derived to overcome the limitations of the general LDF kinetics equation. The new equation includes the knowledge of adsorption isotherm and activation energy, and can predict the adsorption capacity from the Henry's region to the saturated pressure.

Aristov et al. [43] measured kinetics of water adsorption on loose grains of composite sorbent $CaCl_2$ confined to mesoporous silica gel (SWS-1L) at temperature of 33.69 ℃ and vapor

pressure of 8.70 mbar over water uptake range 0-0.47 g/g for various particle sizes (between 0.355 and 1.4 mm). The measurements were performed in a constant pressure unit based on a CAHN microbalance under isothermal external conditions. Results showed that decreasing the particle size leads a remarkable enhancement in the adsorption rate. Girnik et al. [46] addressed a dynamic study on methanol adsorption in compact adsorbent layers. The commercial active carbon ACM-35.4 and polyvinyl alcohol were used as an adsorbent and a binder, respectively. Influence of the carbon grain size and the layer thickness on the Volumetric Large Temperature Jump (V-LTJ) dynamics was studied at a fixed binder content of 12 wt.%. It was noticeable that the binder can enhance heat and mass transfer in an adsorption cooling bed. For the compact layers, the process became faster by a factor of 1.5-3.5 as compared to packed beds. Sapienza et al. [86] studied the equilibrium and dynamics of water adsorption on a commercial silica gel Siogel. Equilibrium data for Siogel were described by a simple characteristic curve with two fitting parameters. Besides, the data for Siogel were very close to the ones reported for Fuji silica RD type. In addition, adsorption dynamics were measured for a monolayer configuration of loose Siogel grains with the characteristic time between 20 and 40 s, which allows reaching a very high initial cooling power of 6-8 kW/kg. Teo et al. [87] presented the adsorption characteristics of Aluminum Fumarate (Al-Fum) and water for the temperatures ranging from 25 to 60 ℃ and pressures up to saturation conditions. The amount of water uptakes was measured by a gravimetric analyzer under static and dynamic conditions. Based on the isotherms and kinetics data, Al-Fum/water showed a potential working for heat transmission applications such as heat pump and desalination.

Since the effective thermal conductivity of an adsorbent packed bed is low (~0.1-0.4 W/m.K) [88, 89] and if the adsorbent is not very near (1 or 2 mm) from a heat transfer surface, the local adsorbent temperature will increase significantly and the adsorption rate will be much

reduced due to the release of heat of adsorption. Accordingly, enhancing the effective thermal conductivity of adsorption bed directly affects its adsorption kinetics and hence increases the performance of adsorption chillers. Demir et al. [90] added metallic additives of copper, brass and aluminum up to 15% to silica gel to enhance heat transfer rate through an adsorption bed. It was noticed that the effective thermal conductivity of a pure silica gel bed is enhanced by 242% by addition of 15 wt.% of aluminum pieces. Based on the results of Demir et al. [90], influence of the contact resistance on the performance of finned tube heat exchanged packed with silica gel was studied [91]. Results showed that using aluminum additives by 15% improved the performance of adsorption bed by 58.2%. Zheng et al. [62] proposed a new composite solid desiccant material to enhance thermal conductivity and adsorption performance of silica gel. The new adsorbent was fabricated by combining silica gel with expanded natural graphite treated with sulfuric acid (ENG-TSA) as a host matrix. Experimental results showed that the highest thermal conductivity of consolidated composite adsorbents is 19.1 W/m.K, which is 270 times higher than that of pure silica gel. Effect of using metallic additives on thermal conductivity of granular activated carbon was investigated [92]. Fillings of iron, copper and aluminum at different mass concentrations ranging from 10 to 30% were studied. The experimental results indicated that the adsorbent thermal conductivity is increased by 110% with aluminum filling of 30%. This caused a decrease in cycle time by 50% and an increase in specific cooling power by 100%. Fayazmanesh et al. [93] enhanced the thermal conductivity of $CaCl_2$-silica gel composites adsorbent by adding natural flakes graphite, and consolidating the mixture with a binder. The results showed that addition of graphite flakes into consolidated adsorbent increases thermal conductivity from 0.13 to 0.57 W/m.K when tested at 2% RH and 35℃.

3.3 System Performance Studies

Over the past few decades, many studies have been conducted out to enhance the performance of adsorption cooling/heating systems. Restuccia et al. [47] numerically investigated the heat and mass transfer properties of a new zeolite-coated adsorbent bed to be employed in sorption air conditioning systems. Analysis of the model results demonstrated that the heat transfer enhancement is mainly related to the good adhesion between metal and adsorbent. This led to an enhancement in heat and mass transfer in the new adsorbent bed. Chan et al. [94] built and tested a compact dual adsorber adsorption cooling system (ACS) prototype using the zeolite 13X/$CaCl_2$ composite adsorbent with water as the adsorbate. Finned heat exchangers were coated with composite adsorbent to enhance the heat and mass transfer performance. It was found that the specific cooling power (SCP) is largely improved from 106 W/kg to 377 W/kg (256% improvement) under desorption temperature of 85℃ and chilled water inlet temperature of 14℃. Also, performing the pre-heating & pre-cooling cycle further increased the SCP to 401 W/kg. Tatlier [95] determined the performance of metal heat exchanger coated with zeolite and metal-organic framework (MOF) for various operating conditions of adsorption cooling systems. A mathematical model was used to calculate the optimum coating thicknesses of the adsorbents. The cooling power provided by coatings of zeolite X in Li form was generally about 10-20% higher than that obtained for zeolite X coatings in Na form. The coating of zeolite X in Na and Li form did not perform well due to the relatively slow diffusion especially at the lower temperatures.

San et al. [49] investigated a lab-scale adsorption heat pump with four aluminum alloy finned tubes adsorbers. Maximum SCP of 93 W/kg of silica-gel was produced and COP of 0.31 was calculated at regeneration temperature of 77.5℃ and optimum cycle time of 11 min. Also, it was found that a proper design of evaporator has a great effect on the performance of adsorption

heat pump. Saha et al. [96] applied a multi-bed arrangement to improve the performance of thermally activated silica gel–water adsorption refrigeration cycle. Three-bed chiller was designed to work as a highly efficient single-stage adsorption chiller using a driving source temperature between 60℃ and 95℃ and a coolant at 30℃. Also, a cycle simulation computer program was developed to analyze the influence of operating conditions on the performance of the system. The calculations indicated that the COP of the three-bed chiller is 0.38 with a driving source, coolant inlet and chilled water inlet temperature at 80℃, 30℃ and 14℃, respectively. Simulation results also showed that waste heat recovery efficiency is boosted by about 35% when three beds are used instead of two beds. Saha et al. [97] studied the performance of a dual-mode silica gel-water adsorption chiller. This adsorption chiller utilizes effectively low temperature solar or waste heat sources of temperature between 40 and 95℃. Simulation results indicated that the optimum COP values are obtained at driving source temperatures between 50℃ and 55℃ in three-stage mode, and between 80℃ and 85℃ in single-stage mode.

Wang et al. [98] designed a novel zeolite-water adsorption air conditioner that supplies 8-12℃ chilled water for the fan coil in the locomotive operator cabin. The simulation results depicted that this machine could produce cooling power of 10 kW at gas inlet temperature of 450℃ and evaporating temperature of 6.5℃. Deshmukh et al. [99] proposed a new design of solar operated adsorption cooling system with two identical small and one large adsorber beds, which is capable of producing continuous cooling. Results indicated that the system is capable of providing a cooling capacity of 0.8 kW for 24 h, with average COP of 0.63 at a generation, condenser and evaporator temperatures of 368 K, 303 K and 283 K, respectively. Al-Mousawi et al. [51] studied different multi-bed water adsorption systems to generate cooling and electricity at the same time using 9 different cases including 7 bed configurations and 7 time ratios. Effect of using different

cases on the overall system performance was investigated using a MATLAB Simulink program for cooling and power generation. Using three-bed configuration with time ratio of ½ produced the highest specific cooling power (SCP) Results also showed that maximum COP of 0.64 can be achieved using Silica-gel, while maximum SCP and adsorption power efficiency of 650 W/kg and 4.6%, respectively achieved using AQSOA-Z02. Mitra et al. [100] presented a numerical and thermodynamic study of a two-stage, 2-bed silica gel/water adsorption system for simultaneous generation of cooling power and potable water. It was indicated that decreasing the heat source temperature increases the optimum cycle time, whereas COP is relatively insensitive to such alterations. The thermodynamic analysis provided a theoretical limit for minimum desorption temperature and optimal inter-stage pressure for a two-stage adsorption cycle. Wang et al. [101] proposed a novel solar adsorption refrigeration system employing an enhancing mass transfer method based on dropping the internal pressure of the system in the desorption process. The experimental results proved that the novel method is effective for low adsorbent temperature operation, which may increase the COP by 16.4%.

As fresh-water, energy and environment nexus of are intertwined and interconnected, researchers proposed an integration between Multi-Effect Desalination (MED) cycle and adsorption cycle (MEDAD) [102, 103]. This integration allows the last stages of MED cycle to operate at temperatures below the ambient temperature. So, the distillate production from the combined cycle increases by a factor of 2 to 3 compared with the conventional MED cycle [103]. As the production rate from MED cycle depends of its dynamic response, the dynamic performance of MED using different configurations has been studied and investigated at various operating conditions [104-110].

3.4 Conclusion of Previous Studies

Performance of adsorption cooling (AC) systems with different design configurations and operating conditions has been investigated in the literature. It is concluded the prospect of using adsorption cooling technology as an alternative to mechanical vapor refrigeration system. Compared to mechanical system, adsorption cooling system has low maintenance and the absence of moving components is a very important feature that makes this type of system suitable for many applications such as air-conditioning and cooling food storage units. The absence of harmful and hazardous products such as CFCs, together with a substantial reduction of CO_2 emissions due to very low consumption of electricity, is impressive and creates an environmentally safe technology.

However, the adsorption cooling technology is restricted by the poor heat and mass transfer inside the adsorber packed bed, which is the main obstacle to commercialization of AC units. Significant efforts to enhance performance of adsorbents are required to increase the specific cooling power (SCP) of AC systems and propose more compact units. There are different ways to solve these problems, one is to develop a new adsorbent material which would have a better adsorption capacity and kinetics; another, could be to propose a new design of adsorption bed that could enhance the heat and mass transfer.

CHAPTER 4 EXPERIMENTAL WORK

4.1 Introduction

Selection of a suitable adsorbate/adsorbent pair is critical for an adsorption cooling cycle. The surface characteristics and thermo-physical properties of the adsorbent, and the adsorption rate of adsorbate are key parameters in making the selection. This chapter presents design and construction of an experimental test facility that is used to measure the adsorption kinetics and isotherm of different working pairs. Also, it is used to evaluate the heat and mass transfer processes in an adsorption bed, which is typically applied in adsorption cooling cycle.

4.2 Experimental Setup Description

In the development of any adsorption system design, it is essential to study the characteristics of adsorption isotherm and kinetics of the adsorbate/adsorbent pair. Volumetric and gravimetric approach are the common methods that are used for measuring the adsorption isotherm [12, 111]. The volumetric approach is suitable only when the amount of adsorbent is very small so that the adsorption process can be considered as quasi-isobaric. The gravimetric approach uses a larger amount of adsorbent and allows the possibility to weigh the adsorption uptake directly.

Based on the gravimetric approach, the present experimental test rig is designed to be simple and to monitor the adsorption rate at a desired pressure and temperature. It also can be used to investigate the performance of adsorption beds with different structures and various working pairs. The present test rig consists of a measuring chamber, evaporator/condenser, cooling water circulating system, chilled water circulating system and electrical heating system as shown in Fig. 4-1. In this test facility, evaporation and condensation are performed in one heat exchanger chamber to make the system simpler. It performs as an evaporator in the adsorption process and

as a condenser in the desorption process. This vessel is filled with clean water as the source or sink of adsorbate vapor. Since water contains calcium and/or magnesium mineral ions, the evaporator/condenser chamber should be regularly drained, cleaned and refilled with water to avoid insoluble mineral deposits and scaling. The water temperature is controlled by the water that flows inside the copper coil that is connected to the thermal bath 1 (TB1) as indicated in Fig. 4-2. Furthermore, a vacuum pump is connected to the evaporator/condenser chamber to suck air out and provide the required vacuum conditions.

The second vessel represents the measuring unit which contains adsorbent placed on a flat plate heat exchanger (120×40 mm) mounted on a single point load cell/load gauge. The load cell has a range of 600 g and it is calibrated using a very precise balance of ± 0.001 g accuracy. The accuracy of the load cell is estimated to be less than 1% with a time response faster than 0.1 s. The heat exchanger is connected to TB2 and TB3 by flexible tubing to control the sample temperature by providing external cooling/heating fluid passing through the inner tubes of the heat exchanger to remove or provide heat to the adsorbent throughout the isobaric adsorption/desorption process. The position of the flexible tubes and flow velocity inside are adjusted before the test to eliminate the vibrations that could affect the load cell response.

When the pressure inside the tank is lower than that on the outside, the acrylic cover pushes onto the silicon gasket. The deformation makes the gasket contact the cover perfectly and prevent ambient air from leaking inside. With this sealing method, a high vacuum level inside the evaporator/condenser tank is achieved. The results of the leakage test indicate that the measuring unit chamber and evaporator/condenser chamber gain only 20 Pa/day. The measuring unit is equipped with 10 T-type thermocouples, with accuracy of ±0.5℃, to measure the sample temperature at different locations during the test. Two MKS pressure transducers with accuracy of

± 0.25% are used to measure the pressure of each chamber. All measurements are connected to a data acquisition system.

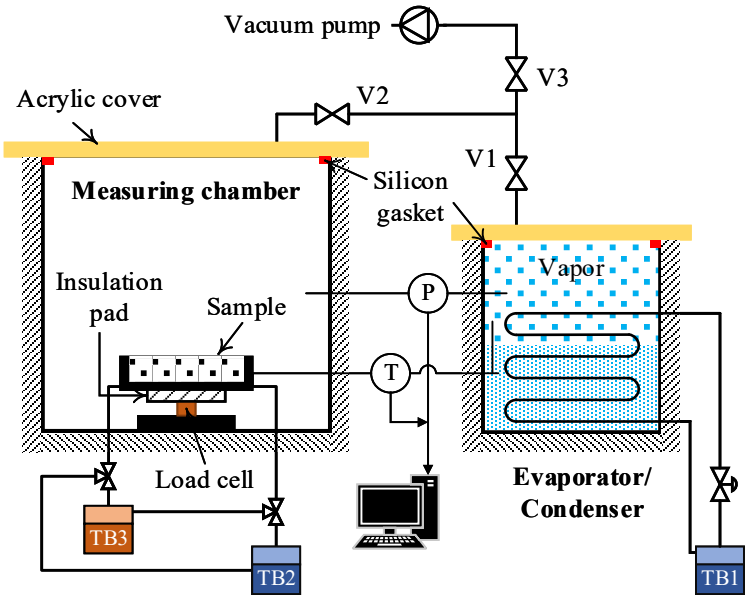

Figure 4-1 Experimental test rig

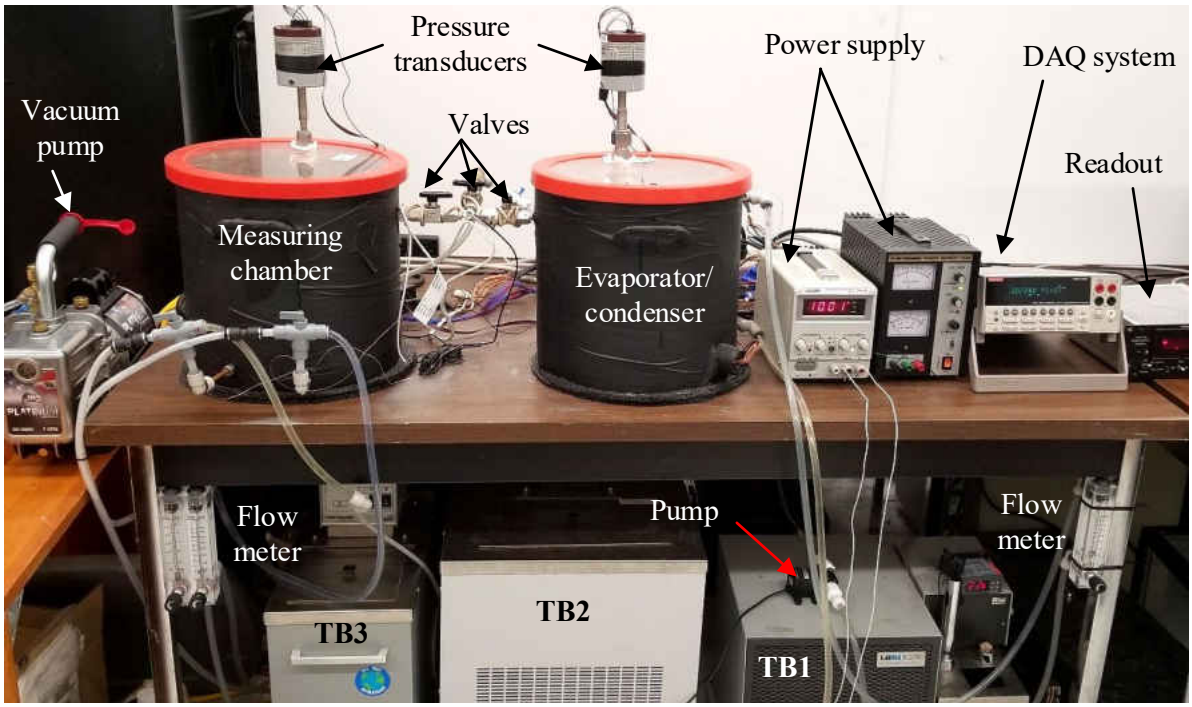

Figure 4-2 Pictorial view of the entire test rig

Each component of the test facility is described in the following sections, including the measuring unit chamber, evaporator/condenser, water pumps, valves, vacuum pump, pressure transducers and thermocouples.

4.2.1 Measuring unit chamber

The measuring unit vessel is a cylindrical stainless-steel tank with a diameter of 13 in and a height of 13 in. It has one hole for load cell wiring connections, one hole for thermocouples and one hole for vacuum pump and vapor entering during the adsorption period or leaving during the desorption process. Single point load cell, manufactured from aluminum as shown in Fig 4-3, is used to measure the mass change of the adsorbent during the adsorption and desorption process. The load cell is available in ranges from 600 grams to 200 kilograms, highly accurate and suitable for many applications such as electronic scales and weighing machines. This single point design is highly resistant to eccentric loading, allowing direct mounting to the scale base and weighing platform. It is also a moisture resistant, so it is uses in damp environments.

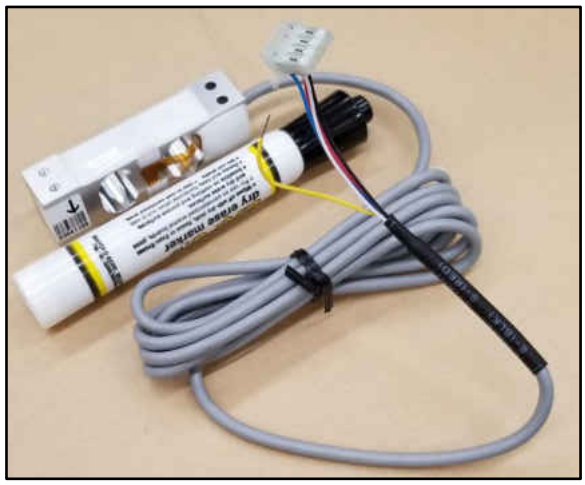

Figure 4-3 Pictorial view of the load cell used in this study

In this work, the load cell is excited by 5 Vdc and calibrated with the heat exchanger and flexible tubing (see Fig. 4-4) using a very precise balance of ± 0.001 g accuracy as presented in

Fig. 4-5. The accuracy of the load cell is calculated to be less than 1% with a time response faster than 0.1 s and hysteresis of 0.02%. The heat exchanger is made of aluminum and has internal flow channels. The heat exchanger is rested on acrylic stand, which is attached to load cell. The acrylic stand separates between the load cell and heat exchanger to keep the load cell temperature is less than 60°C during the desorption process. The temperature of the heat exchanger is controlled using two thermal baths; one for adsorption process and another for desorption process. On the other hand, the load cell output is recorded without the adsorbent at different cooling water temperatures and mass flow rates. It is determined that the flexible tubing and cooling water do not lead to significant uncertainty in the load cell measurements. In addition, tubing position are adjusted before the test to eliminate the vibrations.

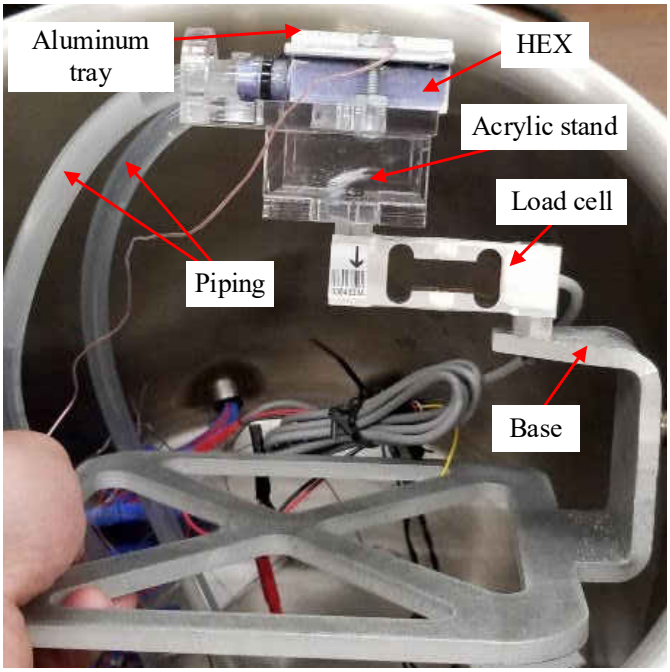

Figure 4-4 Load cell arrangement

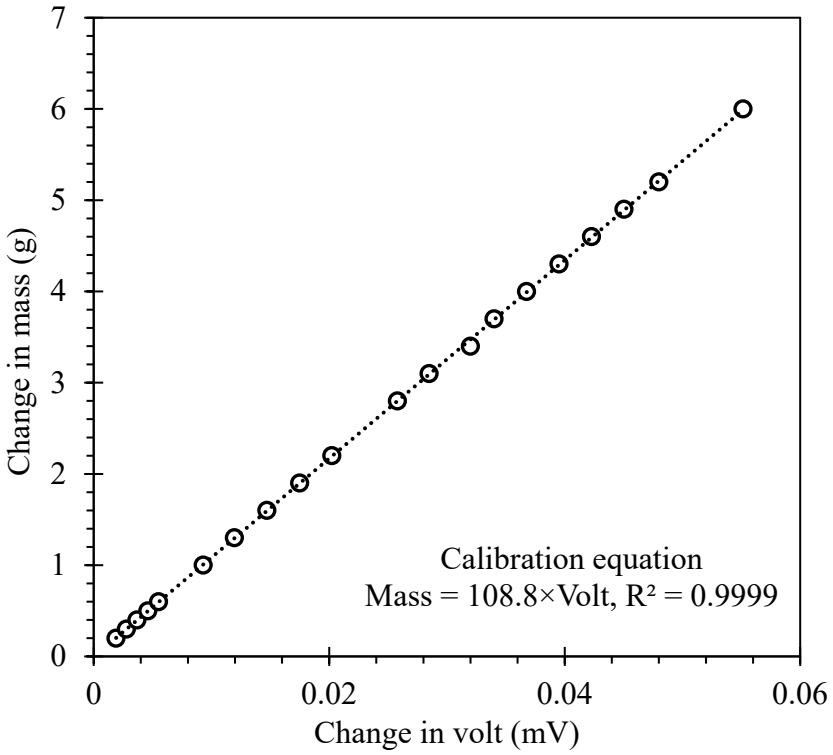

Figure 4-5 Load cell calibration curve

4.2.2 Evaporator/condenser vessel

In the test facility, there is only one adsorption bed investigated every test. So, the adsorber is connected to an evaporator during the adsorption mode and to a condenser during the desorption mode. Therefore, the evaporator and condenser can be integrated into one chamber. The evaporator/condenser is a cylindrical stainless-steel tank with a diameter of 13 in and a height of 13 in. On the wall, there are two holes for cooling/heating fluid inlet and outlet and another hole for thermocouples measuring the temperature of the refrigerant vapor and Liquid, as shown in Figure 4-6. Also, there is one hole for vacuum pump and refrigerant vapor entering/leaving this chamber. The outer wall of chamber is covered with thermal insulation material to reduce heat losses to or from the surrounding.

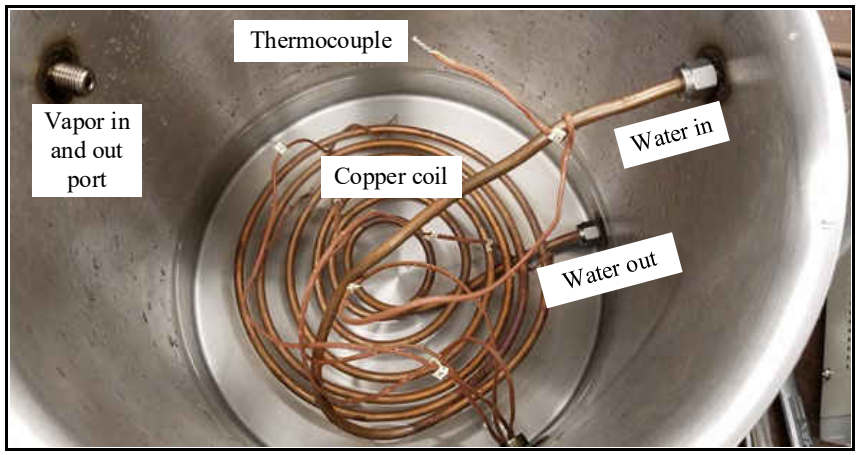

Figure 4-6 Pictorial inside view of the evaporator/condenser chamber

Water flows inside a copper coil is used to keep the evaporator/condenser temperature constant by extracting the heat of condensation during the desorption or supply the heat of evaporation during the adsorption period. The coil is made of ¼ in outer diameter tube and has several turns in the same plane, laid at the bottom of the chamber and submerged in the liquid refrigerant as presented in Fig. 4-6. The temperature of water is controlled using thermal bath (LAUDA K-2/RD). A diaphragm circulation pump is used to pump water through the copper coil. The pump is powered by DC volt up to 12 V and capable of circulating a water flow rate up to 8 L/min. The input DC voltage of the pump is adjusted to circulate a certain amount of water flow rate that is measured by flowmeter.

4.2.3 Sealing method

The cover of each chamber is made from acrylic and has one hole for the pressure transducer. The measuring chamber and evaporator/condenser chamber is sealed through a rubber gasket. During the test, the pressure inside the chambers is smaller than that outside so, the acrylic cover pushes onto the rubber/silicon gasket, as shown in Figure 4-7. This deformation makes the gasket contact the cover perfectly and prevent ambient air from going inside the chambers. With

this sealing method, a high vacuum level inside the vessels is achieved. In the absence of water and adsorbent, the pressure of the two chambers are monitored and recorded to estimate the leakage. The results of the leakage test indicate that the pressure of measuring unit chamber and evaporator/condenser chamber increases only 20 Pa during a day, which is sufficient to evaluate the performance of adsorption bed or measure the adsorption isotherm for any working pair.

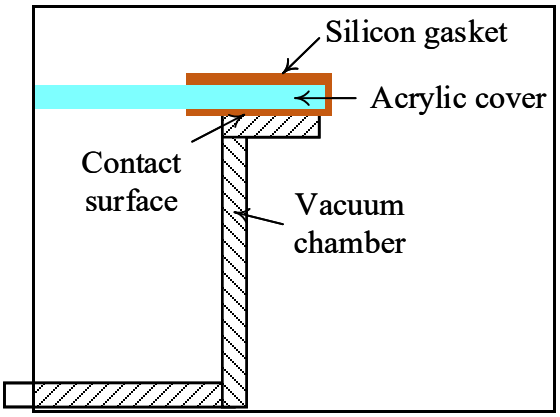

Figure 4-7 Sealing method used for the two vacuumed chambers

4.2.4 Temperature measurements

T-type thermocouples are installed at different positions in the test rig to measure the temperatures of the adsorption bed/adsorbent, heat exchanger, water in evaporator/condenser chamber and heating/cooling fluid flowing through the heat exchanger and copper coil. The adsorbent temperature is measured at different locations using 30 AWG gauge thermocouples wires, which have a dimeter of 0.01 in. This type of thermocouple can measure temperature up to 350ºC with accuracy of less than 0.5ºC according to the manufacturer's instructions. It is worth to mention that these wires are soft and do not negatively affect the load cell response. A thermocouple feedthrough, shown in Fig. 4-8, is a component used to conduct the thermocouples wires through bulkhead of the chamber to external instrumentation. The used feedthroughs can

afford a pressure up to 8 bar and temperature up to 120ºC. This type of fitting is also used to transfer the load cell wires through the vacuum measuring chamber to DAQ system.

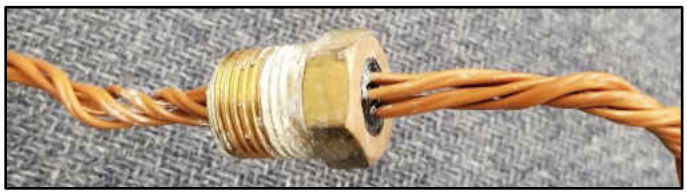

Figure 4-8 Thermocouple feedthrough used in evaporator/condenser chamber

4.2.5 Pressure measurements

Pressure of each chamber is measured using MKS Baratron 622A pressure transducer. The pressure transducer requires ±15 VDC input voltage provided by MKS readout while the output is 0-10 VDC analog signal that is linear with pressure as illustrated in Fig. 4-9. The pressure transducers are calibrated using another pressure transducer calibrated by the manufacture. Figure 4-9 shows the calibration curve of each transducer with accuracy of ± 0.25%.

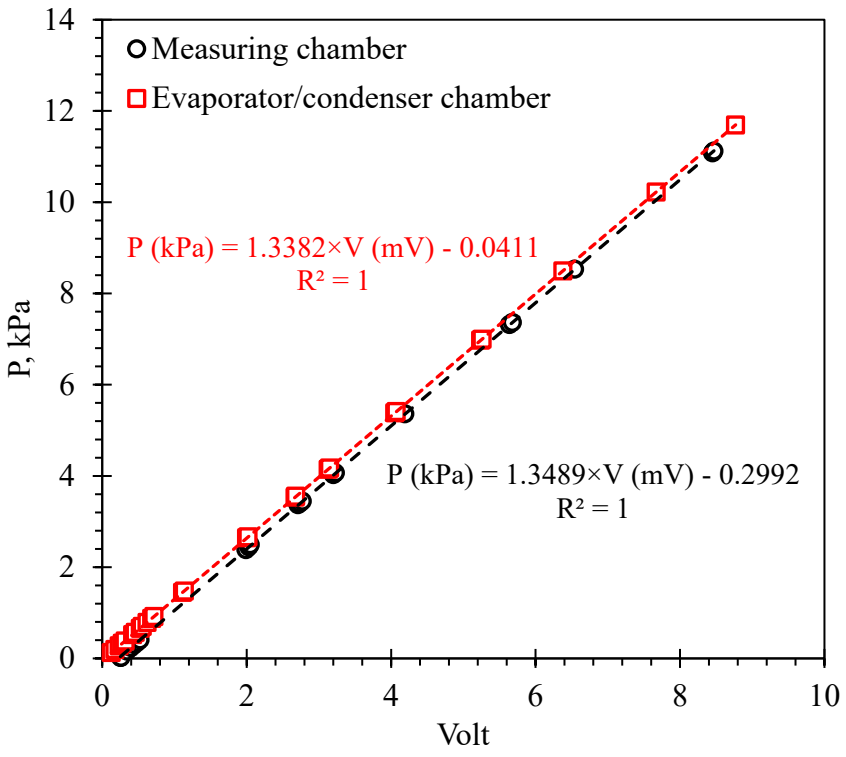

Figure 4-9 Calibrations of the pressure transducers

4.3 Test Procedure

The present experimental test rig can be used to measure the adsorption isotherm and kinetics of different working pairs and the performance of adsorption bed. Measurements of the load cell, temperature and pressure are monitored and recorded simultaneously using a data logger and computer. The testing methodology, regardless the type of measurement, has three stages: preparation, desorption, and adsorption.

The first stage of the testing methodology is the integration of the heat exchanger and adsorbent with the load cell as well as the calibration of the latter. After the installation, a standardized procedure is followed to guarantee high reproducibility of the measurements. Each test is run more than once to check the repeatability of the experimental set-up and the repeated measurements for the same operating conditions vary by no more than ±2%.

4.3.1 Measuring of adsorption isotherm and kinetics

Adsorption isotherms and kinetics of Fuji silica-gel RD and RD-2060 are experimentally measured. Silica-gel RD and RD-2060 are in granular form and have particle size ranges of 1.0-2.0 mm and 0.18-1.0 mm, respectively.

The following steps describe the testing procedure for adsorption isotherm and kinetics.

1. The evaporator/condenser is filled with water and thermal bath 1 is set at specific temperature and then the vacuum pump is run until equilibrium condition is reached.

2. The sample of the adsorbent is placed on the heat exchanger and its temperature is controlled by the thermal bath 2 or 3.

3. Small known dead loads are placed on the load cell and the load cell response is monitored to ensure that the flow through the flexible tubes does not affect the load cell response and the accuracy is still less than 1%.

4. The sample is heated and the measuring chamber is evacuated by the vacuum pump to reach a relative pressure less than 10^{-4}. The sample is assumed to be completely dry when the load cell response becomes constant for 2 h, then the degassed dry sample is weighed.

5. The sample is cooled down to the desired adsorption temperature and then the two chambers are connected to start the adsorption process.

6. During the adsorption, the sample temperatures and the load cell response are monitored over time. The adsorption process is assumed to be completed when the uniform sample temperature is achieved and equals the inlet water temperature.

In case of measuring the performance of an adsorption bed, the first three steps are the same. Then, the tested bed is heated to the desorption temperature and evacuated by the use of a vacuum pump to reach condenser pressure while the two chambers are disconnected. Subsequently, the dry tested bed is cooled to the initial adsorption temperature of the isobaric adsorption process. Then, valves 1 and 2 are opened to feed the measuring unit chamber with water vapor, allowing the adsorbent material to adsorb water vapor. After reaching equilibrium conditions, cool water at temperature T_c is introduced to cool the adsorbent to the final temperature (T_c) (see Fig. 4-1). During the step, an increase in the adsorbent weight can be observed, using the load cell, which directly corresponds to the amount of water adsorbed (i.e., the change in uptake).

4.4 Measurements Repeatability

All instruments of the test facility are examined through a repeatability test. Three independent tests using the same procedure are conducted at the same operating conditions. The time difference between the three tests is more than 24 hours to make sure the temperature of the system is the same as the ambient temperature (22^{o}C) at the beginning of each test. The fitting of the load cell response and average temperature of the adsorbent of the three repeated tests are reordered and plotted in Fig. 4-10. It is evident from this figure that the experimental measurements are nearly the same for the same operating conditions of a test, which guarantee the measurements repeatability and consistency of the instruments used.

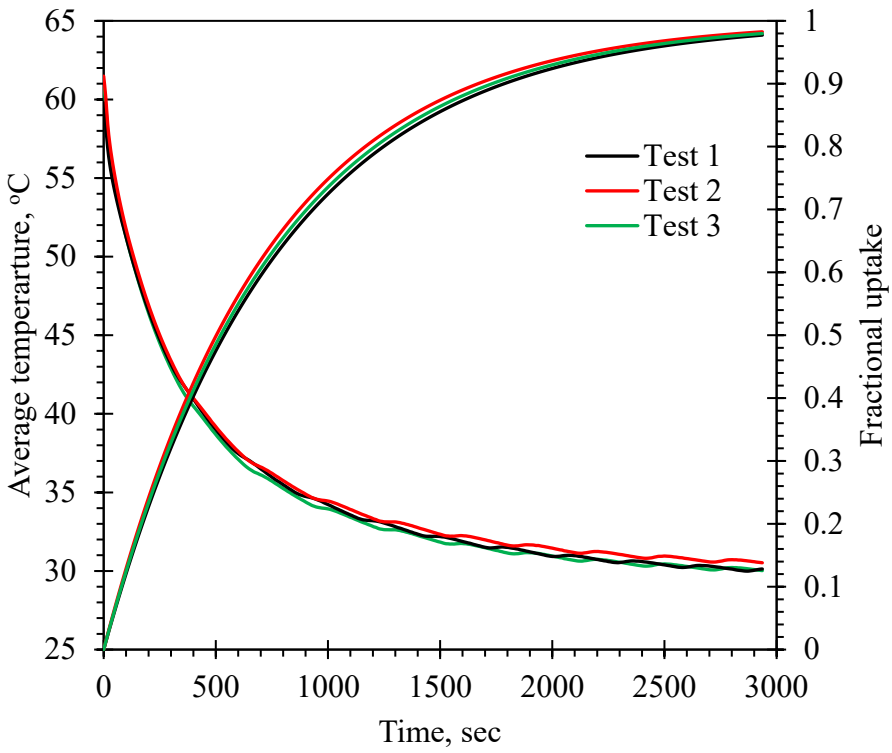

Figure 4-10 Average adsorbent temperature and fractional uptake for different tests at the same conditions

4.5 Error Analyses

The factors that lead to errors in the load cell, temperature and pressure measurements are the accuracy of the load cell (E_0), thermocouple (E_1), pressure transmitter (E_2), data logger (E_3) and errors due to connections (E_4). The total errors in the load cell reading (E_{LC}) temperature (E_T) and mean pressure (E_P) measurements can be determined as follow [112, 113]:

$$E_{LC} = \sqrt{E_0^2 + E_3^2 + E_4^2} \quad (11)$$

$$E_T = \sqrt{E_1^2 + E_3^2 + E_4^2} \quad (12)$$

$$E_P = \sqrt{E_2^2 + E_3^2 + E_4^2} \quad (13)$$

As the surface diffusivity is a function of temperature, the error associated with it can be written as:

$$E_{D_s} = \frac{dD_s}{dT} E_T = \frac{D_s E}{RT^2} E_T \Rightarrow \frac{E_{D_s}}{D_s} = \frac{E}{RT^2} E_T \quad (14)$$

Based on the above equations, the maximum error of load cell, temperature and pressure measurements is found to be 1.5%, 2% and 1.5%, respectively. The error in calculating the surface diffusivity is about 2.5%, and the error in the surface diffusivity due to the temperature variation of the sample during the adsorption (maximum difference should be less than 2°C) is found to be 3.5%.

CHAPTER 5 MEASUREMENTS OF ADSORPTION ISOTHERM AND KINETICS

5.1 Introduction

The choice of a suitable adsorbate/adsorbent pair is critical for an adsorption cooling cycle. The surface characteristics and thermo-physical properties of the adsorbent, and the adsorption rate of adsorbate are key parameters in making the choice. Through literature review, it is found that there are disagreements among the experimental measurements and various equations/models used to describe adsorption isotherms and surface diffusivity of water in silica-gel. The experimental setup described in detail in Chapter 4 is used to measure the sorption kinetics and equilibrium uptake of two different types of silica gel: silica gel RD-2060 and silica gel RD. Using the newly measured data, those from the manufacturers and from the literature, these inconsistencies are eliminated by utilizing the Dubinin-Astakhov (D-A) model to fit the entire adsorption isotherm curve. Moreover, based on the adsorption rate and the adsorbent temperature measured simultaneously, a new approach is proposed to measure the surface diffusivity in the temperature and pressure ranges typical of those during the operating conditions of adsorption cooling systems. The findings of this study have been presented in International Journal of Applied Thermal Engineering and International Journal of Refrigeration [**].

5.2 Inconsistencies in Adsorption Models of Silica-Gel/Water

The Freundlich, Tòth and Dubinin-Astakhov (D-A) equations are used to fit experimental measurements of adsorption isotherm. The Freundlich and Tòth equations do not estimate the

** The content of this chapter has been published in

1. R. H. Mohammed, O. Mesalhy, M. L. Elsayed, S. Hou, M. Su, L. C. Chow, Physical properties and adsorption kinetics of silica-gel/water for adsorption chillers, Applied Thermal Engineering 137, 368-376, 2018.
2. R. H. Mohammed, O. Mesalhy, M. L. Elsayed, M Su, L. C. Chow, Revisiting the adsorption equilibrium equations of silica gel/water for adsorption cooling applications, International Journal of Refrigeration 86, 40-47, 2018.

uptake correctly when the relative pressure is less than 0.15. The D-A equation, which is widely used, was originally developed based on the Polanyi adsorption theory and has different forms [53, 114]. The uptake could be a function of the operating pressure and adsorbent temperature as in Eq. 15 and 16 which are the same, or a function of the operating temperature as in Eq. 17.

$$\frac{X_o}{X_m} = exp\left\{-\left(-\frac{RT_s}{E}\ln\left(\frac{P_v}{P_s}\right)\right)^n\right\} \quad (15)$$

$$\frac{X_o}{X_m} = exp\left\{-D\left(\ln\left(\frac{P_s}{P_v}\right)\right)^n\right\} \quad (16)$$

$$\frac{X_o}{X_m} = exp\left\{-k\left(\frac{T_s}{T_v}-1\right)^n\right\} \quad (17)$$

where X_o is the equilibrium adsorbate mass per unit mass of adsorbent (kg/kg) at vapor pressure P_v and adsorbent temperature T_s, P_s is the saturation vapor pressure at T_s, T_v is the vapor temperature, X_m is the maximum adsorbent capacity, $\frac{P_v}{P_s}$ is the relative pressure (RP), D is the affinity coefficient, R is the universal gas constant, n is the uploading factor, k is constant depends on adsorption isotherm and E is the characteristic energy of adsorption (J/mol).

Silica-gel (SiO_2) is widely used in many industries due to its strong hydrophilicity towards water. There are many types of silica-gel such as A, B, A5BW and A^{++}. Silica-gel RD is commonly employed in adsorption cooling systems and dehumidification applications. The adsorption isotherm of silica-gel/water is measured by either the gravimetric or volumetric methodology, while the isothermal or non-isothermal approach was proposed to extract the surface diffusivity. Although there are many publications in the adsorption characteristics, there are inconsistencies among the different experimental measurements of the surface diffusivity. Also, there are

significant discrepancies among the adsorption equilibrium equations used to describe the adsorption isotherm of silica-gel RD/water.

Chihara and Suzuki [1] used the gravimetric method to measure the adsorption properties of Fuji silica-gel with water vapor. Xia et al. [2] used Eq. 16 to fit these experimental measurements and obtained values for X_m=0.348 kg/kg, n=1.6 and D=0.449. Also, Eq. 17 with values for X_m=0.346 kg/kg, n=1.6 and k=5.6 was used to correlate the same experimental data, and this equation has been widely used in numerical simulations of adsorption cooling systems [45, 115-117]. Figure 5-1 shows large discrepancies among the experimental measurements of the adsorption isotherm of silica-gel/water and the calculated ones using the D-A model. So, new sets of parameters for the D-A model should be proposed to appropriately fit the measurements. Choosing X_m=0.346 kg/kg, D=0.64, and n=1.0 for Eq. 16 and X_m=0.346 kg/kg, k=11, and n=1.0 for Eq. 17 can minimize the discrepancy. The resulting isotherms using these new sets of parameters are also plotted in Fig. 5-1. It is clear that the predicted uptakes using the new sets of coefficients have a good agreement with the experimental measurements.

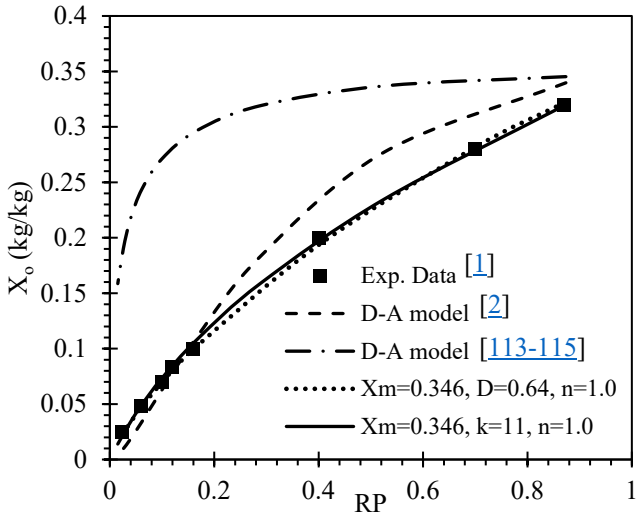

Figure 5-1 Comparison between the measured isotherm of silica-gel/water and the predicated one using D-A model.

The surface diffusivity of water in silica-gel was measured using isothermal and non-isothermal approaches. Based on hopping mechanism, Sladek et al. [10] proposed a simple Arrhenius-form equation for surface diffusion (D_s) of water vapor onto silica gel as follows [5]:

$$D_S = \frac{1.6\times10^{-6}}{\tau} exp\left(-\frac{A\cdot H}{T_S}\right) \quad (18)$$

where τ is the solid tortuosity factor which is equal 2.8 for regular density silica gels, T_s is the adsorbent temperature, A is a constant which is equal to 0.974 for silica gel, and H is the heat of adsorption that is calculated for silica-gel/water from the following relationship:

$$H = -1400X_o + 2950 \quad \text{for } X_o \geq 0.05 \quad \left(\frac{kJ}{kg}\right) \quad (19)$$

Based on the Isothermal Differential Step (IDS) method, a CAHN 2000 thermo-balance was used to measure the equilibrium uptake of water vapor onto RD silica-gel at a temperature range from 30 to 150 ºC and a vapor pressure range from 1 to 5 kPa [118]. The surface diffusivity was found to be an Arrhenius function of temperature (Eq. 20) with activation energy (E_a) of 41.5 kJ/mol and pre-exponential factor (D_{so}) of 2.9×10^{-4} m^2/s. These measured values are close to those obtained in [1] for Fuji Davison silica-gel type A. This is may be because of the similar nanostructure in these silica-gels.

$$D_S = D_{so}\, exp\left(-\frac{E_a}{RT_S}\right) \quad (20)$$

Figure 5-2 compares the aforementioned measured surface diffusivity of water onto silica-gel. It is found that the measured surface diffusivity by Aristov et al. [118] is close to the measured one by Chihara and Suzuki [1]. The measured surface diffusivity by Sladek et al. [10], which depends on the water concentration, is close to the others at low uptake, but it is about 2.6 times

higher at uptake of 0.3 at 350 K as presented in Fig. 5-2. Due to these inconsistencies, a new approach for measuring the surface diffusivity is proposed and validated.

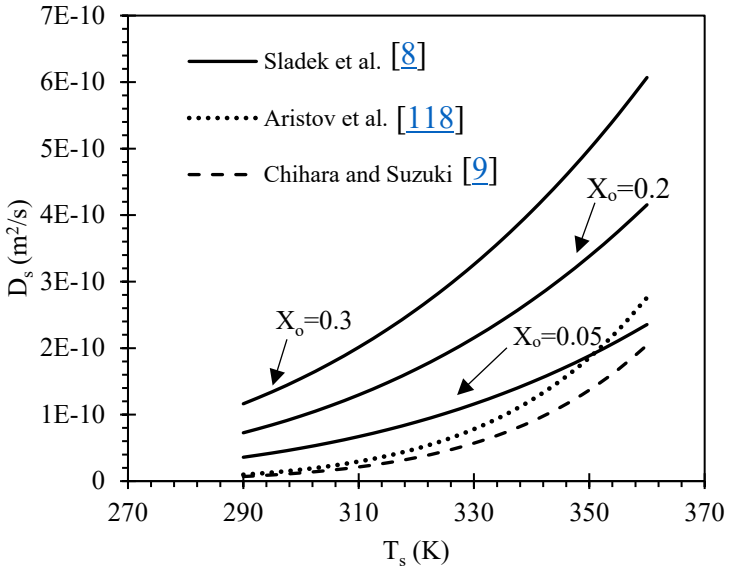

Figure 5-2 Surface mass diffusivity of water vapor onto silica gel obtained from previous studies

5.3 Experimental Work

5.3.1 Physical properties measurements

The surface characteristics such as the specific surface area, pore volume and pore size distribution of the silica gel RD and RD-2060 are analyzed using a surface area analyzer (Quantachrome, NOVAe) [119-121]. Nitrogen is used as the adsorbate under the environment of liquid nitrogen (77K). Figure 5-3 shows the adsorption isotherms of Fuji silica-gel RD and RD-2060. Both types show a type IV adsorption isotherm [6], which indicates that the nitrogen molecules first form monolayer followed by multilayer on the silica walls. The pore sizes within the silica beads fall in the mesoporous range, which facilitates capillary condensation of vapor inside the silica. The specific surface area, pore volume and average pore diameter of these two types of silica beads are listed in Table 5-1. It is shown that silica gel RD has larger surface area

and pore volume than the other one, while the average pore diameter of the two types are nearly the same.

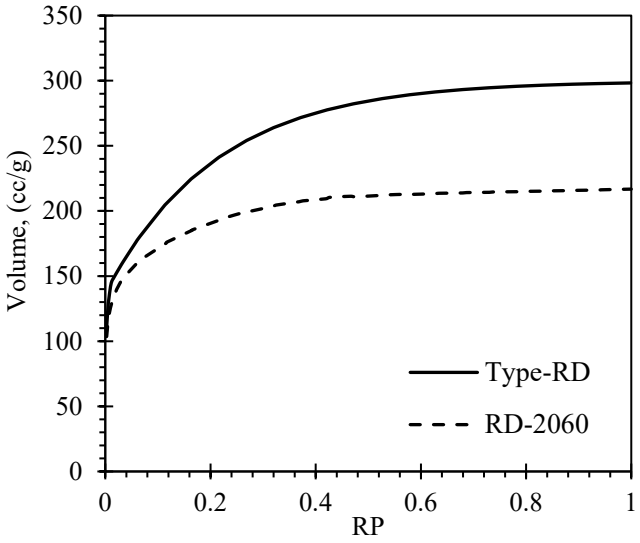

Figure 5-3 N_2 uptake by two types of porous silica-gel beads

Table 5-1 The physical properties of type-RD and RD-2060 silica-gel beads.

Silica-gel	RD	RD-2060
Surface area (m^2/g)	827.5	686.3
Pore volume (cc/g)	0.462	0.335
Pore diameter (nm)	3.24	3.19

Figure 5-4 shows the statistical result of particle size distribution of the two types of porous silica beads. Silica beads are well dispersed in a petri dish with a diameter of 3 cm for the optical images. A MATLAB program is used to distinguish the contour of the beads from the background based on the contrast difference as shown in Fig. 5-4A and 5-4B. The diameter (or equivalent diameter in type RD-2060) of each bead is calculated by the program and the statistical results are shown in Fig. 5-4C and 5-4D. For type RD silica beads, the most probable diameter falls in the range of 0.80~0.89 mm, while that of RD-2060 silica beads is 0.50~0.59 mm. Compared to RD-2060, RD has a wider distribution (from 0.7 to 2.0 mm), which leads to a higher level of

heterogeneity. The average diameters are 0.835 and 0.540 mm for RD and RD-2060 silica beads, respectively.

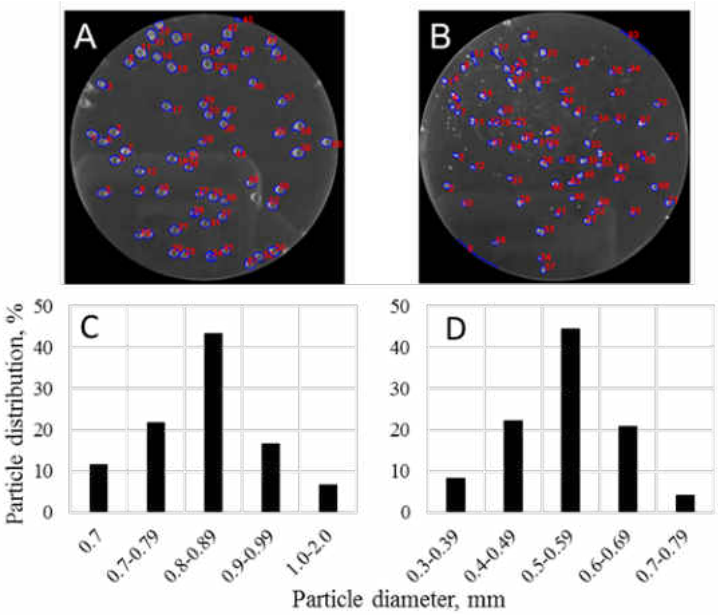

Figure 5-4 Optical images of (A) type-RD and (B) RD-2060 porous silica beads with computer-aided statistical analysis; particle size distribution of (C) RD and (D) RD-2060 porous silica beads.

5.3.2 Testing procedure of adsorption isotherm and kinetics

The following steps describe the testing procedure in detail, including preparation, desorption, and adsorption.

1. The evaporator/condenser is filled with water and thermal bath 1 is set at specific temperature and then the vacuum pump is run until equilibrium condition is reached.
2. The sample of the adsorbent is placed on the heat exchanger and its temperature is controlled by the thermal bath 2 or 3.
3. Small known dead loads are placed on the load cell and the load cell response is monitored to ensure that the flow through the flexible tubes does not affect the load cell response and the accuracy is still less than 1%.

4. The sample is heated and the measuring chamber is evacuated by the vacuum pump to reach a relative pressure less than 10^{-4}. The sample is assumed to be completely dry when the load cell response becomes constant for 2 hr, then the degassed dry sample is weighed.
5. The sample is cooled down to the desired adsorption temperature and then the two chambers are connected to start the adsorption process.
6. During the adsorption, the sample temperatures and the load cell response are monitored over time. The adsorption process is assumed to be completed when the uniform sample temperature is achieved and equals the inlet water temperature.

The adsorption isotherms of Fuji silica-gel RD and RD-2060 are measured by following the above procedure. Silica-gel RD and RD-2060 are in granular form and have particle size ranges of 1.0-2.0 mm and 0.18-1.0 mm, respectively. Each test is run more than once to check the repeatability of the experimental set-up and the repeated measurements for the same operating conditions vary by no more than ±4%.

5.4 Results and Discussion

5.4.1 Adsorption equilibrium

The equilibrium uptakes of water vapor onto silica-gel RD-2060 and Type-RD at different pressure and temperature range from 20°C to 60°C are presented in Fig. 5-5 and Fig. 5-6, respectively. The measured uptakes of RD-2060 show a good agreement with the previous available experimental measurements [122]. The present measurements indicate that the maximum uptakes of silica-gel RD-2060 and Type-RD are about 0.38 kg/kg and 0.48 kg/kg, respectively. The isosteric heat of adsorption of Fuji silica-gel Type-RD is calculated by plotting Clausius-Clapeyron equation (Eq. 21) as illustrated in Fig. 5-7. The slope of the lines represents ($-\Delta H$). The

plot is also repeated for Fuji silica-gel RD 2060. The results show that the heats of adsorption for silica-gel RD-2060 and Type-RD are nearly the same and have a value of 2415 kJ/kg with a deviation ranging from 0.65% to 10.56% from published data as shown in Table 5-2.

$$\left.\frac{\partial \ln P_v}{d(T_S)}\right|_x = -\frac{\Delta H}{RT_S^2} \Rightarrow \ln(P_v) = constant - \frac{\Delta H}{RT_S} \qquad (21)$$

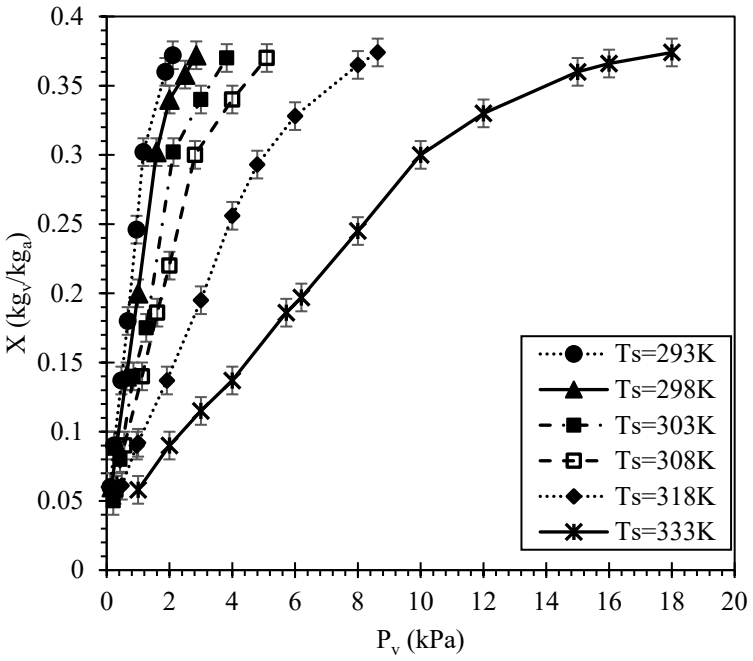

Figure 5-5 Equilibrium uptake of RD-2060 at different pressures and temperatures

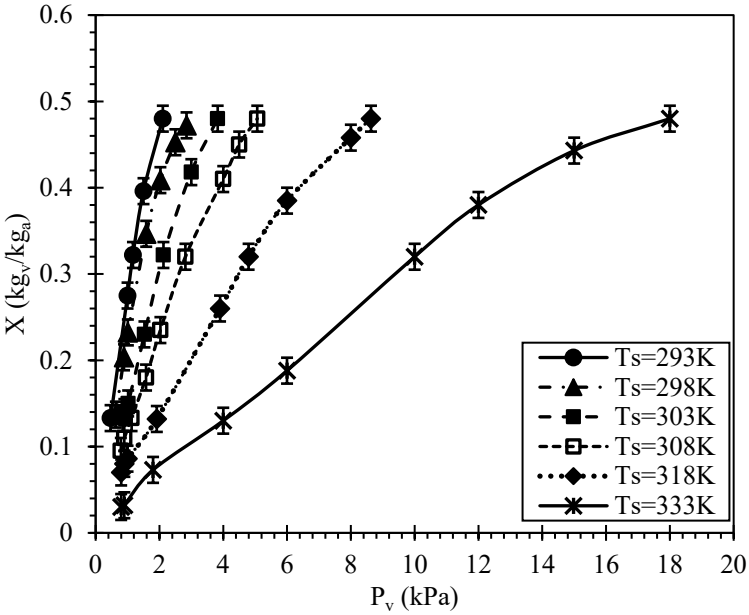

Figure 5-6 Equilibrium uptake of Type-RD at different pressures and temperatures

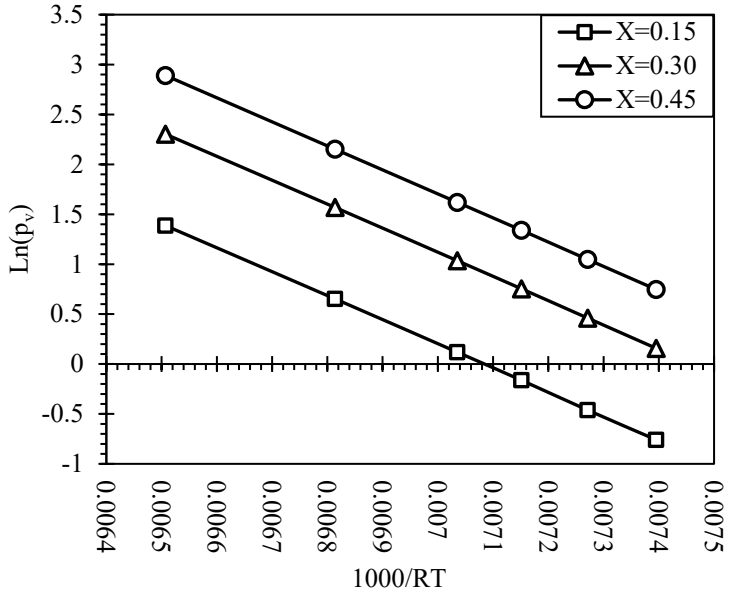

Figure 5-7 Isosteres of Type-RD silica-gel/water

Table 5-2 Isosteric heat of adsorption of Fuji RD silica-gels

Reference	ΔH (kJ kg^{-1})	Deviation (%)
[122]	2430	0.62
[48, 123]	2510	0.96
[28, 72, 124]	2693	10.32
[4]	2700	10.56

5.4.2 Data analysis and regression

By plotting equilibrium uptake (X) versus relative pressure, the water adsorption isotherms of these two types of Fuji silica-gel could be classified as Type IV [53] as shown in Fig. 5-8 and 5-9. The experimental measurements show good agreement with the data provided by the manufacturer. Although the maximum uptakes of Type-RD and RD-2060 silica gels are not the same, both of them have similar equilibrium uptake from a relative pressure of 0.05 till 0.5. Because the relative pressure of the adsorption cooling cycles normally varies from 0.05 to 0.3 [53, 125], both adsorbents are expected to have the nearly the same change in the uptake under the same operating conditions, but the silica-gel RD-2060 is recommended as it has a smaller particle diameter which enhances the diffusion process during the adsorption process and hence increases performance.

The measured isotherm curves show an inflection point at relative pressure (RP) ≈ 0.4 and 0.35 for silica-gel RD and RD-2060, respectively. This is attributed to the fact that the region of the water adsorption isotherm where the relative pressure is more than 0.4 (RP>0.4) is typically dominated by capillary condensation. Despite the limited validity of the corrected Kelvin equation for microporous materials, it is commonly used to describe the apparent capillary condensation regime, and is written as [6, 125]:

$$\frac{P_v}{P_s} = \exp\left(-\frac{2\sigma V_L \cos(\beta)}{(r_p - t_m) R T_s}\right) \qquad (22)$$

where r_p is the pore radius, R is the universal gas constant, and T_s is the adsorbent temperature, σ is the surface tension of water, V_L the molar volume of water, β is the contact angle of water on the silica-gel pore walls. The parameter t_m is the statistical thickness of the adsorbed water layer

and is calculated by dividing the volume of water adsorbed prior to the capillary condensation by the surface area of the adsorbent [125].

Here, the properties of water at 30ºC are used for the calculation. Based on this equation and the adsorbent properties, the contact angle is found to of 44º and 36º for silica-gel Type-RD and RD-2060, respectively. Interestingly, the contact angle of silica-gel Type-RD deviates by 1º from the previous reported data [126, 127]

As shown in Figs. 5-8 and 5-9, it is clear that by setting the characteristic energy E as a function of relative pressure, the D-A model can be used to fit the experimental measurements accurately over all the entire adsorption relative pressure range. The dependence of E on the relative pressure can be attributed to the fact that E represents the affinity of the adsorbent surface for the adsorbate. During the adsorption process, the surface changes from partially dry to multilayer condition. Partially dry surface has a higher affinity for vapor molecules than a surface covered with an adsorbate layer. In other words, E should decrease as the relative pressure increases. With the correlation of E=f(RP) as shown in Table 5-3, the D-A model can fit the experimental measurements appropriately for the entire range of relative pressure with a standard deviation of 0.006.

Also, it is found that the D-A model with constant values of n and E cannot fit the experimental uptakes accurately for the entire range of relative pressure. Furthermore, the experimental measurements are also fitted using the Tòth model and plotted in Fig. 5-8 and 5-9. The coefficients of this model are presented in Table 5-3 with standard deviation of 0.017. It is clear that the Tòth model does not predict the uptake correctly at relative pressure less than 0.15. Although it predicts the equilibrium uptakes accurately when the relative pressure is more than 0.15, it cannot be used to simulate the performance of adsorption chillers because the relative

pressure at the beginning of adsorption is about 0.05. Therefore, the specific cooling power estimated by Tòth equation can be 13% higher than the accurate one.

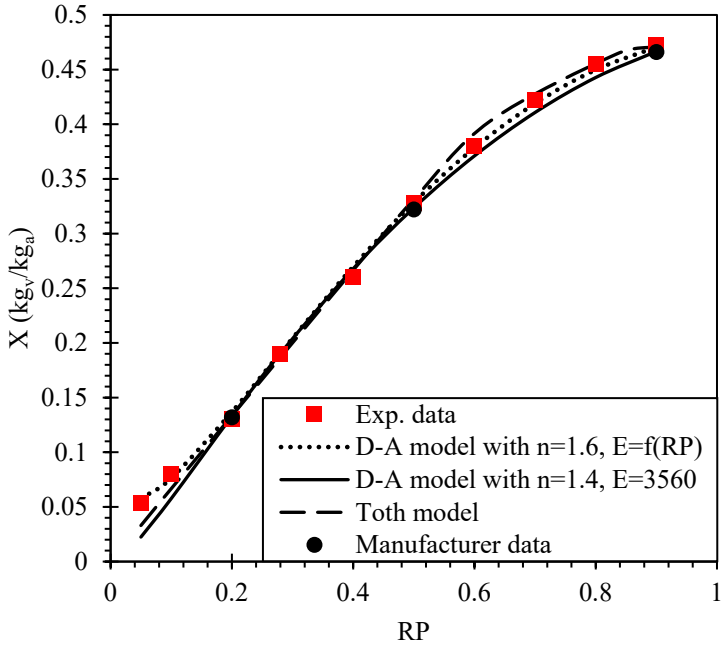

Figure 5-8 Data fitting of the experimental water sorption isotherm of silica-gel Type-RD

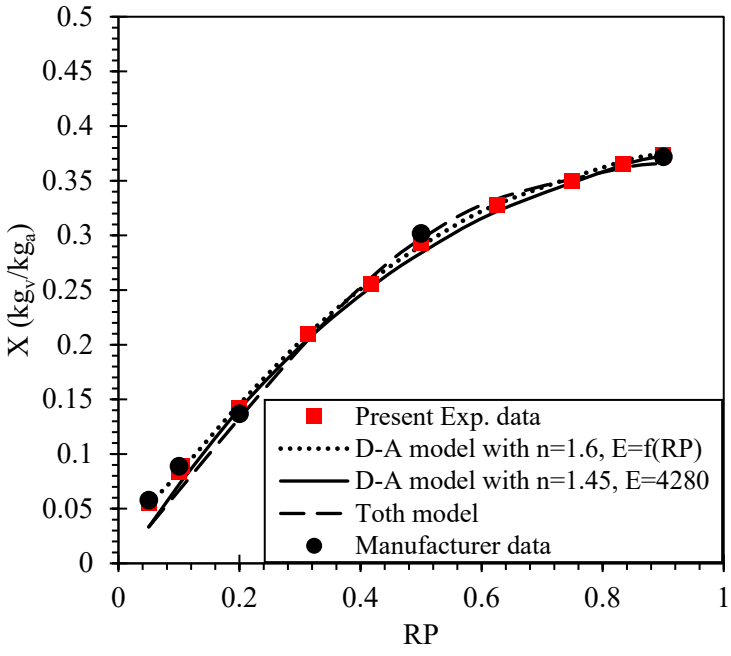

Figure 5-9 Data fitting of the experimental water sorption isotherm of silica-gel RD-2060

Table 5-3 Coefficients of D-A and Tòth model for the tested silica-gels

Silica gel type	Tòth model				D-A model		
	X_o (kg/kg)	t	ΔH (kJ/kg)	b_o	X_o (kg/kg)	n	E (J/mol)
Type-RD	0.48	8	2415	$5x10^{-9}$	0.48	1.6	$3030 + 192\ RP^{\frac{-1}{1.3}}$
RD-2060	0.38	4	2415	$5x10^{-9}$	0.38	1.6	$3980 + 103\ RP^{\frac{-1}{1.2}}$

By using a simple relationship between the saturation pressure and temperature of water ($T=191.054\times P^{0.0554}$) [5], the characteristic energy can be set as a function of (T_v/T_s) instead of (P_v/P_s) as shown in Eq. 23 and 24 and then Eq. 17 can be used to calculate the equilibrium uptakes.

$$Type - RD \Rightarrow E = 3030 + 192\left(\frac{T_v}{T_s}\right)^{-13.89} \quad \text{(J/mol)} \qquad (23)$$

$$RD - 2060 \Rightarrow E = 3980 + 103\left(\frac{T_v}{T_s}\right)^{-15.04} \quad \text{(J/mol)} \qquad (24)$$

So, it is recommended for the designers of the silica-gel/water adsorption cooling systems to use the D-A model with a variable characteristic energy E to determine the equilibrium uptake over the entire relative pressure range. This approach needs X_o, n, and the coefficients for the correlation of E. By fixing the value of n to be 1.6 and choosing X_o to be the maximum uptake, the coefficients for E can be determined by fitting the limited manufacturer data.

5.4.3 Adsorption kinetics

The adsorption kinetics characterizes the degree of saturation. Linear driving force (LDF) (Eq. 25) for vapor adsorption kinetics is successfully used to fit the experimental adsorption rate with standard deviation of 0.012 as shown in Fig. 5-10.

$$\frac{dX}{dt} = \frac{60D_s}{d_e^2}(X_o - X) = k_m(X_o - X) \rightarrow \frac{X(t)}{X_o} = 1 - \exp(-k_m t) \qquad (25)$$

where d_e is the effective diameter of the tested sample and D_s is the surface diffusivity that can be calculated from Eq. 20.

During the adsorption period, the silica gel sample temperature is nearly isothermal. The difference between the maximum and minimum temperature of the silica gel at all times is found to be less than 2°C for all tested cases. This small difference in temperature is due to using a small thickness ($< 7\ mm$) of the adsorbent. Accordingly, uniform temperature within the sample during the adsorption test is assumed and the average sample temperature is used to represent the sample temperature. The average effective diameter is calculated based on the exact solution of the diffusion equation (Fick's law). The exact solution of vapor diffusion onto porous particle of diameter d_p is [6]:

$$\frac{m_v(t)}{m_o} = A\sqrt{t}\,, \quad for\ \frac{m_v(t)}{m_o} < 0.3 \qquad where\ A^2 = \frac{144 D_s}{\pi d_p^2} \tag{26}$$

where m_v is the mass adsorbed at certain time t, m_o is the maximum mass adsorbed at $t \to \infty$.

The uptake of a sample with different particles sizes after specific time could be calculated as:

$$m_{v1} + m_{v2} + m_{v3} + \cdots = m_{o1}A_1\sqrt{t} + m_{o2}A_2\sqrt{t} + m_{o3}A_3\sqrt{t} + \cdots = m_o A\sqrt{t} \tag{27}$$

Then

$$\frac{m_{o1}A_1}{m_o} + \frac{m_{o2}A_2}{m_o} + \frac{m_{o3}A_3}{m_o} + \cdots = A \qquad where\ \ m_{o1} = X_{o1}m_{s1} \tag{28}$$

where $m_o A\sqrt{t}$ is the total mass adsorbed, m_{o1} is the maximum mas adsorbed by particles of diameter d_{p1} whose mass is m_{s1}.

As the sample has the same adsorbent, $X_{o1} = X_{o2} = X_{o3} = X_o$ and Eq. 28 can be rewritten as:

$$\frac{m_{s1}A_1}{m_s} + \frac{m_{s2}A_2}{m_s} + \frac{m_{s3}A_3}{m_s} + \cdots = A \rightarrow \frac{y_1}{d_{p1}^2} + \frac{y_2}{d_{p2}^2} + \frac{y_3}{d_{p3}^2} + \cdots = \frac{1}{d_e^2} = \sum_{i=1}^{n} \frac{y_i}{d_{pi}^2} \quad (29)$$

where y_i is the mass fraction of the particles of diameter d_{pi}.

Accordingly, the effective particle size can be calculated based on the particle size distribution of the tested sample.

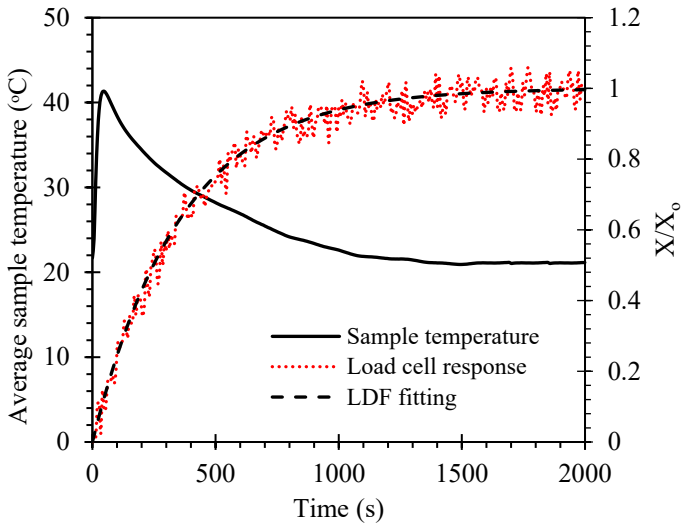

Figure 5-10 Load cell response and silica gel RD temperature during adsorption process

Figure 5-11 presents the procedure of calculating the activation energy (E_a) and pre-exponential factor (D_{so}) using the measured instantaneous adsorption uptake and the average adsorbent temperature. First, initial values for the activation energy and pre-exponential factor are assumed. Based on the instantaneous average temperature of the sample during the adsorption, the surface diffusivity is calculated using Eq. 20, then the instantaneous uptake is estimated from Eq. 25. According to the difference between the estimated uptake and the measured one, the values of the activation energy and pre-exponential factor are modified to keep this difference is less than

0.001 kg/kg. Adsorption rates of the two types of silica-gel are measured at different operating pressures (1.0-20.0 kPa) and adsorbent temperatures (10-70^{o}C). Multiple samples of silica-gel with different particles sizes are tested (see Table 5-5). It is found that the calculated activation energy at different adsorption conditions varies from 40 to 41.2 kJ/mol and the pre-exponential factor from 2.5×10^{-4} to 2.8×10^{-4} m^2/s. These values deviate from the published data by less than 4.5% [128-130]. It is worth to mention that using either the maximum or minimum temperature of the sample instead of the average sample temperature to calculate the surface diffusivity changes the calculated activation energy by less 0.3%.

Figure 12 and 13 depict the measured adsorption rate and the predicted one based on the calculated surface diffusivity using the new approach. It is evident from these figures that this proposed approach shows a good agreement between the measured and predicted adsorption rate despite of the particle size distribution. This good agreement is established for all tested samples shown in Table 5-5. Although Eq. 26 is valid only for uploading ratio (X/X_o) less than 0.3, the calculated effective particle size of the sample still provides reasonable results of the surface diffusivity. It is worth to mention that this approach is valid as long as the time response of the load cell and thermocouple is comparable because both the instantaneous temperature measurements and load cell response are used to calculate the surface diffusivity. Also, the thickness of the sample should be less than 5 mm, which is comparable to the thickness of adsorbent layer in real adsorption bed, to be able to achieve uniform temperature distribution within the tested sample. As a result, this proposed approach is applicable in measuring the surface diffusivity in nanoporous adsorbents under operating conditions like those in the real adsorption cooling systems.

Table 5-4 Tested silica-gels samples

Silica gel type	Fuji RD-2060	Fuji Type-RD
Particles sizes (mm)	0.3-0.49	0.7-2.0
	0.5-0.79	
	0.3-0.79	

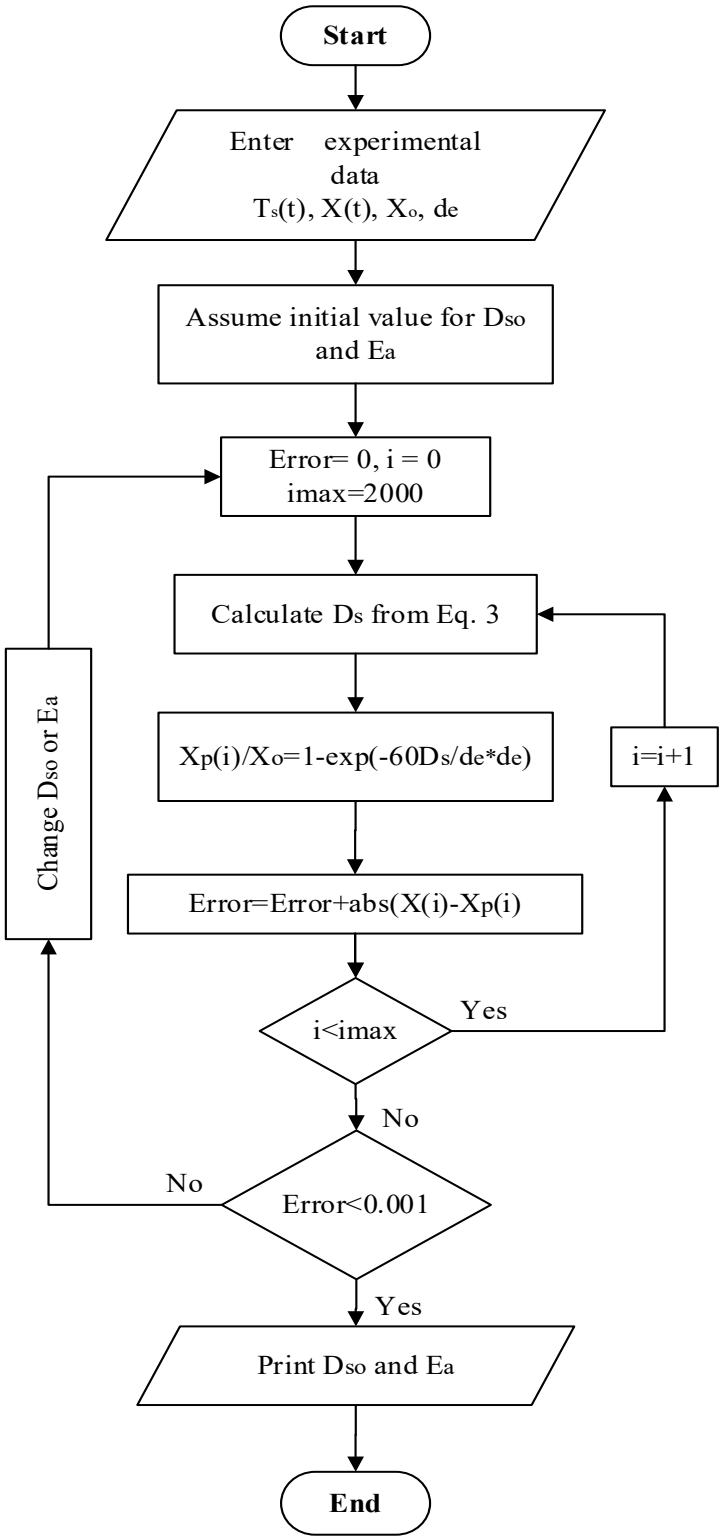

Figure 5-11 Procedure of calculating the activation energy and pre-exponential factor

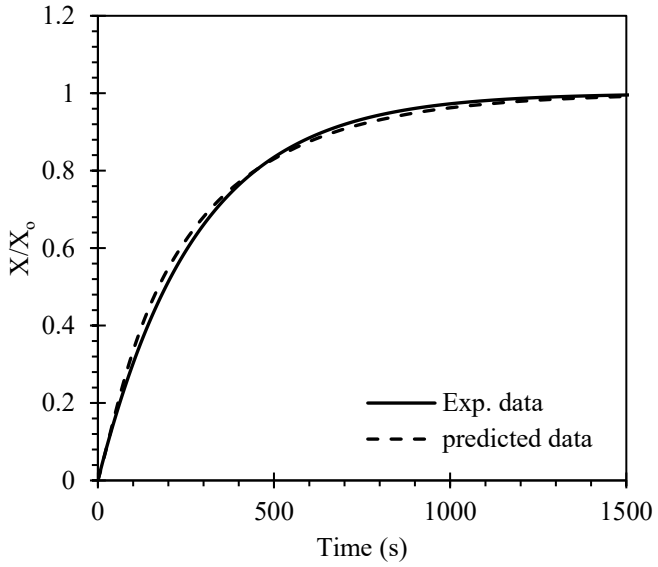

Figure 5-12 Experimental and predicted adsorption rates for 5 g silica-gel RD-2060 with particles sizes of 0.3-0.79 mm

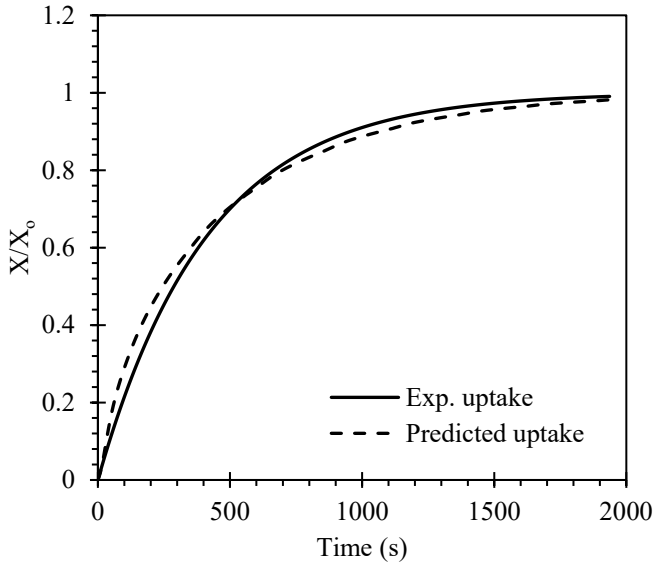

Figure 5-13 Experimental and predicted adsorption rates for 20 g silica-gel RD with particles sizes of 0.7-2.0 mm

5.5 Conclusions

Due to the limited availability of experimental measurements, a simple but accurate experimental setup is designed and constructed to measure the equilibrium uptake of any working pairs at any operating conditions. Apparent capillary condensation is observed at a relative

pressure of 0.4 and 0.35 for silica-gel RD and RD-2060, respectively. The estimated contact angles based on the corrected Kelvin equation are 44^{o} and 36^{o} for silica-gel Type-RD and RD-2060, respectively. To be able to successfully fit the adsorption isotherms for the entire relative pressure, the characteristic energy in the D-A model is proposed to be a function of the relative pressure instead of a constant value. The characteristic energy decreases as the relative pressure increases, because the attraction force (surface effect) decreases as the thickness of the adsorbed phase increases.

A new approach for calculating the surface diffusivity which allows the sample temperature to be time dependent is proposed to overcome the limitations and complexities of the other methodologies. The key advantage of this approach, beside its simplicity, is the possibility of measuring the surface diffusivity under the real operating conditions of adsorption cooling cycles. This proposed methodology is validated by comparing the calculated surface diffusivity of water vapor onto silica-gels with the published data, and good agreement is established. The calculated activation energy at different adsorption conditions varies from 40.0 to 41.2 kJ/mol and the pre-exponential factor varies from 2.5×10^{-4} to 2.8×10^{-4} m^2/s.

CHAPTER 6 ASSESSMENT OF THE NUMERICAL MODELS

6.1 Introduction

A significant amount of efforts has been carried out to evaluate the Specific Cooling Power (SCP) of adsorption cooling systems using either a Lumped Parameter (LP) model or a Coupled Heat and Mass Transfer (CHMT) model. However, there are no comprehensive studies comparing the results from the two models and assessing their validity and accuracy in predicting the performance of adsorption cooling units. In this study, the experimental test rig is used to study the thermal response and adsorption kinetics of a lab-scale silica gel packed bed. The test rig is then used to estimate the bed performance under various operating conditions. A detailed coupled heat and mass transfer (CHMT) model and a lumped parameter (LP) model are implemented to evaluate the performance of an adsorption cooling system using silica gel/water as the working pair. Experimental measurements from the lab-scale adsorption bed are used to validate the numerical models. The SCP estimated from the experimental measurements is compared with that from the CHMT model at various evaporation temperatures, mass flow rate of the chilled water and cycle times. This allows one to identify the optimal cycle time and address the deviation between the experimental measurements and numerical results from the CHMT model. A modified version of CHMT model is proposed to reduce this deviation and provide a more accurate value for the SCP of the adsorption bed. In addition, the LP model is implemented to investigate the performance of the adsorption cooling system at various evaporator sizes, evaporation temperatures, adsorbent particle sizes and chilled water mass flow rates. This allows a critical investigation of the validity and accuracy of LP model for estimating the actual SCP of practical adsorption cooling systems. Moreover, this study points out the importance of designing an

effective evaporator to provide maximum cooling power from the adsorption cooling system. The results of this study have been published in International Journal of Refrigeration[**].

6.2 Experimental Work

6.2.1 Measurements procedure

An amount of silica gel is placed on the heat exchanger, as shown in Fig. 6-1, and its temperature is controlled by the thermal bath 2 or 3. After placing the adsorber bed on the load cell, a standard procedure is followed to measure the performance of the bed. The system is evacuating by using a vacuum pump. While the two vessels are disconnected, distilled water is added into the evaporator/condenser chamber and its temperature is adjusted to the desired evaporation temperature (T_e) using the thermal bath (TB1). At the same time, the adsorber bed in the measuring chamber is heated to the desorption temperature (T_d=80°C) by using hot water from the thermal bath (TB3). The measuring chamber is then evacuated by using a vacuum pump to reach the condenser pressure (4.5 kPa). After reaching equilibrium condition, cooling water from a thermal bath (TB2) is used to cool the bed to the initial adsorption temperature (T_i) which is uniquely determined by the operating conditions and the adsorption isotherm of the working pair. As soon as the pressure and temperature of the bed reach the evaporator pressure and the initial temperature (T_i), respectively, the valve (V3) is opened to feed the bed with vapor. During the adsorption period, the bed is cooled down and the increase in the adsorbent weight is measured using the load cell. Recording the load cell response directly gives the amount of water adsorbed (i.e., the change in uptake). At the same time, the chilled water inlet and outlet temperatures are recorded for estimating the evaporator capacity and the specific cooling power (SCP). Also, these

[**] R. H. Mohammed, O. Mesalhy, M. L. Elsayed, L. C. Chow, Assessment of numerical models in the evaluation of adsorption cooling system performance, International Journal of Refrigeration 99, 166-175, 2019.

temperatures are used to estimate the overall heat transfer coefficient of the evaporator, that is used as an input parameter for numerical simulation described later in the paper.

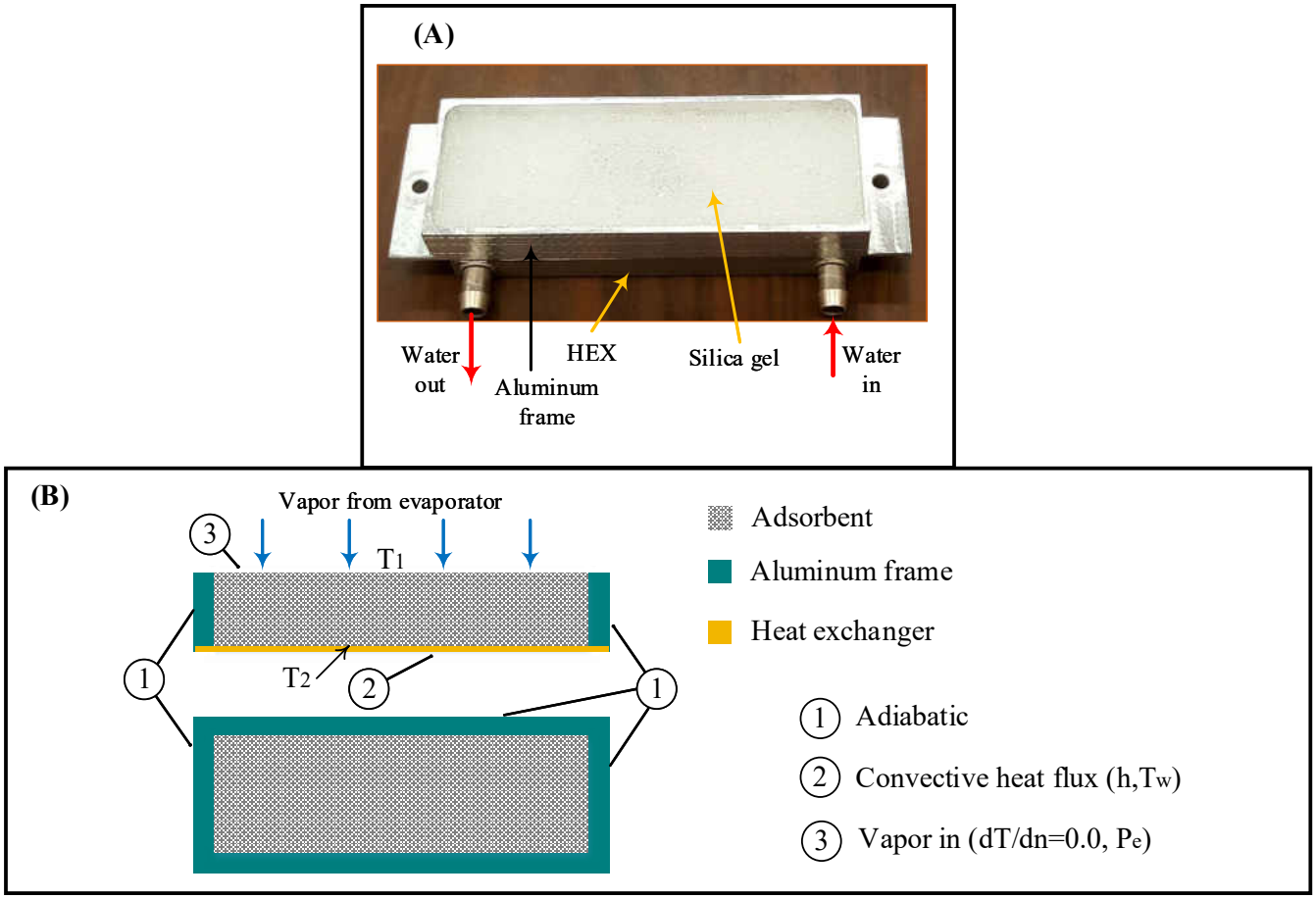

Figure 6-1 Schematic diagram of (A) experimental test rig, (B) pictorial view of the tested bed, and (C) computational domain

6.3 Numerical Modeling

6.3.1 Coupled heat and mass transfer (CHMT) model

Heat and mass transfer inside a silica gel packed bed shown in Fig. 6-1 is studied using a transient three-dimensional local thermal non-equilibrium (LTNE) model. The LTNE was discussed in details elsewhere [5]. The Darcy's equation and LDF model are solved simultaneously

to account for the inter-particle permeation resistance and intra-particle mass diffusion resistance, respectively.

$$\vec{U} = -\frac{K}{\mu}\nabla P \qquad (30)$$

where μ is the vapor dynamic viscosity and K is the bed permeability and is calculated as:

$$K = \frac{d_p^2 \varepsilon_b^3}{150(1-\varepsilon_b)^2} \qquad (31)$$

$$\frac{\partial X}{\partial t} = \frac{60 D_s}{d_p^2}(X_o - X) \qquad (32)$$

where D_s and X_o are the surface diffusivity and equilibrium uptake, respectively which are estimated from the following equations [41, 131]:

$$D_s = D_{so}\, exp\left(-\frac{E_a}{RT_s}\right) \qquad (33)$$

$$X_o = X_\infty\, exp\left(-\left(\frac{RT_s}{E} ln\left(\frac{P_s}{P}\right)\right)^n\right) \qquad (34)$$

where P_s is the saturation pressure at the solid (i.e., adsorbent) temperature T_s and is calculated as [5]:

$$P_s = 8.143 \times 10^{10} \exp\left(-\frac{5071.7}{T_s}\right) \qquad (35)$$

The mass conservation equation for the adsorbate gas is written as [132, 133]:

$$\varepsilon_b \frac{\partial \rho_v}{\partial t} + \nabla.\left(\rho_v \vec{U}\right) + \rho_b \frac{\partial X}{\partial t} = 0 \qquad (36)$$

Two different energy conservation equations are used to calculate the temperature field of the gas and solid phases.

- The energy equation for the porous solid phase can be expressed as [45]:

$$\rho_b\left[C_{ps} + X C_{pw}\right]\frac{\partial T_s}{\partial t} = \nabla.(k_b \nabla T_s) + \rho_b H_a \frac{\partial X}{\partial t} + q_{sf}(T_f - T_s) \qquad (37)$$

- The energy equation for the vapor phase can be written as:

$$\varepsilon_b \rho_f C_{pf}\frac{\partial T_f}{\partial t} + \rho_f C_{pf}\vec{U}.\nabla T = \nabla.\left(k_f \nabla T_f\right) + \rho_b C_{pf}\frac{\partial X}{\partial t}\left(T_f - T_s\right) - q_{sf}(T_f - T_s) \qquad (38)$$

- The energy equation for the aluminum frame is written as [112, 113, 134]:

$$\frac{\partial T_{AL}}{\partial t} = \alpha_{AL}\nabla^2 T_{AL} \quad (39)$$

where $q_{sf} = a_{sv}h_{sf}$ represents the heat transfer exchange between the vapor and solid phase, a_{sv} gas-solid interface area per unit volume which is defined as $a_{sv} = \frac{6(1-\varepsilon_t)}{d_p}$ and the interfacial heat transfer coefficient h_{sf} is estimated as [135]:

$$Re = \frac{\rho U d_p}{\mu} \quad (40)$$

$$Nu = 2.0 + 1.1Pr^{0.33}Re^{0.6} \quad (41)$$

$$\frac{1}{h_{sf}} = \frac{d_p}{k_f Nu} + \frac{d_p}{10k_f} \quad (42)$$

SCP produced by an adsorption bed, based on CHMT model, can be calculated as [5]:

$$SCP_{CHMT} = \frac{h_{fg}\times(X_{max}-X_{min})}{t_c} = \frac{h_{fg}\times\Delta X}{t_c} \quad (43)$$

where t_c is the cycle time, h_{fg} is the latent heat of vaporization at the evaporator pressure and ΔX is the bed capacity.

The overall heat transfer coefficient of adsorption bed depends on the porosity of the adsorbent material, thermal conductivity of the adsorbent and the thickness of the adsorbent layer. These parameters directly affect the thermal response and adsorption rate of the adsorption bed during the adsorption process. The CHMT model provides the instantaneous temperatures of the adsorbent layer that can be used to estimate the overall heat transfer coefficient of the bed which is needed for the LP model as follows:

$$UA_b = \frac{hA_s(T_2-T_w)}{T_1-T_2} \quad (44)$$

where A_s is the surface area exposed to cooling fluid, T_1 is the average temperature of the adsorbent surface exposed to vapor from evaporator and T_2 is the average temperature of the surface exposed to cooling fluid as shown in Fig. 6-1B.

The boundary conditions are shown in Fig. 1C. Constant pressure is assumed at the surface exposed to vapor from the evaporator. The thermo-physical properties of the silica-gel/water working pair and the simulation parameters required for the CHMT model are given in Table 6-1. The CHMT model is built in COMSOL Multiphysics 5.2 and solved numerically using finite element technique with a relative tolerance of 10^{-5}.

Table 6-1 Input parameters and operating conditions for CHMT model [41]

Parameter	Value	Unit
d_p	0.35	mm
E_a	42,000	$J/(mol.K)$
E	4,280	J/mol
n	1.15	--
X_∞	0.37	kg_v/kg_a
D_{so}	2.54×10^{-4}	m^2/s
k_b	0.198	$W/m.K$
k_f	0.024	$W/m.K$
ρ_b	740	kg/m^3
H_a	2415	kJ/kg
h	600	$W/m^2.K$
T_e	10	°C
T_w	30	°C
T_d	80	°C
T_i	58	°C
C_{ps}	924	$J/kg.K$
ε_b	0.37	--
ε_t	0.65	--

6.3.2 Lumped parameter (LP) model

The lumped parameter (LP) model used in this study is built based on the principle of energy and mass balances across the evaporator and adsorption bed. The assumptions used to develop this model are as follows:

- The lumped method is considered for the adsorber bed and evaporator. Hence, the temperature and pressure variation within these components are neglected.
- The vapor adsorbed by the adsorbent is assumed to behave like a liquid. Therefore, it has the same thermodynamic properties of its liquid phase.
- Cold water temperature is assumed to be constant.
- Pressure drops in vapor flow circuit are neglected.

Dynamic study of an adsorption system requires modeling the adsorption kinetics, mass balance, and energy balance across each component. The energy balance in the evaporator and adsorber bed is described using the lumped approach. The evaporator interacts with the adsorber bed, and the energy balance equations for the evaporator and bed are written as [28]:

$$\left(MC_p\right)_e \frac{dT_e}{dt} = -M_{sg}\left(\frac{dX}{dt}\right) h_{fg,T_e} - \dot{m_{ch}} C_{pw}\left(T_{ch,o} - T_{ch,i}\right) \quad (45)$$

$$\left(\left(MC_p\right)_b + \left(XM_{sg}C_{pw}\right)\right)\frac{dT_b}{dt} = M_{sg}\left(\frac{dX}{dt}\right) H_a - \dot{m_{cw}} C_{pw}\left(T_{cw,o} - T_{cw,i}\right) \quad (46)$$

The LHS in the above equations represents the sensible energy change of the evaporator and adsorber bed. $\left(MC_p\right)_b$ is the heat capacity of the bed and equals to $\left[\left(MC_p\right)_{sg} + \left(MC_p\right)_{AL}\right]$. The term $M_{sg}\left(\frac{dX}{dt}\right) h_{fg,T_e}$ represents the latent heat of vaporization, while the term $M_{sg}\left(\frac{dX}{dt}\right) H_a$ represents the heat of adsorption that is released during the adsorption process. The last terms in the RHS represent the heat transferred to water.

The outlet temperatures of the cooling water of the bed or chilled water are estimated using the Log Mean Temperature Difference (LMTD) method as [129]:

$$T_{cw,o/ch,o} = T_{b/e} + \left(T_{cw,i/ch,i} - T_{b/e}\right) \exp\left(-\frac{(UA)_{b/e}}{\dot{m_{cw,ch}} C_{pw}}\right) \quad (47)$$

During the experimental measurements, the outlet and inlet temperatures of cooling water of the bed and chilled water of the evaporator are recorded and used to calculate the value of the overall heat transfer coefficient of the bed and evaporator, respectively. These values are used as input parameters for the numerical model.

The evaporator capacity is calculated by monitoring the inlet and outlet temperatures of the chilled water during the adsorption period. The specific cooling power (SCP) is then estimated based on the evaporator capacity as follows [28, 129]:

$$\dot{Q}_e = \frac{1}{t}\int_0^{t_c} \dot{m}_{ch} C_{p,w}\left(T_{ch,o} - T_{ch,i}\right)dt \quad (48)$$

$$SCP_{LP} = \frac{\dot{Q}_e}{M_{sg}} \quad (49)$$

The equations above for the LP model are solved using MATLAB 2015 while the water thermodynamics properties are obtained using REFPROP. The characteristics of the adsorption cooling system and the input parameters for the LP model are given in Table 6-2.

Table 6-2 LP model input parameters

Parameter	C_{pw}	$(MC_p)_e$	$(MC_p)_{AL}$	M_{sg}	$\dot{m}_{ch}$	$\dot{m}_{cw}$	$T_{ch,i}$	$T_{cw,i}$	UA_b	UA_e
Value	4190	14.4	0.045	20	0.7	0.7	10	30	0.38	500
Unit	$J/kg.K$	kJ/K	kJ/K	g	LPM	LPM	°C	°C	W/K	W/K

6.4 Validation of Numerical Models

For the CHMT model, a mesh independence study is carried out using various mesh sizes and time steps. A mesh size of 240×14×80 elements and a time step of 0.5 sec are found to be enough to capture the flow and temperature fields with sufficient accuracy.

The lab-scale adsorption bed is operated at an evaporator pressure of 1.23 kPa, condenser pressure of 4.5 kPa and regeneration (desorption) temperature of 80°C. The load cell response, chilled water inlet and outlet temperature, bed temperatures at different locations and pressure transducers are the main measurements monitored during the adsorption process. Experimental measurements are compared with numerical results obtained from CHMT model and LP model and presented in Figs. 6-2 and 6-3. There is a marginal deviation between the numerical results and experimental measurements of the average bed temperature and uptake profiles. The maximum difference between experimental measurements and simulation outcomes at the end of the adsorption process is 2.5% (1.0°C) in the bed temperature and 2.3% in the uptake. However, it can be seen that the CHMT model overestimates the bed uptake at the beginning of the adsorption process because it does not consider the evaporator pressure drop. These good agreements validate the present simulation to compare between both CHMT and LP models in investigating the performance of the adsorption cooling system.

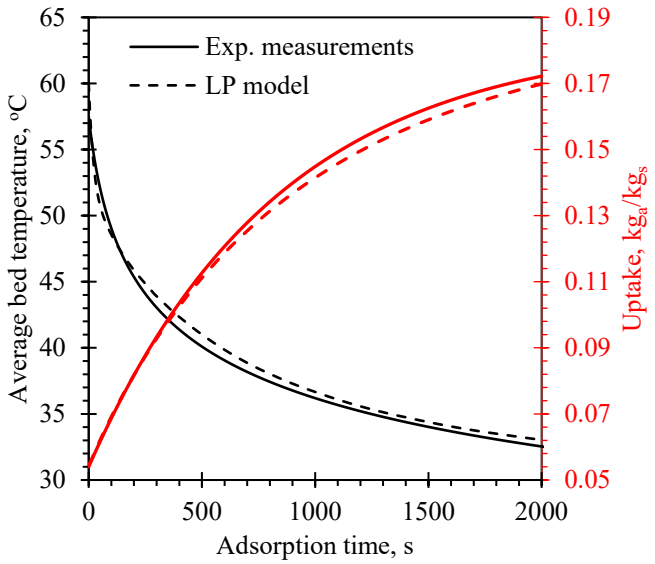

Figure 6-2 Comparison of temperature and uptake profiles obtained from experiments and LP model

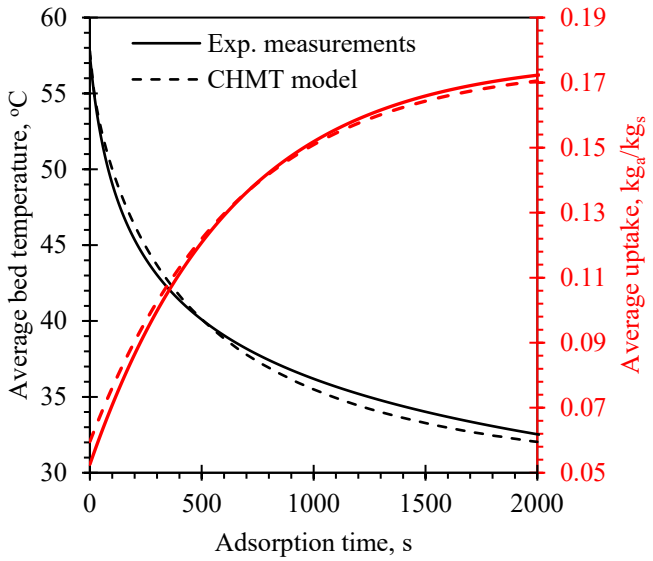

Figure 6-3 Comparison of temperature and uptake profiles obtained from experiments and CHMT model

6.5 Results and Discussion

6.5.1 CHMT model

The CHMT model is widely used to design an adsorption bed and estimate the SCP. The performance of the adsorption bed is evaluated experimentally and numerically using the CHMT model. Figure 6-4 depicts the variation in the SCP of the tested adsorption bed using the experimental measurements and the CHMT model at various evaporation temperatures and cycle times. The experimental results show that the optimal cycle time is about 1200 s, while SCP_{CHMT} continuously declines with increasing the cycle time. It is evident from the figure that there is a noticeable difference between the SCP obtained from CHMT model and the actual one calculated from the experimental measurements. This difference is large at shorter cycle times and continuously declines with increasing the cycle time as presented in Fig. 6-5. Also, this difference does not depend on the evaporator temperature, and this implies that the dynamic behavior of the evaporator is the same regardless of its temperature.

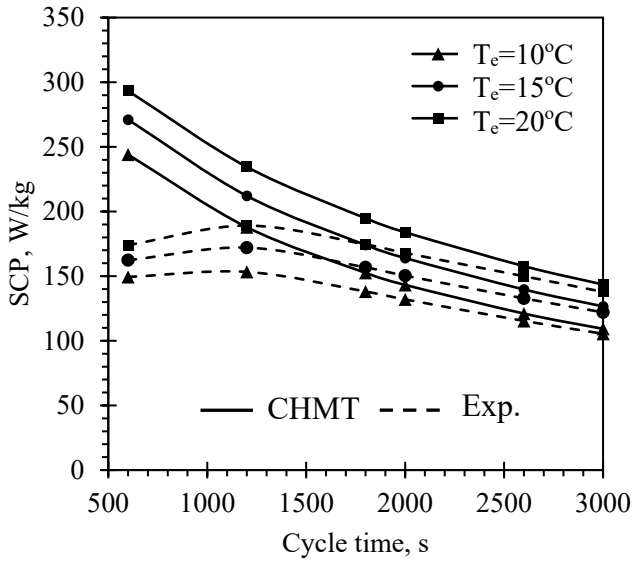

Figure 6-4 SCP of the tested bed at various evaporation temperatures estimated from experimental measurements and CHMT model

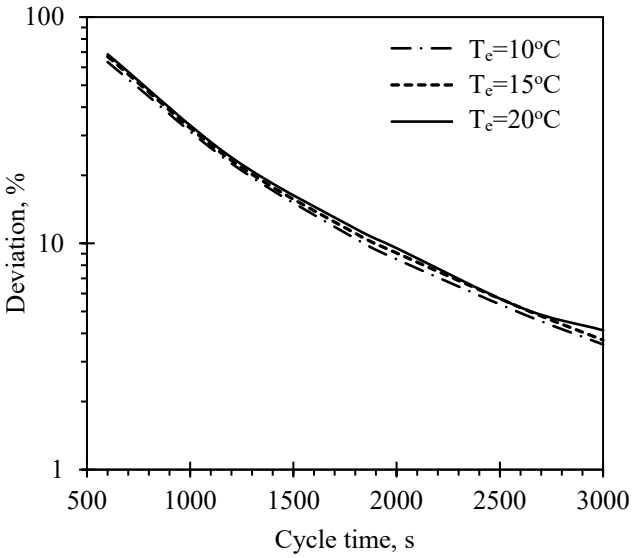

Figure 6-5 Deviation between SCP obtained from experimental results and CHMT model

Figure 6-6 points out the effect of the chilled water flow rate on the SCP obtained from experimental data and the CHMT model at an evaporator temperature of 10°C. It is noted that the SCP_{CHMT} does not depend on the chilled water mass flow rate because the CHMT model does not include the dynamic effect of the evaporator of the adsorption cooling system. The difference between the SCP obtained from the experimental measurements and the CHMT model declines as

chilled water flow rate increases and cycle time increases as presented in Fig. 6-7. This is because increasing the chilled water mass flow rate decreases the pressure drop in the evaporator especially at the beginning of adsorption process as shown in Fig. 6-8. Figure 6-8 depicts that the evaporator pressure decreases sharply at the beginning of the adsorption process. The low mass flow rate of chilled water causes a significant decrease in the evaporator pressure and temperature because the adsorption rate is higher at the beginning of adsorption process and the heat added by the chilled water is not sufficient to generate the required vapor for the adsorption process and keep the evaporator pressure constant. This reduction in evaporator pressure at the beginning of the adsorption process reduces the bed equilibrium uptake which decreases the SCP. After a certain period, the adsorption process slows down and allows the evaporator pressure to increase and reaches the set point again.

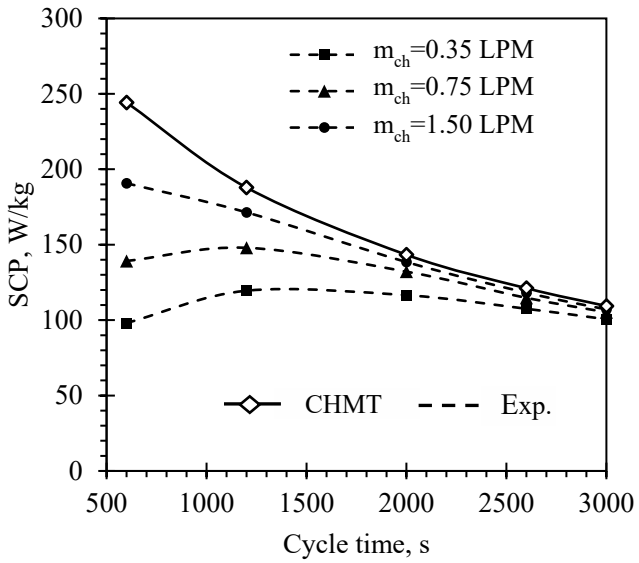

Figure 6-6 SCP of adsorption system at various chilled water flow rates and cycle times

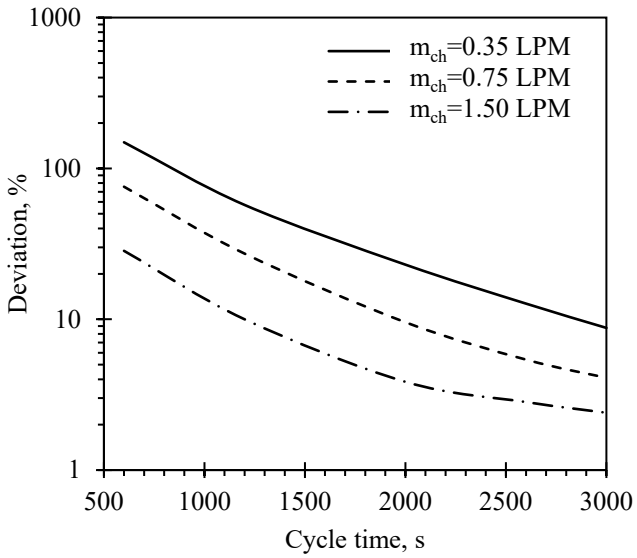

Figure 6-7 Deviation between SCP_{Exp} and SCP_{CHMT} at various chilled water flow rates and cycle times

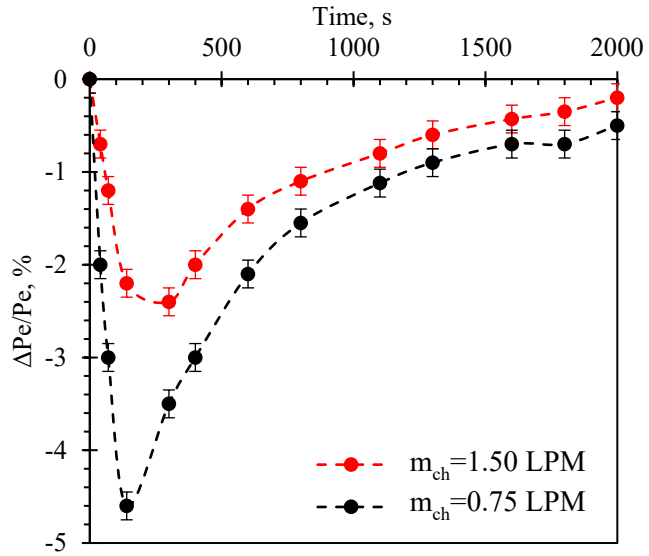

Figure 6-8 Temporal variation of the evaporator pressure during the adsorption period at different chilled water flow rates

As a result, the CHMT model is not an appropriate approach to estimate the actual SCP of the adsorption cooling system because the dynamic response of the evaporator is not considered in the model. In other words, assuming a constant pressure boundary condition for the surface exposed to vapor from the evaporator is not a suitable assumption. This assumption causes the SCP calculated from the CHMT model to overestimate the SCP.

6.5.2 Modified CHMT model

It is previously shown that the SCP obtained from the CHMT model is higher than the one produced by the adsorption bed investigated because a constant temperature and pressure condition in the evaporator is assumed, which may not be acceptable for short cycle times. So, considering the evaporator dynamic response in the model will allow predicting a more realistic value for the SCP of the adsorption bed. Accordingly, a modified CHMT model that assumes a time-dependent boundary condition on the bed surfaces exposed to the evaporator is proposed. Equations 45 and 47 are coupled with the CHMT model to calculate the evaporator temperature during the adsorption process. Based on the calculated evaporator temperature, evaporator pressure is calculated from Equation 35 and added as a boundary condition at the surface exposed to the evaporator (i.e., boundary condition No. 3 in Fig. 6-1B). By adding the energy balance equations of the evaporator to the CHMT model, the SCP can be calculated based on the evaporator capacity as shown in Eq. 49. The differences between the SCP calculated from experimental measurements and the modified CHMT model based on the evaporator capacity are found to be less than 3.5% as depicted in Fig. 6-9. Accordingly, the modified CHMT provides an accurate estimation of SCP produced by an adsorption cooling bed. It is therefore a powerful tool to design adsorption bed as well as estimate the actual SCP when this bed is implemented in an adsorption cooling cycle.

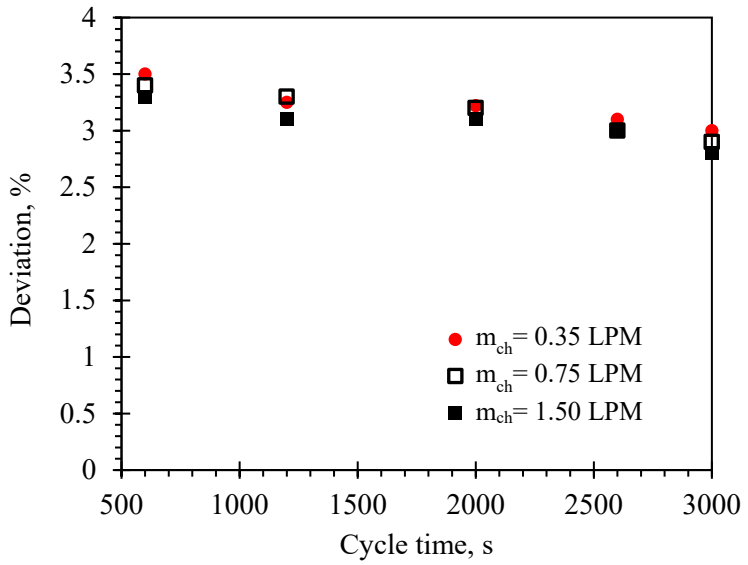

Figure 6-9 Deviation between SCP calculated from Exp. data and modified CHMT model at different cycle times

6.5.3 LP model

The LP model is an alternative approach to calculate the SCP of an adsorption cooling unit. It is sometimes preferred because the computational time is short compared with the CHMT and the modified CHMT model. In addition, it is easier to implement as it involves only a set of ordinary differential equations. However, the overall heat transfer coefficient of the bed that is needed for the LP model can only be estimated from the modified CHMT model in the absence of experimental measurements. It is worth to mention that the overall heat transfer coefficient of the bed estimated from Eq. 44 deviates by less than 4% from the one calculated from the experimental measurements based on Eq. 47.

The LP model is also implemented to investigate the effect of the overall heat transfer coefficient of the evaporator on the SCP as depicted in Fig. 6-10. The results from the LP model is validated using the available experimental measurements at the overall heat transfer coefficient of the evaporator of 500 W/K. A good agreement is established between the numerical results from

the LP model and experimental measurements as shown in Fig. 6-10. Decreasing the overall heat transfer coefficient of evaporator leads to a decrease in the SCP of the adsorption cooling system as presented in Fig. 6-10. This is because the pressure drop in evaporator decreases as its overall heat transfer coefficient increases which directly leads to an enhancement in SCP of adsorption system. However, this improvement levels off to a maximum value at $UA_e \approx 500\ W/K$, beyond which the value of the chilled water outlet temperature equals to the evaporator temperature and no further improvement in SCP can be achieved. The produced cooling capacity indicates an optimum cycle time of 1200 s, independent of the value of the evaporator overall heat transfer coefficient.

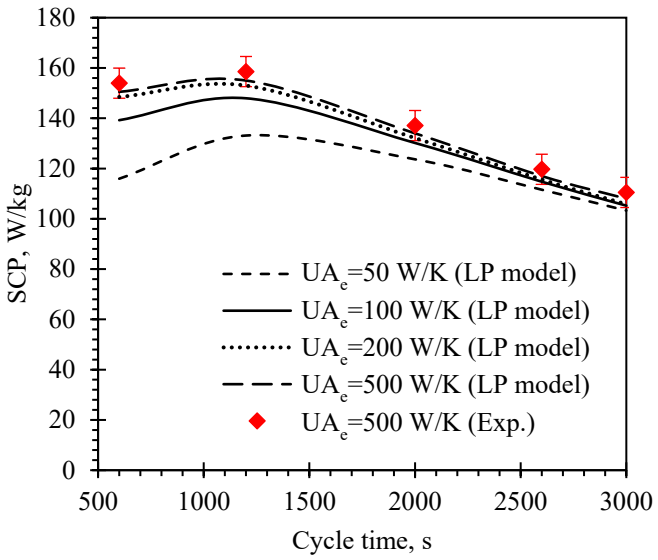

Figure 6-10 SCP of the tested bed at various overall heat transfer coefficient of evaporator

The evaporator heat capacity is proportional to its size and material. Figure 6-11 represents the effect of the evaporator heat capacity on the performance of the tested adsorption bed. It is evident from the figure that the SCP increases as the evaporator heat capacity decreases and reaches to the maximum values (i.e., the SCP estimated from the CHMT model) when a small evaporator is employed. This means that an adsorption cooling system could produce the

maximum cooling power when the amount of water (refrigerant) in the evaporator is just sufficient to feed the adsorber bed during the adsorption process. This scenario means that the evaporator will be completely dry after the adsorption process which is not applicable to the practical adsorption cooling systems where the evaporator coil is submerged in water all the time. Therefore, it can be concluded that the generated cooling power from the adsorption cooling system is affected by the height of water column in the evaporator. Figure 6-12 shows the difference between the two solutions at various heat capacities and cycle times. It can be seen that the deviation in SCP decreases as the cycle time increases and heat capacity of the evaporator decreases. The deviation is about 2% at heat capacity and cycle time of 1.4 kJ/K and 600 s, respectively. Accordingly, the evaporator design and its heat capacity are key parameters in designing an adsorption cooling system.

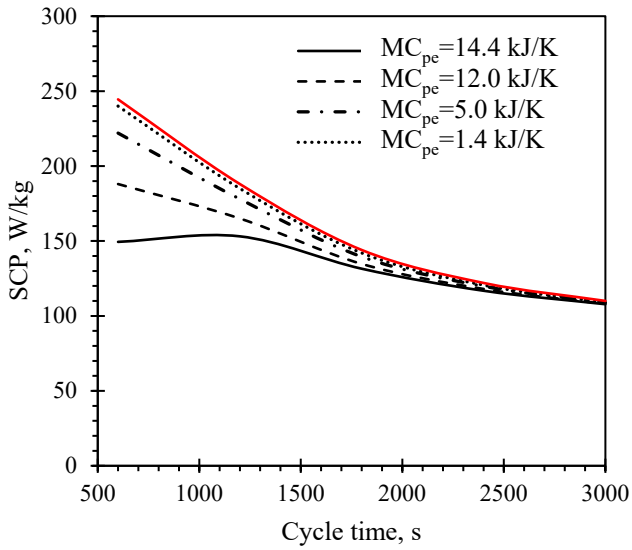

Figure 6-11 SCP of the tested bed at various heat capacities and cycle times estimated from CHMT (red line) and LP model (black lines)

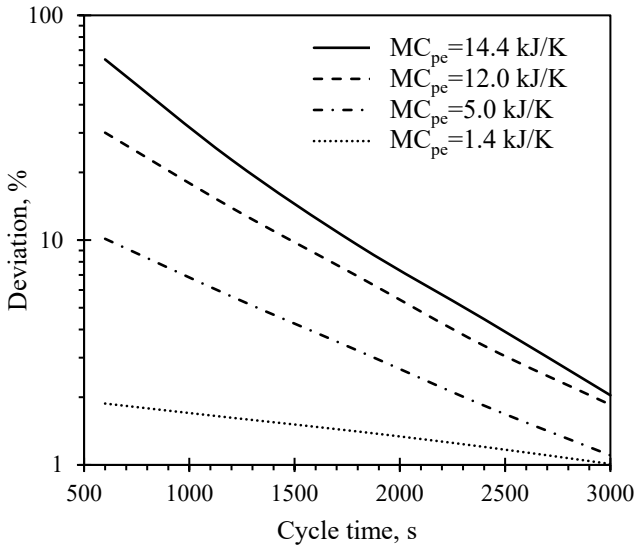

Figure 6-12 Deviation between SCP_{LP} and SCP_{CHMT} at various heat capacities and cycle times

6.6 Conclusions

An experimental setup is designed and constructed to investigate the thermal response and adsorption kinetics of a lab-scale silica gel packed bed. Experimental measurements and results from the CHMT model and the LP model are compared to evaluate the validity of the CHMT model and the LP model in estimating the SCP of adsorption cooling systems. Furthermore, the dynamic effect of the evaporator on the performance of an adsorption cooling system is studied and addressed at various values of evaporator temperature, evaporator overall heat transfer coefficient, chilled water mass flow rate and evaporator heat capacity. Based on a comparison among the experimental measurements and simulation results, the following conclusions can be highlighted:

- The SCP of an adsorption cooling system calculated from the CMHT model is found to be overestimated because the dynamic effect of the evaporator is not included in the model.
- At short cycle times, a noticeably large difference between the SCPs obtained from experimental data and CHMT model is observed, and it declines at longer cycle times.

- A modified CHMT model that considers the dynamic response of the evaporator during the adsorption period is proposed. The modified CHMT mode is found to be a suitable approach to design an effective adsorption bed for cooling applications by investigating its adsorption kinetics and thermal response as well as to estimate the SCP produced by this bed.
- The modified CHMT model can be used to calculate the overall heat transfer coefficient of the designed bed and the mass of the adsorbent, which are needed as input parameters for the LP model. The LP model provides the optimal adsorption cycle time.
- The accuracy of the LP model in predicting the SCP of an adsorption cooling cycle is evaluated. It is found that the LP model is an appropriate tool to calculate the SCP and study the effect of the evaporator design parameters on the cycle performance.
- Remarkable enhancement in the SCP of an adsorption cooling system can be achieved by using an evaporator with a high overall heat transfer coefficient and high chilled water mass flow rate. Therefore, the selection of the evaporator characteristics is a critical step in the design and construction of an effective adsorption cooling system.

CHAPTER 7 SCALING ANALYSIS

7.1 Introduction

The low performance of adsorption cooling system reported in previous studies is due to the high thermal resistance and high intra-particle mass diffusion resistance within the adsorption bed packed with adsorbent beads. The main goal of this study is to derive new scaling parameters that can be used to specify the optimal bed dimensions and select the appropriate working pair to achieve the maximum cooling power. Therefore, the study performs an order of magnitude analysis and scaling analysis on the terms in the governing conservation equations to identify the importance of each term on the bed performance. In addition, a numerical study is performed to illustrate the roles played by the newly derived scaling parameters. The results of this study have been published in International Journal of Thermal Sciences[**].

7.2 Theory of Heat and Mass Transfer in an Adsorption Packed Bed

An adsorption bed is basically a heat exchanger packed with a nanoporous adsorbent whose particle diameter is in the range of 0.18-3.0 mm. The different bed configurations can be simplified as a layer of adsorbent with vapor adsorbate coming from an evaporator. The other side is a cold wall that could be a fin or a surface exposed to a cooling fluid as presented in Fig. 7-1a. Vapor penetrates into the void spaces between particles, which is characterized by the inter-particle permeation resistance as shown in Fig. 7-1b. The inter-particle permeation resistance causes a pressure drop across the adsorbent-adsorbate layer. When the vapor reaches the surface of the adsorbent particles, adsorption occurs via mass diffusion through the nanopores of the adsorbent

[**] The content of this chapter has been published in R. H. Mohammed, O. Mesalhy, M. L. Elsayed, L. C. Chow, Scaling analysis of heat and mass transfer processes in an adsorption packed bed, International Journal of Thermal Sciences 133, 82-89, 2018.

particles (i.e., intra-particle mass diffusion resistance) and it is accompanied with the release of heat of adsorption. The heat generated is removed by a cooling fluid facilitating continuous adsorption. However, this heat must first be conducted through the adsorbent bed to the heat transfer surface for the adsorption process to continue. Since the effective thermal conductivity of a packed bed is low, the adsorbent layer should be small to reduce its thermal resistance. The particles eventually reach an equilibrium condition and no further adsorption occurs. The change in uptake depends on the bed pressure and temperature during the adsorption period. Accordingly, adsorption bed performance is controlled by inter-particle permeation resistance, intra-particle mass diffusion resistance, heat diffusion through the adsorbent-adsorbate layer and convective heat transfer resistance [29]. Figure 7-1c summarizes the thermal resistances of adsorbent embedded heat exchanger in a typical adsorption heat transfer process [136].

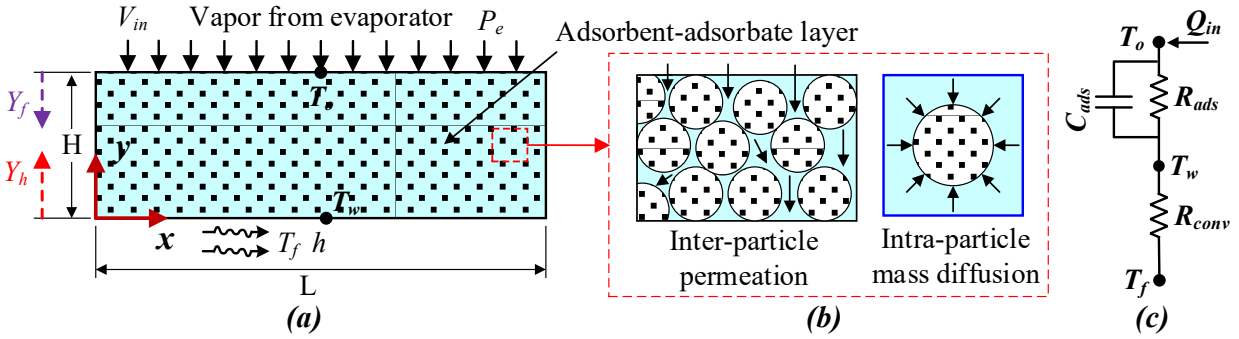

Figure 7-1 Schematic representation of (a) an adsorbent embedded heat exchanger, (b) mass transfer resistances, and (c) thermal resistances of a bed

7.3 Scaling/Order-of-Magnitude Analysis

Two different time scales control the bed performance. The first one is the mass diffusion time scale, which is defined as the time required for the adsorbate to penetrate into the adsorbent particle. The second time scale is the thermal time scale that represents the time required for the heat generated inside the bed to transfer to the cooled surface through the bed.

The mass diffusion time scale can be obtained from the LDF equation as:

$$\underbrace{\frac{\partial X}{\partial t}}_{\frac{\Delta X}{t_d}} = \underbrace{\frac{15 D_s}{r_p^2}(X_o - X)}_{\frac{D_s(T_i)}{r_p^2}\Delta X} \qquad (50)$$

where $D_s(T_i)$ is the surface diffusion calculated at the initial temperature of the bed and ΔX is the change in uptake.

So, the time scale of mass diffusion in a particle is $t_d \approx \frac{r_p^2}{D_s(T_i)}$, which can be also estimated from Fickian the diffusion equation $\left(i.e., \frac{\partial X}{\partial t} = D_s \frac{\partial^2 X}{\partial x^2}\right)$, similar to what was introduced elsewhere [5].

Based on the bed configuration illustrated in Fig. 1a, the mass conservation equation for adsorbate gas (Eq. 1) can be written as:

$$\underbrace{\varepsilon_b \frac{\partial \rho_v}{\partial t}}_{\left(\frac{\varepsilon_b \Delta \rho_v}{t_a}\right)} + \underbrace{\rho_v \frac{\partial v}{\partial y}}_{\left(\rho_v \frac{V_{in}}{Y_f}\right)} = \underbrace{-\rho_b \frac{\partial X}{\partial t}}_{\left(\rho_b \frac{\Delta X}{t_d}\right)} \qquad (51)$$

As the change in vapor density during the adsorption is extremely small, the first term on the left-hand side in Eq. 36 can be ignored compared to the other terms. The vapor velocity scales as the difference in the vapor velocity at the surface and at the end of the adsorbent layer. This velocity equals the inlet velocity coming from evaporator at the surface of the adsorbent. The length scales as Y_f, which is the vapor penetration distance from the bed surface in the direction of vapor flow. This scaling analysis yields $V_{in} \approx \left(\frac{\rho_b \Delta X}{\rho_v t_d} Y_f\right)$.

Revisiting Darcy's law using appropriate scaling parameters shows the following:

$$\underbrace{\vec{U}}_{\mathrm{V_{in}}} = \underbrace{-\frac{K}{\mu}\nabla P}_{\left(\frac{\mathrm{K}}{\mu}\frac{\Delta P}{Y_f}\right) = \left(\frac{\mathrm{K}}{\mu}\frac{\mathrm{P_e}}{Y_f}\right)\delta} \qquad (52)$$

where ΔP is the pressure drop through across the vapor penetration depth Y_f and $\delta = \frac{\Delta P}{P_e}$ is the pressure drop ratio.

Thus, the scaling analysis of mass conservation and Darcy's equation shows that:

$$V_{in} \approx \left(\frac{\rho_b \Delta X}{\rho_v t_d} Y_f\right) \approx \left(\frac{K}{\mu}\frac{P_e}{Y_f}\right)\delta \Rightarrow Y_f^2 = \left(\frac{\rho_v r_p^2 K P_e}{\rho_b \Delta X D_s \mu}\right)\delta \quad (53)$$

Based on the thermo-properties shown in Table 7-1, $Y_f^2 \sim \mathcal{O}(10^{-4} - 10^{-1})\, m^2$ for a pressure drop percentage of $\mathcal{O}(10^1)\%$ and particle diameter in the range of 0.18-3.0 mm, which is commonly used in adsorption cooling systems.

Table 7-1 Thermo-physical properties of common working pairs [74, 137-139]

Working pair	C_{ps} (J/kg.K)	k_b (W/m.K)	ρ_b (kg/m^3)	Q_a (kJ/kg)	k	X_∞ (kg/kg)	n
Silica-gel/water	924	0.198	740	2415	14.0	0.37	1.15
Zeolite/water	921	0.155	650-850	3300-4200	5.36	0.26	1.73
Activated carbon/ammonia	711	0.017	431-520	2000-2700	3.57	0.29	1.38
Activated carbon/methanol	711	0.017	431-520	1800-2000	13.38	0.45	1.5

The energy equation can be rearranged, and the unsteady and thermal diffusion terms can be scaled with the appropriate scaling terms as follows:

$$\underbrace{\left(\varepsilon_b \rho_v C_{pv}\right)\frac{\partial T}{\partial t}}_{\frac{\varepsilon_b \rho_v C_{pv} \Delta T}{t_a}} + \underbrace{\rho_v C_{pv} v.\frac{\partial T}{\partial y}}_{\frac{\rho_v C_{pv} V_{in} \Delta T}{Y_h}} = \underbrace{-\rho_b \left[C_{p,b} - Q_a \frac{\partial X}{\partial T}\right]\frac{\partial T}{\partial t}}_{\rho_b \left[C_{p,b} + Q_a \frac{\Delta X}{\Delta T}\right]\frac{\Delta T}{t_a}} + \underbrace{k_b \frac{\partial^2 T}{\partial y^2}}_{k_b \frac{\Delta T}{Y_h^2}} \quad (54)$$

$$\frac{\varepsilon_b \rho_v C_{pv}}{t_a k_b} Y_h^2 \qquad \frac{\rho_v C_{pv} V_{in} Y_h}{k_b} \qquad \frac{\rho_b C_{p,app}}{t_a k_b} Y_h^2 \qquad 1$$

where $C_{p,b} = C_{ps} + \bar{X} C_{pw}$ is the effective heat capacity of the bed and $\bar{X}$ is the average bed uptake.

The temperature difference (ΔT) scales as the difference between the initial temperature of the bed and final equilibrium temperature that is equal to the cooling fluid temperature $\{\Delta T = (T_i - T_f)\}$. The length scales as Y_h, which represents a distance from the cooled surface where

significant effect of a cooling fluid is felt and within which the thermal diffusion process is dominant. It should be noted that when the two scaling expressions on the left-hand side have the same order of magnitude, the effective thermal conductivity of the bed and it thickness will be sufficient to conduct the heat generated in the bed to the cooling fluid though the adsorption time (t_a).

The change in internal energy of the vapor phase is negligible comparing to the internal energy of the adsorbent-adsorbate layer due to the extremely low heat capacitance of the vapor phase. The convective term can be ignored in comparison to the thermal diffusion term if $V_{in} \ll \frac{k_b}{\rho_v C_{pv} Y_h}$. Previously, the vapor velocity is scaled from mass conservation equation as $V_{in} \approx \left(\frac{\rho_b \Delta X}{\rho_v t_d} Y_f\right)$. So, the inequality can be rewritten as $\left(\frac{\rho_b \Delta X C_{pv} Y_h}{t_d} Y_f\right) \ll k_b$. This inequality is valid for all practical operating conditions of adsorption cooling beds and commonly used working pairs, and hence the convective term can be negligible compared to the thermal diffusion term. The inequality $V_{in} \ll \frac{k_b}{\rho_v C_{pv} Y_h}$ indicates that increasing the bed thermal conductivity and/or decreasing the bed thickness allow an increase in the vapor velocity in the void spaces and hence enhancing the thermal diffusion in adsorption bed.

On the other hand, if the length is scaled as H in Eq. 54, instead of Y_h, the time would scale as the thermal diffusion time (t_{th}) that represents the time scale for a bed of thickness H to cool down from the initial temperature to the cooling fluid temperature in the presence of adsorption, and can be calculated as $t_{th} = \frac{H^2}{\alpha_{b,app}}$. This finding is similar to what was introduced in a previous study [5].

The apparent thermal diffusivity of a bed may be estimated as $\alpha_{b,app} \approx \frac{k_b}{\rho_b C_{p,app}} \approx \frac{Y_h^2}{t_a}$. The apparent thermal diffusivity of the bed is less than the bed thermal diffusivity $\left(i.e.,\ \alpha_b = \frac{k_b}{\rho_b C_{p,b}} > \alpha_{b,app}\right)$ due to the presence of the heat of adsorption, which slows down the bed thermal response. Based on thermo-physical properties of various working pairs presented in Table 7-1, $Y_h^2 \sim \mathcal{O}(10^{-6} - 10^{-5})\ m^2$ that is much lower than the order of magnitude of Y_f^2 for $\delta \sim \mathcal{O}(10^1)$%. This implies that the adsorption bed performance is not controlled by heat diffusion or inter-particle permeation if its thickness (H) is less than the heat penetration depth (Y_h).

Interestingly, the expression for the apparent thermal diffusivity provides significant guidelines for calculating the maximum bed thickness as well as the optimum adsorption time based on the adsorption characteristics of the working pair, thermo-physical properties of the adsorbent and cycle operating conditions. The Fourier number of an adsorbent-adsorbate layer can be introduced as $F_o = \frac{\alpha_{b,app} t_a}{H^2} \Rightarrow F_o = \left(\frac{Y_h}{H}\right)^2$. Accordingly, the thermal diffusion process does not control the performance of an adsorption bed when Fourier number of the adsorbent-adsorbate layer is more than 1.0 $\left(i.e., F_o = \frac{\alpha_{b,app} t_a}{H^2} = \left(\frac{Y_h}{H}\right)^2 > 1.0\right)$. This also means that the adsorption bed performance is not controlled by the heat transfer through the bed when the adsorption time (cycle time) is longer than the thermal diffusion time $\left(i.e., t_a > \frac{H^2}{\alpha_{b,app}}\right)$.

Next, the effect of the external convective resistance on the bed performance is studied. Concerning the transient heat and mass transfer in the adsorbent-adsorbate layer, the net rate of heat rate passes through the adsorbent layer is equal to the total heat (i.e., heat generated) minus the rate of stored energy in the adsorbent due to its capacitance as presented in Fig. 7-1c [136].

The temperature difference across the adsorbent-adsorbate layer can be calculated from the following equation:

$$\frac{T_o - T_w}{R_{ads}} = \frac{(T_o - T_w)}{H/k_b A} = Q_{in} - C_{ads}\frac{dT_{ads}}{dt} = hA\left(T_w - T_f\right) \qquad (55)$$

where R_{ads} is the conductive thermal resistance of adsorbent-adsorbate layer, T_{ads} is the average instantaneous adsorbent-adsorbate layer temperature, T_w is the instantaneous wall temperature of the cooling passage, T_f is the temperature of the cooling fluid, C_{ads} is the adsorbent-adsorbate layer capacitance and Q_{in} is the heat generated due to adsorption $\left(Q_{in} = m_{ads} Q_a \frac{dX}{dt}\right)$.

The upper value of convective heat transfer coefficient can be estimated when $\frac{dT_{ads}}{dt} \to 0.0$.

$$T_w - T_f \approx \frac{\rho_b H Q_a}{h}\frac{dX}{dt} \Rightarrow \Theta = \frac{T_w - T_f}{T_i - T_f} \approx \frac{\rho_b H Q_a}{(T_i - T_f)\,h}\frac{\Delta X D_s(T_i)}{r_p^2} \qquad (56)$$

where Θ is a new parameter called the dimensionless temperature ratio that can be used to estimate the upper limit of convective heat transfer coefficient, beyond which the external resistance (R_{conv}) has only a marginal effect and the bed performance is controlled by the thermal resistance of adsorbent-adsorbate layer as it will be shown later.

7.4 Numerical Work

Heat and mass transfer in the adsorbent-adsorbate layer shown in Fig. 7-1a is studied by using the transient 2-D local thermal equilibrium model that is previously discussed. The model includes vapor flow in packed bed layer, heat transfer from the adsorbent layer to the cooling fluid and mass diffusion into the silica gel particles. The numerical model is built in COMSOL Multiphysics 5.2 and solved numerically with a relative tolerance of 10^{-5}.

7.4.1 Computational domain and initial and boundary conditions

Consider a rectangular adsorber domain with a width (L) of 100 mm and height (H) of 7 mm as shown in Fig. 7-1a. Silica gel-water is selected as the working pair as it is one of the common working pairs used in adsorption cooling systems. Bed porosity, particle porosity and particle diameter are chosen to be 0.37, 0.42 and 0.35 mm, respectively. Surface diffusion of water adsorbate into silica gel is calculated using the Arrhenius equation as follows [5]:

$$D_s = 2.54 \times 10^{-4} \exp\left(-\frac{5051.72}{T}\right) \quad (57)$$

Initially, solid and gas temperature, pressure and uptake distributions inside the adsorbent bed are considered to be uniform. The initial temperature and pressure of the bed are 60℃ and 1228 Pa, respectively, and the initial water vapor uptake is based on the initial conditions from D-A model. A cooling fluid with a temperature of 30℃ and convective heat transfer coefficient of 500 W/m^2.K is used to cool down the bed during the adsorption period. Boundary conditions are listed in Table 7-2. The governing equations are solved numerically using COMSOL Multiphysics 5.2 software with a relative tolerance of 10^{-4}.

Table 7-2 Boundary conditions used in this study

Boundary location	Flow	Temperature
$y = H$	P_e	$dT/dy = 0$
$y = 0.0$	$u = v = 0$	$h(T - T_f) = k_b(dT/dy)$
$x = 0.0$	$u = v = 0$	$dT/dy = 0$
$x = L$	$u = v = 0$	$dT/dy = 0$

7.4.2 Mesh sensitivity and Code validation

Grid independence study is carried out using various sizes of structured mesh and time steps. It is found that mesh size of 250×21 elements with a time step of 0.5 s is enough to capture the flow and temperature fields with high accuracy and reasonable computational time.

Experimental set-up described in [41] is used to measure the adsorption rate and average bed temperature during the adsorption time. These experimental results are compared with those obtained from the numerical simulation as depicted in Fig. 7-2. It is clear that there is a good agreement, with a maximum temperature difference of 1.5℃ between the experimental measurements and numerical results. This quite small deviation demonstrates the suitability of the proposed model and the numerical solution to simulate the heat and mass transfer throughout the adsorption bed.

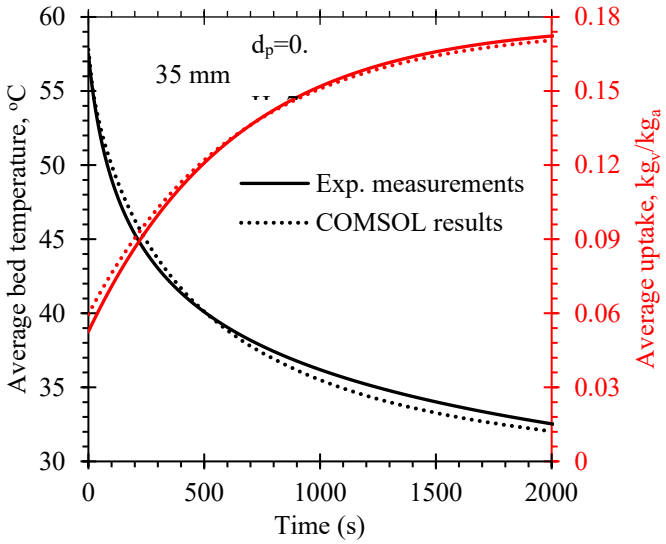

Figure 7-2 Comparison between the experimental measurements and the numerical results

7.5 Results and Discussion

The scaling analysis of the governing equations yields important scaling parameters that depend on the thermo-physical properties of the working pair and the operating conditions as summarized in Table 7-3. These scaling parameters provide guidelines to select the appropriate working pair and to design adsorption bed that could produce the maximum cooling power. The importance of scaling parameters presented in the previous sections is studied using the validated numerical simulation performed for the two-dimensional domain.

Table 7-3 Summary of the scales discussed in this study and their physical meanings

Scaling parameter	Relationship	Physical meaning
Mass diffusion time (t_d)	$\frac{r_p^2}{D_s(T_i)}$	Time required an adsorbate to penetrate through an adsorbent particle of radius r_p and achieve equilibrium uptake.
Vapor penetration depth (Y_f)	$\sqrt{\left(\frac{\rho_v r_p^2 \mathrm{K}\Delta\mathrm{P}}{\rho_b \Delta X D_s \mu}\right)}$	Adsorbent layer thickness that produces pressure drop (ΔP).
Apparent heat capacity ($C_{p,app}$)	$C_{p,b} + Q_a \frac{\Delta X}{\Delta T}$	Apparent heat capacity of the bed taking into account the heat of adsorption.
Heat penetration depth (Y_h)	$\sqrt{\frac{k_b \times t_a}{\rho_b C_{p,app}}}$	Adsorbent depth up to which the heat generation can be conducted to the cooled surface.
Heat diffusion time (t_{th})	$\frac{H^2}{\alpha_{b,app}}$	Time required for a bed of thickness H to cool down from T_i to T_f in the presence of heat of adsorption.
Bed Fourier number (F_o)	$\frac{\alpha_{b,app} t_a}{H^2}$	Ratio between heat penetration depth and bed thickness $\left(\frac{Y_h}{H}\right)^2$.
Dimensionless temperature ratio (Θ)	$\frac{\rho_b H Q_a}{\Delta T\, h} \frac{\Delta X D_s(T_i)}{r_p^2}$	Ratio between heat generated inside bed and heat transfer by convection which can be calculated as $\frac{T_w - T_f}{\Delta T}$.

7.5.1 Vapor penetration depth

The scaling analysis of the continuity and momentum equation results a relationship between pressure drop, thermo-physical properties of working pair, particle diameter and bed thickness. Various silica gel particle diameters and bed thicknesses in the range of 0.18-3 mm and 5-25 mm, respectively are studied to investigate their effects on the pressure drop across the adsorbent-adsorbate layer. These ranges are the typical values used in adsorption cooling beds. Figure 7-3 depicts the percentage of pressure drop across silica gel-water layer estimated from scaling analysis and numerical simulations for various particle diameters and bed thicknesses. The numerical results show that the pressure drop across adsorption bed depends on the particle diameter to bed thickness ratio, and not on the particles diameter or bed thickness separately, as demonstrated by the scaling analysis. Furthermore, the scaling analysis provides a good estimation of the pressure drop through the adsorbent-adsorbate layer. For silica gel/water, it is evident from

the figure that the pressure drop is not significant when the particle size to bed thickness ratio is more than 0.1. The inter-particle permeation resistance is negligible when the ratio is higher than 0.1. As there is a good agreement between the scaling analysis and numerical results, the vapor penetration depth can be used to estimate an acceptable value for the pressure drop across adsorption packed based on the working pair properties and bed dimensions.

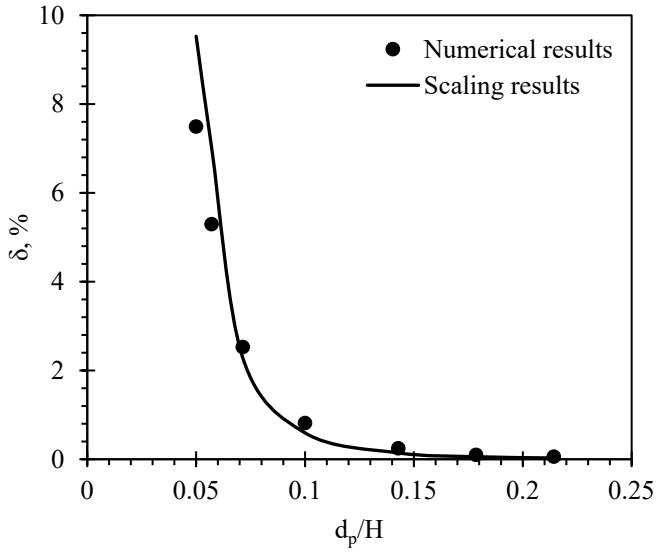

Figure 7-3 Comparison between the pressure drop calculated from numerical simulation and scaling analysis at various particle diameter to bed thickness ratios

7.5.2 Apparent heat capacity

The apparent thermal diffusivity can be used to simplify the energy equation (Eq. 54) to a transient 1-D heat diffusion problem $\left(i.e., \frac{\partial T}{\partial t} = \alpha_{b,app} \frac{\partial^2 T}{\partial y^2}\right)$ that can be solved analytically and then the uptake can be separately calculated by solving the LDF equation. This step assumes uniform heat generation and apparent heat capacity of the adsorbent can be used to calculate the temperature field inside the adsorbent-adsorbate layer. Solving the 1-D heat diffusion equation using the apparent heat capacity provides an approximate solution for the temperature field inside a bed, which can then be used to get a reasonable estimate for the produced cooling power. Figure

7-4 compares the spatial variations of adsorbent temperature obtained from the numerical calculations and exact solution [140] of 1-D heat diffusion equation using the apparent heat capacity of silica gel at various adsorption times. Based on the exact solution of the bed temperature, the uptake is calculated using Eq. 2. The average temperature and uptake of the bed packed with 0.35 mm of silica gel beads are plotted in Fig. 7-5. It is clear that the silica gel bed temperature calculated from the exact solution is higher than that obtained from the numerical simulation for shorter times of adsorption. This is because the heat generated is lower at the beginning of the adsorption process. Later, as the adsorption bed cools further, the rate of adsorption increases and heat of adsorption slows down the bed thermal response. Analysis of results shows less than 3% deviation between the two solutions. Accordingly, the apparent specific heat $\left(C_{p,app}\right)$, which is lower than the actual bed specific heat, provides a suitable method to couple heat transfer and adsorption processes into a single parameter and predict the average bed temperature and uptake as obtained in Fig. 7-5.

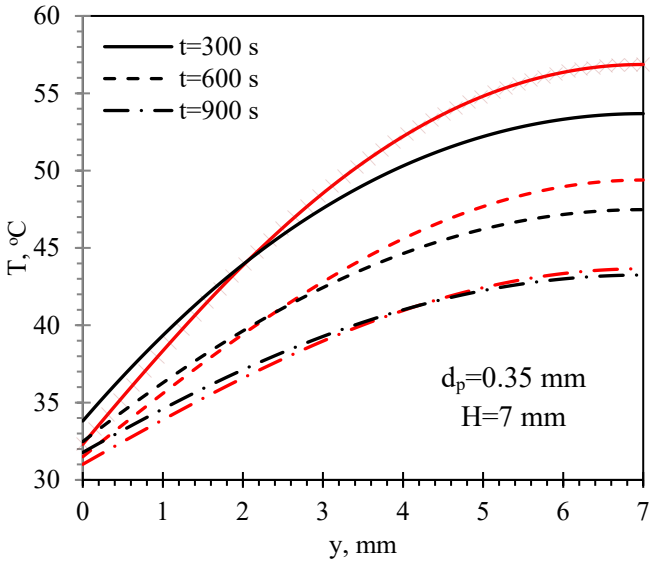

Figure 7-4 Comparison of bed temperature variation obtained from numerical simulation (black lines) and exact solution (red lines) at various adsorption times

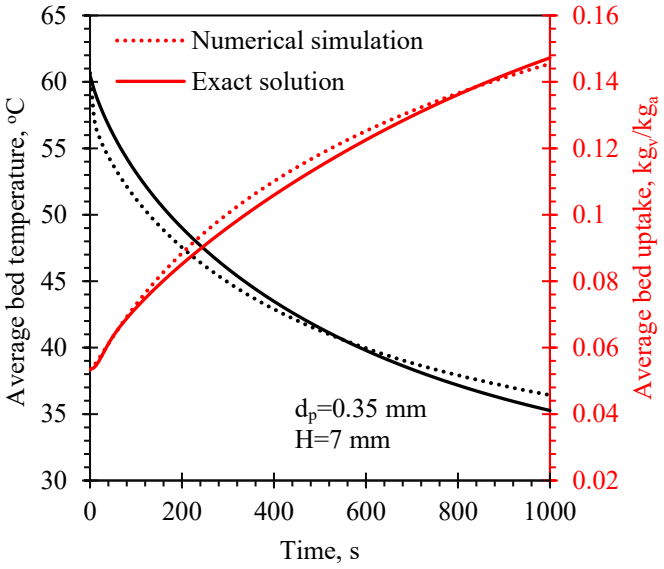

Figure 7-5 Comparison of average bed temperature and uptake calculated of exact solution and numerical simulation

7.5.3 Fourier number

Figure 7-6 illustrates the effect of increasing the silica gel thermal conductivity on the average bed temperature and uptake at the upper value of the convective heat transfer coefficient and silica gel particle diameter of 0.35 mm. It is found that increasing the silica gel thermal conductivity from 0.198 W/m.K to 1.75 W/m.K leads to an increase in cooling power produced after 600 s by 50%. However, the thermal response of the bed is not affected by the bed thermal conductivity when it is higher than 1.75 W/m.K.

The specific cooling power produced by an adsorption cooling bed can be estimated as [5]:

$$SCP = \frac{(X(t) - X_i) \times h_{fg}}{t_a} \quad (58)$$

where h_{fg} is the latent heat of vaporization at the evaporator pressure.

The influence of Fourier number on SCP produced by different bed thicknesses is plotted in Fig. 7-7. It is found that SCP increases as Fourier number of the adsorbent-adsorbate layer (F_o) increases and levels off to a maximum value at $F_o \approx 1$, beyond which the value of the bed thermal conductivity is high enough to conduct the amount of heat generated to the cooling fluid.

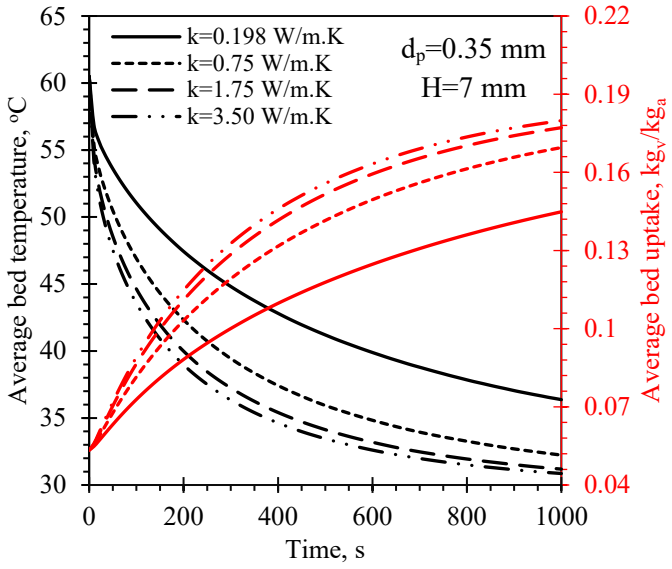

Figure 7-6 Temporal variation of average bed temperature and uptake at various bed thermal conductivity.

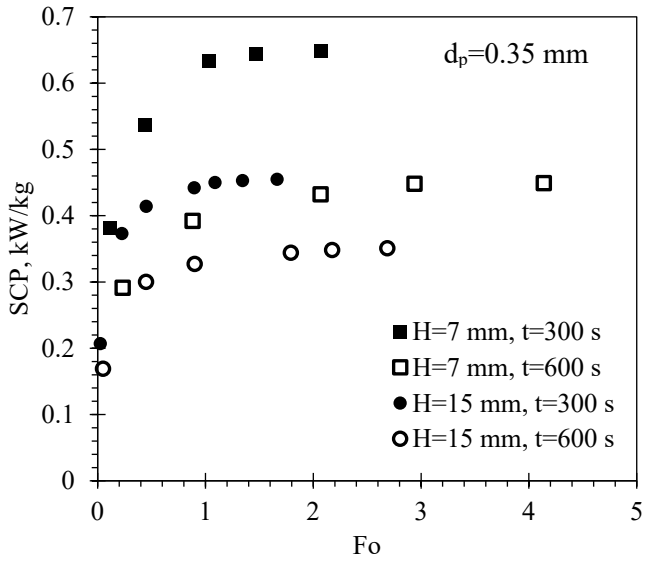

Figure 7-7 Effect of Fourier number of the adsorbent-adsorbate layer (F_o) on SCP for various bed thicknesses

Figure 7-8 depicts the influence of silica gel particle size on the SCP at different Fourier numbers. As the particle size decreases, the intra-particle mass diffusion resistance decreases, which leads to a noticeable increase in the SCP. It is evident from the figure that the inter-particle permeation resistance does not control the performance of silica gel bed when silica gel particle

diameter to bed thickness ratio $\left(\frac{d_p}{H}\right)$ is more than 0.1, as previously shown in Fig. 7-3. The dotted lines in Fig. 8 illustrate the predicted SCP in the absence of the inter-particle permeation resistance effect. It is clear that the inter-particle permeation resistance has a remarkable effect on the performance of adsorption bed when $\frac{d_p}{H}$ is less than 0.1. It is found that existence of the inter-particle permeation resistance decreases the SCP by 11% for silica gel particle diameter of 0.3 mm. For silica gel particle size of 1 mm, the SCP increases by 21% when the effective thermal conductivity of the bed increases by a factor of 6. Also, decreasing the particle diameter from 1 mm to 0.7 mm leads to an increase in the SCP by 32%. Further decreasing in the particle diameter does not prominently enhance the SCP at low bed thermal conductivity, because the bed is mainly controlled by the thermal diffusion resistance in this range. Analysis of such results concludes that the intra-particle mass diffusion resistance governs the performance of adsorption bed when the mass diffusion time (t_d) is more than the adsorption time (t_a). Likewise, the heat diffusion resistance dominates the bed performance when the thermal diffusion time (t_{th}) is more than the adsorption time.

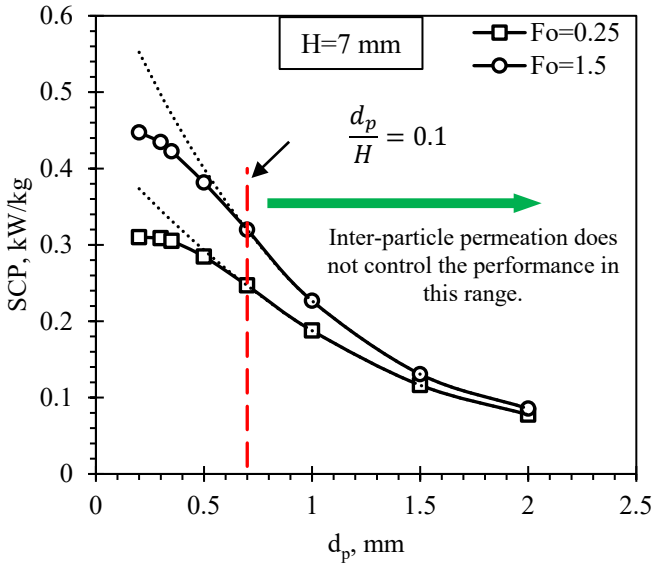

Figure 7-8 SCP produced after 600 s by silica gel bed at various particle sizes.

7.5.4 Dimensionless temperature ratio

Figure 7-9 presents the effect of the convective heat transfer coefficient on the average silica gel packed bed temperature and uptake at a particle size of 0.35 mm. It is clear that increasing the convective heat transfer coefficient has a very noticeable effect on the thermal response of the bed. However, the effect becomes insignificant when the convective heat transfer coefficient is increased beyond 400 W/m^2.K due to the low thermal conductivity of the adsorbent material. Furthermore, the effect of the dimensionless temperature ratio (Θ) on the bed performance is investigated at various particle sizes and bed thicknesses as depicted in Fig. 7-10. It is also evident from this figure that decreasing the dimensionless temperature ratio (i.e., increasing the convective heat transfer coefficient) below 0.2 does not enhance the silica gel packed bed performance. This means that the silica gel bed performance is controlled by heat diffusion when $\Theta < 0.2$ and enhancing the bed thermal conductivity will increase the SCP. By using this range of Θ, the upper limit of convective heat transfer coefficient can be specified based on the working pair properties and adsorbent-adsorbate layer thickness.

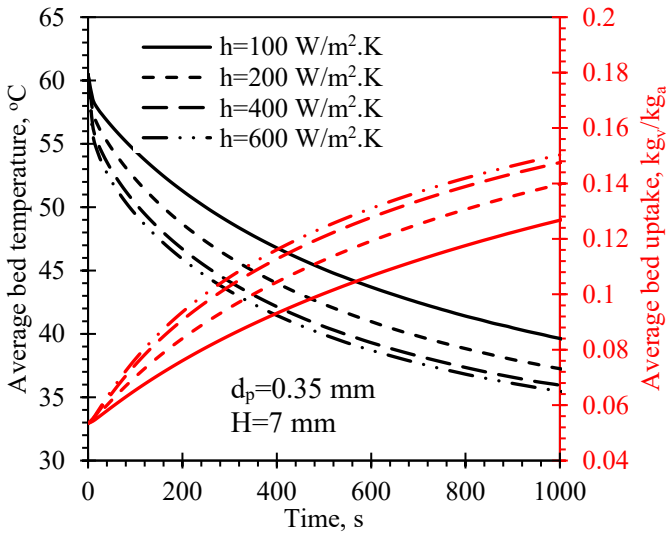

Figure 7-9 Temporal average silica gel bed temperature and uptake of bed thickness of 7 mm at various convective heat transfer coefficient

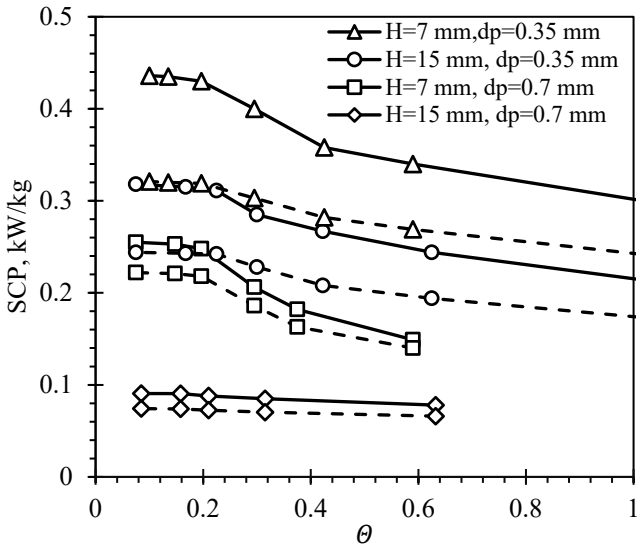

Figure 7-10 Effect of dimensionless temperature ratio parameter (Θ) on SCP produced at 300 s (solid lines) and 600 s (dashed lines)

7.5.5 Design criteria for an efficient silica gel/water adsorption bed

The importance of the newly derived scaling parameters is previously discussed. These scaling parameters depend on the thermo-physical properties of the working pair and the operating conditions of the adsorption cooling cycle. An efficient silica gel/water adsorption bed can be designed by fulfilling the following criteria:

- The particle diameter to bed thickness ratio should be larger than 0.1 for the inter-particle permeation resistance to have only a marginal effect on the adsorption bed performance.
- The appropriate particle diameter should be selected with the adsorption time set longer than the mass diffusion time. This guarantees that the intra-particle mass diffusion resistance is not limiting the bed performance.
- An optimal convective heat transfer coefficient can be determined and implemented when the dimensionless temperature ratio (Θ) is less than 0.2.
- The Fourier number of the adsorbent-adsorbate layer should be more than 1 to significantly reduce the effect of the conduction resistance on the bed performance.

7.6 Conclusion

This paper presents a scaling analysis of heat diffusion and vapor adsorption in a porous adsorbent bed. It is found, from the working pair properties and bed dimensions, that the vapor penetration depth can provide an acceptable estimate for the pressure drop across the adsorbent-adsorbate layer. The apparent heat capacity of the adsorbent derived from the scaling analysis can be used to get an approximate solution for the temperature and uptake fields inside the adsorption bed. As a result, an acceptable estimation for the SCP can be obtained.

Analysis of results indicates that the performance of an adsorption silica gel packed bed is not controlled by the conduction resistance when Fourier number of adsorbent-adsorbate layer (F_o) is more than 1. The convective heat transfer resistance has only a marginal effect on the adsorption bed performance when the dimensionless temperature ratio parameter (Θ) is less than 0.2. The performance of an adsorption silica gel packed bed is limited by the inter-particle permeation resistance when the particle diameter to adsorbent layer thickness ratio is less than 0.1. Also, the intra-particle mass diffusion resistance is found to have a considerable influence on the bed performance when the mass diffusion time is longer than the adsorption time. Finally, the scaling parameters introduced in this study can provide insights and design criteria for efficient adsorption beds.

CHAPTER 8 PERFORMANCE EVALUATION OF NEW BED DESIGN

8.1 Introduction

Though the performance of adsorption cooling (AC) systems with different design configurations and operating conditions has been investigated in the literature, AC systems still suffer from poor heat and mass transfer inside the adsorption bed, which is the main obstacle to commercialization of AC units. Therefore, improvements should be made to obtain more efficient and more compact units. Accordingly, a newly designed packed bed for use in AC systems is proposed and evaluated in this research. The bed is modular and can be scaled for a given cooling load. The effective thermal conductivity of a silica gel/water adsorption packed bed is significantly enhanced by placing the silica gel particles in a high-porosity aluminum (AL) foam. The enhancement could lead to several folds increase in the specific cooling power (SCP), cooling capacity per unit volume (CPv) and coefficient of performance (COP) of an adsorption cooling (AC) chiller. The thermal response and adsorption kinetics of various silica-gel/AL foam beds under typical operating conditions are investigated experimentally and numerically. The effect of pores per inch (PPI) of the foam, silica-gel particle size, bed height and adsorption isotherm of different types of silica gel on the bed performance are investigated. The results of this study have been presented in International Journal of Applied Thermal Engineering [**].

[**] The content of this chapter has been published in

1. R. H. Mohammed, O. Mesalhy, M. L. Elsayed, L. C. Chow, Performance evaluation of a new modular packed bed for adsorption cooling systems, Applied Thermal Engineering 136, 293-300, 2018.
2. Performance enhancement of adsorption beds with silica-gel particles packed in aluminum foams, International Journal of Refrigeration, 2019. (Accepted).

8.2 Description of the New Modular Packed Bed Design

The proposed design consists of repeated packed bed cells (modules) as shown in Fig. 8-1A. Each module is an open-cell aluminum foam, as shown in Fig. 8-2, packed with silica gel to enhance the overall thermal conductivity of the bed from 0.198 to 5.8 W/m.K [141]. The physical characteristics of aluminum foams used in this study are shown in Table 8-1. 10 PPI and 20 PPI AL foams with a porosity of 90% are used. The surface area of a 20 PPI foam is about twice that of a 10 PPI foam. The large surface area helps in the dissipation of the heat released during adsorption. Each AL foam module is brazed to an aluminum substrate from the bottom side and filled with silica-gel beads. Fuji silica-gel with a particle size in the range of 0.2-0.5 mm and 0.5-0.9 mm with average particle diameter of 0.35 mm and 0.7 mm, respectively are used in the experimental measurements. The modules are cooled down or heated up using a fluid running under each module. The modules are arranged vertically and their numbers can be selected based to the required cooling power. The modules are subjected to a vapor from/to evaporator/condenser from vapor passages left between them. The module width and length are designed to be much larger than its thickness.

Table 8-1 Physical characteristics of the aluminum foams used in this study [141]

Property	Value	Unit
Specific heat	895	$J/kg.K$
Bulk thermal conductivity	5.8	$W/m.K$
Melting point	660	°C
Relative density $(1-\varepsilon_{fo})$	10	%
Pores per inch (PPI)	10, 20	PPI
Surface area	10 for 10 PPI	cm^2/cm^3
	21 for 20 PPI	cm^2/cm^3

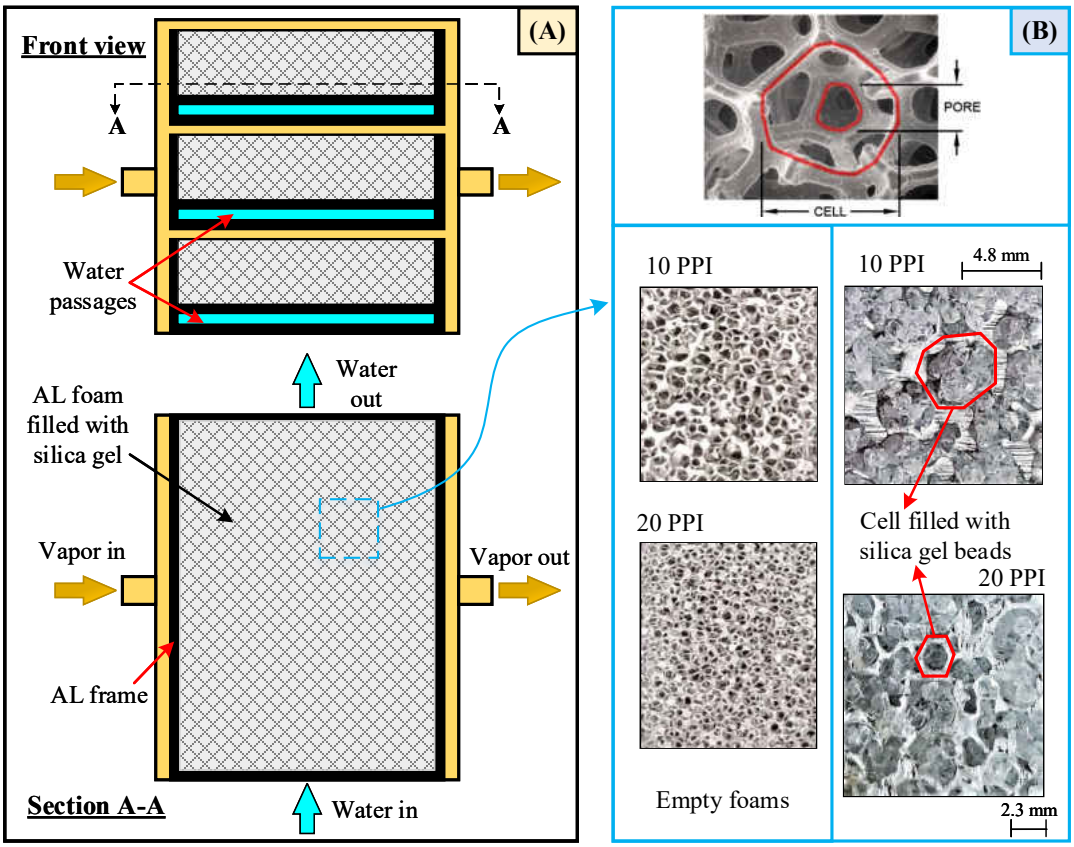

Figure 8-1 (A) schematic drawing for the proposed bed and (B) pictorial views of 10 and 20 PPI foams with/without silica-gel

8.3 Heat and Mass Transfer Mechanisms in Silica-Gel/AL Foam Bed

A schematic of an open-cell aluminum foam packed with silica-gel particles is shown in Fig. 8-2. The ability of adsorbate vapor from an evaporator penetrating into the void spaces between the adsorbent particles is characterized by the inter-particle permeation resistance (flow resistance). The inter-particle permeation resistance causes a pressure drop across the height of the bed. When the vapor reaches the particle surface, adsorption occurs via mass diffusion through the nanopores of the adsorbent particles (i.e., intra-particle mass diffusion resistance). This diffusion is accompanied by the release of heat of adsorption. The heat generated in a particle is conducted through the other particles to reach to the surface of a foam ligament. Then, the heat conducts through the foam to the heat transfer fluid. So, using a foam provides a large contact surface area

between foam ligament and silica gel particles. In the absence of the foam, heat generated is conducted through the particles of the adsorbent (i.e., absorbent layer) that has relatively high thermal resistance. Accordingly, the ligaments of the foam provide an effective heat transfer path for the heat generated. This path significantly enhances the cooling rate of the adsorption bed during the adsorption process. It is clear that the number of particles in each foam cell could affect the effective thermal conductivity of the AL foam bed and hence affect its thermal response. So, in the present study, the influences of the cell size of the foam (i.e., PPI) and the particle size of the adsorbent on the bed performance are also investigated.

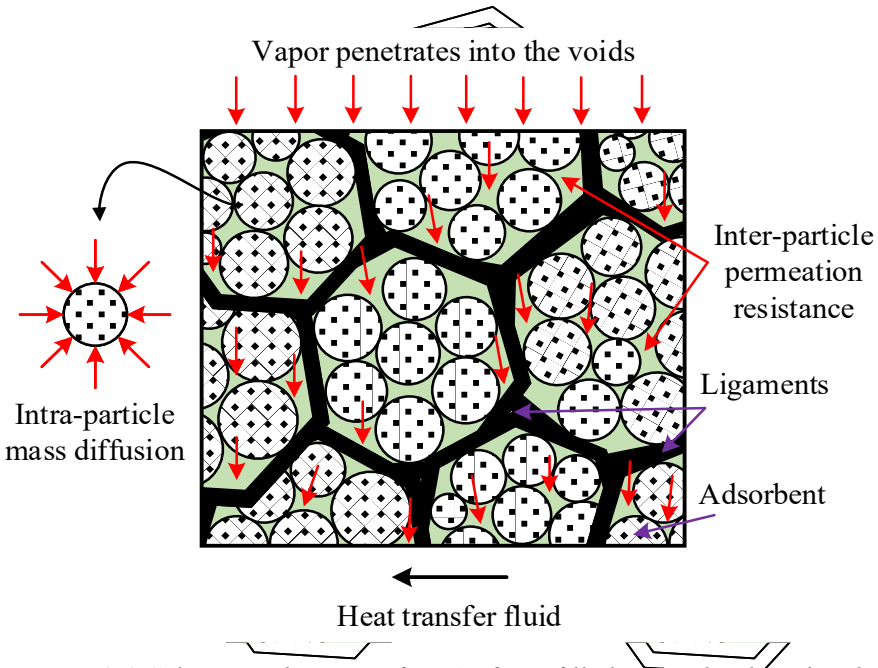

Figure 8-2 Schematic drawing of an AL foam filled with adsorbent beads

8.4 Testing Methodology

The first stage of the testing methodology is the filling of the AL foam with silica gel beads and measure the bed porosity $\left(\varepsilon_b = 1 - \frac{m_{sg}}{(1-\varepsilon_p)\rho_s V \varepsilon_{fo}}\right)$. It is found that the bed porosity of the silica gel/AL foam bed varies from 0.41 to 0.44, depending on the silica gel particle diameter and PPI of foam. This small variation in the bed porosity has only a small effect on the bed performance

[142, 143]. The bed is integrated to heat exchanger using a thermal paste and then rested on the load cell as shown in Fig. 8-3. The load cell is calibrated with cooling water flowing in the flexible tubes and the heat exchanger. After calibration, the load cell response is recorded at various mass flow rates and cooling water temperatures. The main conclusion is that the flexible tubing and cooling/heating water do not add significant uncertainty in the load cell readings.

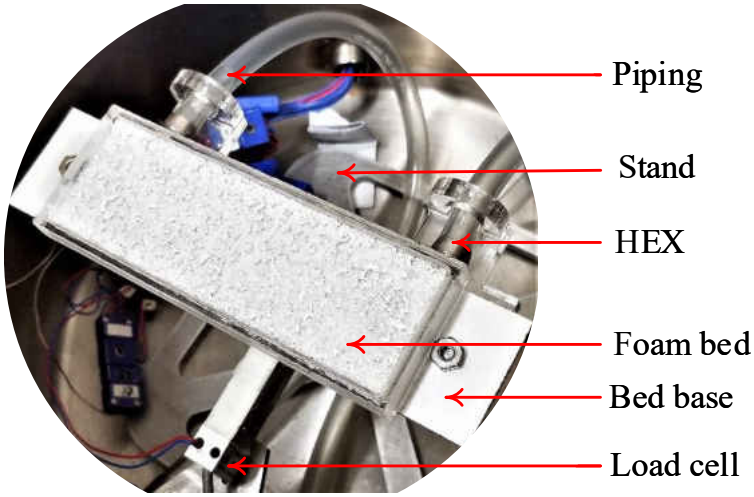

Figure 8-3 Pictorial view of the tested module arrangement

After the installation of the bed and load cell calibration, the Gravimetric Large Temperature Jump method [12] is followed to study the dynamics of the foam bed under typical operating conditions. The temperature and pressure of water in the evaporator/condenser vessel are adjusted. Hot water from the thermal bath is used to heat the bed to the desorption temperature, while the vacuum pump is run to evacuate the measuring unit chamber to make the sample almost completely dry. After reaching a constant load cell reading for 1 h, the temperature of the dry bed is adjusted using hot/cold water from the thermal baths. This temperature represents the initial adsorption or desorption temperature which is uniquely determined by the adsorption isotherm of the working pair and the operating conditions of the simulated cycle. When the bed temperature reaches the initial adsorption or desorption temperature, Valve 1 and 2 are opened and the

measuring chamber is fed with water vapor from the evaporator/condenser chamber allowing the silica gel to adsorb water vapor. After reaching a constant average bed temperature and a load cell measurement for 1 h, the bed is cooled down in case of adsorption or heated up in case of desorption. The adsorption or desorption process is completed when the weight and the average bed temperature is constant for 1 h. During this step, the increase or decrease in the load cell response is recorded, which directly corresponds to the change in uptake during the adsorption or desorption process. The evaporator and condenser pressure are kept almost constant at 1.24 kPa and 4.2 kPa during the adsorption and desorption process, respectively. During the desorption process, the inlet and outlet temperatures of the hot water are reordered to be used in calculating the COP.

8.5 Numerical Study

This section presents the description of the computational domain of the proposed bed, various assumptions made to simplify the mathematical model, and the operating and boundary conditions chosen to simulate the adsorption cooling cycle.

8.5.1 Computational domain description

Computational domain shown in Fig. 8-4 is chosen to examine heat and mass transfer inside the proposed silica-gel/AL foam bed and simulate its performance. The computational domain consists of two sub-domains; silica gel/AL foam and a solid aluminum substrate with 2 mm thickness. As the AL foam is brazed to the aluminum sheet, the contact resistance between them is negligible. The top surface is exposed to vapor coming from the evaporator while the bottom surface is cooled using a heat transfer fluid (water).

In addition, the same computational domain is also used to investigate the performance of a layer of silica gel without the AL foam. The same initial and boundary conditions are used. The effective thermal conductivity is set to be 0.198 W/m.K [5] in this case instead of 6.0 W/m.K for an AL foam bed.

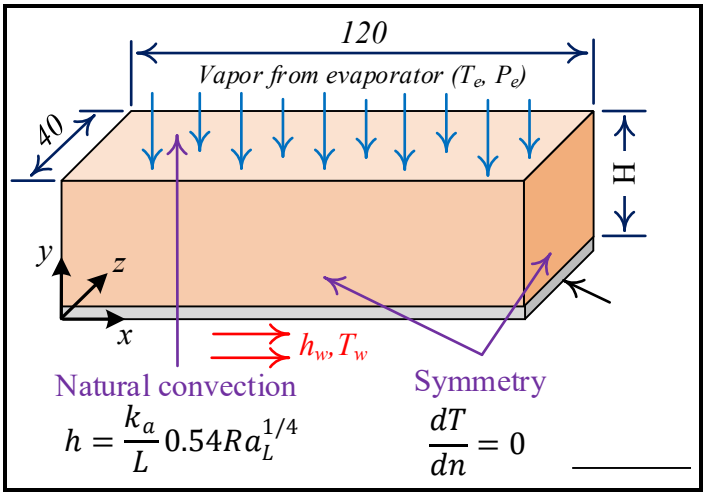

Figure 8-4 Computational domain of the silica gel/AL foam bed

8.5.2 Assumptions

The mathematical model developed in this study is mainly based on the following simplifications and assumptions to simplify the computation process [5, 142]:

i. The bed effective thermal conductivity is spatially uniform.
ii. The bed porosity is constant and is equal to 0.42.
iii. The vapor phase of the adsorbate is an ideal gas.
iv. The specific heats, viscosity, and thermal conductivities are temperature independent.

8.5.3 Mathematical Equations

The volume-averaged form of continuity, momentum, and energy conservation equations are the principal governing equations. Appropriate source terms are added to the conservation equations to simulate the adsorption process.

a) Continuity equation

The continuity equation for the adsorbate gas phase is [51, 133]:

$$\varepsilon_b \frac{\partial \rho_v}{\partial t} + \nabla.\left(\rho_v \vec{U}\right) = -(1-\varepsilon_t)\rho_s \frac{\partial X}{\partial t} \quad (59)$$

where ε_b is the bed porosity, ε_t is the total porosity $(\varepsilon_t = \varepsilon_b + (1-\varepsilon_b)\varepsilon_p)$, ρ_v is the vapor density, $\vec{U}$ is the vapor velocity vector, and ρ_s is the density of solid silica-gel.

The linear driving force (LDF) model is used to estimate the adsorption uptake:

$$\frac{\partial X}{\partial t} = \frac{60 D_s}{d_p^2}(X_o - X) \quad (60)$$

where d_p is the average particle diameter. The surface diffusivity (D_s) and equilibrium uptake (X_o) are calculated from the following equations [41]:

$$D_s = 2.54 \times 10^{-4} \exp\left(-\frac{5051.7}{T_b}\right) \quad (61)$$

$$X_o = X_\infty \exp\left(-k\left(\frac{T_b}{T_e} - 1\right)^n\right) \quad (62)$$

where T_b is the bed temperature, T_e is the evaporator temperature, n is heterogeneity factor, X_∞ is the maximum uptake, and k is a constant which depends on the adsorption isotherm.

b) Momentum equation

Inter-particle permeation resistance can lead to a large pressure drop across the bed height. So, Darcy's equation is implemented to calculate the velocity field of the vapor adsorbate in the bed. Due to the very slow velocity of the adsorbate through the voids between the adsorbent particles, inertial effects can be ignored in this study.

$$\vec{U} = -\frac{K}{\mu}\nabla P \quad (63)$$

$$K = \frac{d_p^2 \varepsilon_b^3}{150(1-\varepsilon_b)^2} \quad (64)$$

where K is the bed permeability and μ is the vapor dynamic viscosity.

c) Energy equations

A single energy equation is used to calculate the local bed temperature by assuming local thermal equilibrium (LTE) between the solid and vapor phase. Many previous studies reported the validity of the LTE assumption in simulating the adsorption process [45, 130, 144].

$$\left(\varepsilon_b\rho_f C_{pf} + \rho_{fo}C_{pfo} + (1-\varepsilon_t)\rho_s\left(C_{ps} + XC_{pw}\right)\right)\frac{\partial T_b}{\partial t} + \rho_f C_{pf}\vec{U}.\nabla T = \nabla.(k_b\nabla T_b) + (1-\varepsilon_t)\rho_s H_a\frac{\partial X}{\partial t} \quad (65)$$

The first term on the LHS is the total heat capacity of the bed while the first term on RHS is the thermal diffusion term. The effective bed thermal conductivity is estimated as volume-averaged of thermal conductivity of silica-gel and AL foam. The second term on RHS is the energy generated during the adsorption process.

The heat diffusion equation in the aluminum substrate (i.e., base) that is brazed to the foam is also solved to consider its effect in the spreading of heat [112, 113, 134].

$$\frac{\partial T_m}{\partial t} = \alpha_m\nabla^2 T_m \quad (66)$$

In the above equations, ρ_f is the vapor density, ρ_{fo} is the foam density, C_{pf} is the heat capacity of the vapor phase, C_{pfo} is the specific heat of the foam and C_{ps} is the specific heat silica gel.

The cooling capacity per unit volume (CP_v) and specific cooling power (SCP) delivered by an adsorption bed can be calculated based on the bed capacity as [5]:

$$CP_v = \frac{m_{sg}\times h_{fg}(T_e)\times\Delta X}{V\times t_a} = \frac{(1-\varepsilon_t)\rho_s\times h_{fg}(T_e)\times\Delta X}{t_a} \quad (67)$$

$$SCP = \frac{h_{fg}(T_e)\times\Delta X}{t_a} \quad (68)$$

The rate of heat added during the desorption process can be estimated as:

$$\dot{Q_{des}} = \frac{(mC_p\Delta T)_b}{t_d} + \frac{m_{sg}h_{fg}(T_c)\Delta X}{t_d} \quad (69)$$

The first term on the RHS is the sensible heat added to the bed and the second term is the latent heat added to convert the adsorbate from the liquid to vapor phase.

The coefficient of performance of the cycle (COP) is calculated as:

$$COP = \frac{m_{sg} \times SCP}{Q_{des}} \quad (70)$$

where h_{fg} is the adsorbate (refrigerant) latent heat of vaporization at the evaporator or condenser temperature, ΔX is the change in bed uptake during the adsorption process, V is the volume of the bed (120×40×H), t_a is the adsorption time, t_d is the desorption time which equals t_a in this study, and m_{sg} is the mass of silica gel.

The volume averaged temperature of the bed and uptake are evaluated at each time step as following:

$$T_{bed}(t) = \frac{1}{V} \iiint T_b(x,y,z)\, dV \quad (71)$$

$$X_{bed}(t) = \frac{1}{V} \iiint X(x,y,z)\, dV \quad (72)$$

The main simulation parameters are given in Table 8-2.

Table 8-2 Numerical values of the parameters used in this study

Parameter	Value	Unit	Parameter	Value	Unit
C_{pfo}	895	$kJ/kg.K$	m_{cw}, m_{hw}	0.7	LPM
C_{ps}	924	$kJ/kg.K$	n	1.2	--
d_p	0.35, 0.7	mm	P_e	1.24	kPa
H_a	2415	kJ/kg	T_d	86	°C
H	10, 15	mm	T_e	10	°C
h_w	1800	W/m^2.K	T_c	30	°C
k	16	--	X_∞	0.31	kg_v/kg_s
k_a	0.026	W/m.K	ε_b	0.42	--
k_b	6.0	W/m.K	ε_t	0.66	--
k_f	0.024	W/m.K	ε_{fo}	0.90	--
ρ_s	2027	kg/m^3	ρ_{fo}	270	kg/m^3

8.5.4 Initial and boundary conditions

Suitable numerical values for the initial, boundary and operating conditions are applied to initiate the numerical solution and simulate the kinetics of a practical adsorption cooling cycle. Initially, the distribution of pressure, temperature, and uptake within the bed is set to be uniform. The initial bed pressure and temperature are set to be 1.24 kPa and 62°C, respectively. The initial bed temperature and uptake are estimated based on a desorption temperature of 86°C and a condenser temperature of 30°C. All bed sides are assumed to be adiabatic due to symmetry. The top surface is exposed to a vapor pressure and temperature of 1.24 kPa and 10°C, respectively. The bottom of the computational domain is exposed to a heat transfer fluid with a convective heat transfer coefficient of 2000 $W/m^2 \cdot K$ and a temperature of T_w. In the experimental test, the adsorption process is initiated by imposing a temperature jump (i.e., switching from hot water to cold water). All experimental measurements show that there is a time lag associated with the inlet water temperature (T_w) switching from hot to cold water. This is attributed to the mixing of cold and hot water in the inlet pipe just before the adsorber heat exchanger. For the different configurations of adsorption bed considered in this study, the experimental measurements of the inlet cooling water temperature are fitted with an empirical equation (Eq. 73) which is used as an input to the numerical model. Figure 8-5 presents the experimental measurements of the inlet cooling water temperature and the empirical equation given by Eq. 73. It is found that the empirical equation fits the experimental data with a standard deviation of 0.992.

$$T_w = 30.47 + 33.6 \times 0.91^t - 0.000331 \times t \qquad (73)$$

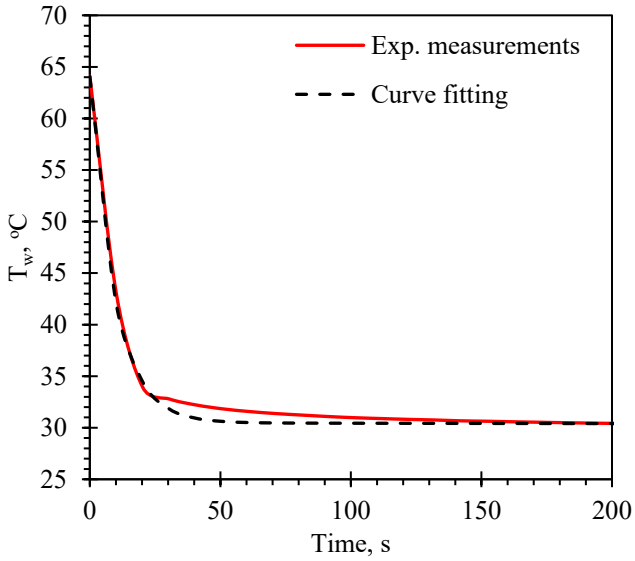

Figure 8-5 Experimental and fitted inlet cooling water temperature profile.

8.5.5 Mesh sensitivity and code validation

The numerical study is carried out using COMSOL Multiphysics 5.2 software, employing the suitable source terms in mass and energy equations. The governing equations are discretized using the finite element method and solved numerically with a relative tolerance of 10^{-5}. Time and mesh independence study is carried out using different time step sizes and various mesh sizes. A time step of 0.1 s and $\Delta x = \Delta y = \Delta z = 0.1$ mm are found to be suitable to capture the temperature and flow fields with reasonable computational time and high accuracy.

20 PPI AL foams with 10 mm and 15 mm height are filled with silica gel of 0.7 mm particle size. The performance of the silica gel/20 PPI AL foam beds is investigated experimentally and numerically. The experimental measurements and numerical results of the average bed temperature and uptake during the adsorption and desorption process are compared and illustrated in Fig. 8-6 and Fig. 8-7, respectively. It is found that the maximum temperature difference between the experimental and numerical results is less than 2.5ºC and 1ºC in case of adsorption and desorption process, respectively. This close agreement between the experimental measurements

and numerical results indicates the suitability of the proposed mathematical model to simulate the heat and mass transfer inside the silica gel/AL foam bed and hence evaluate its performance.

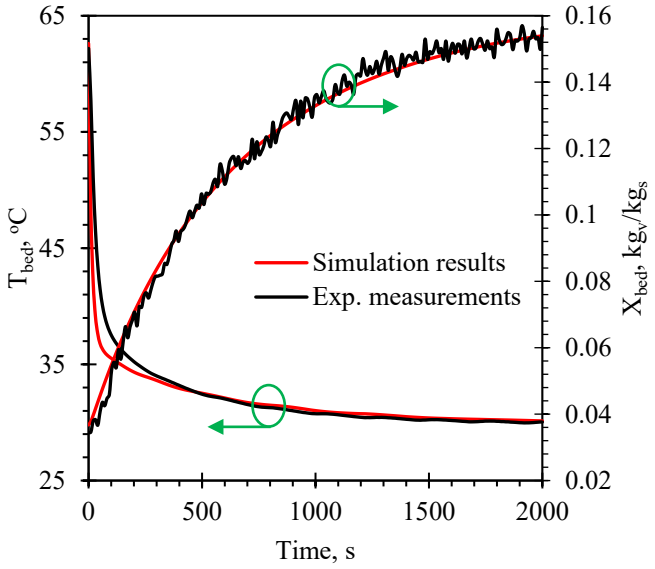

Figure 8-6 Average temperature and uptake of AL foam bed with a height of 10 mm during adsorption process

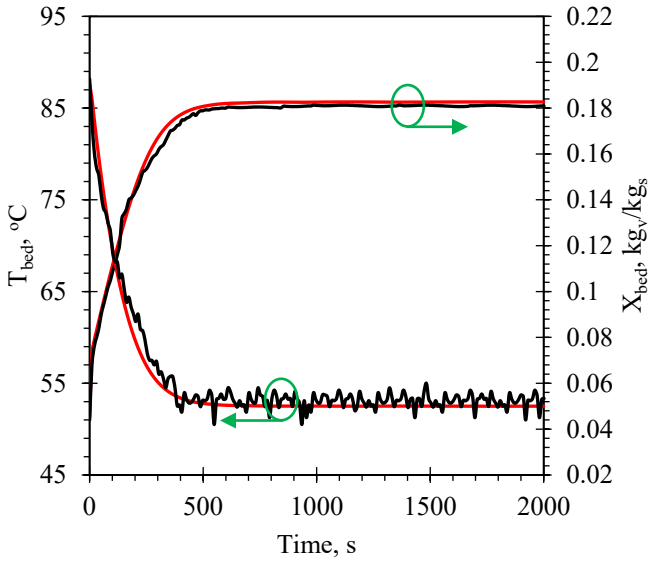

Figure 8-7Average temperature and uptake of AL foam bed with a height of 10 mm during the desorption process

8.6 Results and Discussion

In the following sub-sections, the importance of the intra-particle mass diffusion resistance on the bed performance is studied using the 10 and 20 PPI AL foams filled with 0.35 mm and 0.7 mm silica-gel particles. In addition, the thermal response and adsorption kinetics of silica gel/AL foam bed with a height of 10 mm and 15 mm are discussed. The performance of each AL foam bed filled with silica-gel is compared to a silica-gel bed in the absence of AL foam under the same operating conditions. This comparison aims to reveal the enhancement of bed thermal conductivity on the performance of an adsorption cooling system using open-celled aluminum foams. Finally, the SCP, CP_v and COP for all studied beds are obtained through numerical simulations.

8.6.1 Effect of using AL foam

Silica gel with a particle diameter of 0.7 mm is packed in 10 and 20 PPI AL foam with a height of 15 mm. The adsorbent to foam mass ratio is about 2.3. In another case, a layer of silica gel with a height of 15 mm is rested on the heat exchanger, and its performance is also measured and compared to silica gel/AL foam bed. Temperature contours at 100 s, 600 s and 1200 s for the silica gel layer and silica gel/AL foam bed are presented in Fig. 8-8. There is a substantial temperature difference across the bed height in case of the layer of silica gel at any time during the adsorption process. On the contrary, AL foam is able to conduct the heat generated during the adsorption process to the cooling fluid and make the bed much more isothermal. Figure 8-9 depicts the temporal profile of the volume-averaged temperature of the bed with and without foam. It is apparent from the figure that AL foam is able to cool the bed during the adsorption period much faster than a layer of silica gel without foam because of the low thermal resistance of the foam bed compared to that of the silica gel bed. For instance, the temperature difference between the silica gel layer and silica gel/AL foam bed is about 16°C and 10°C at 500 s and 2000 s, respectively.

Silica gel/AL foam bed reaches the equilibrium temperature (~30ºC) after 1200 s of adsorption, while the silica gel layer needs much more than 2000 s to reach the same equilibrium condition. Interestingly, the average temperature of a bed using 10 PPI AL foam is higher than that using 20 PPI AL foam. This small deviation is less than 2ºC, and is attributed to the lower surface area of the 10 PPI foam compared to 20 PPI foam. Also, the cell size of 10 PPI foam is larger than that of 20 PPI foam. So, more silica gel beads fill each cell of the 10 PPI foam and introduce a non-negligible thermal resistance that decreases the bed effective thermal conductivity.

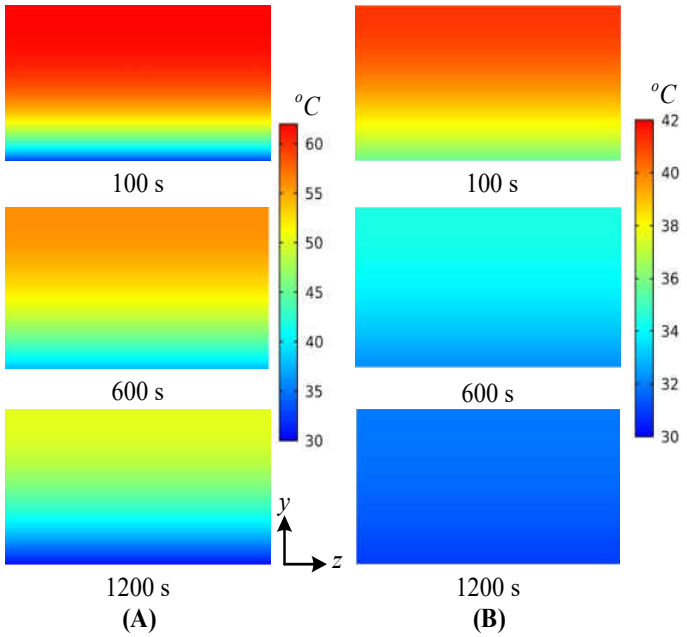

Figure 8-8 Temperature contours at different times for (A) silica gel layer and (B) silica gel/AL foam bed

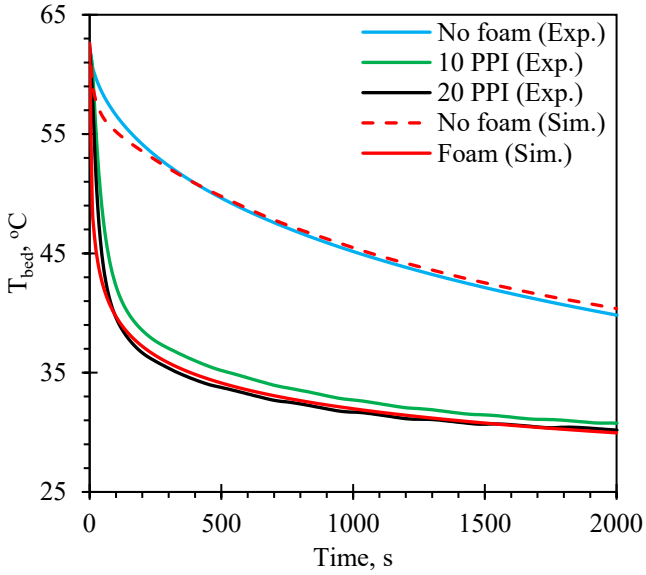

Figure 8-9 Temporal variation of the average bed temperature with and without foam.

Figure 8-10 shows the effect of using foam on the temporal average bed uptake. The uptake curves are plotted by using the load cell readings during the adsorption period. It is found that using AL foams has a considerable influence on the average bed uptake due to the enhancement of the thermal conductivity. The average uptake of silica gel/AL foam bed is higher than a layer of silica gel by ~50% after a 2000 s adsorption period. On the other hand, the 20 PPI AL foam bed outperforms the 10 PPI one in term of the average uptake due to its higher surface area and smaller cell size. Accordingly, AL foam with 20 PPI is better than 10 PPI in adsorption cooling applications.

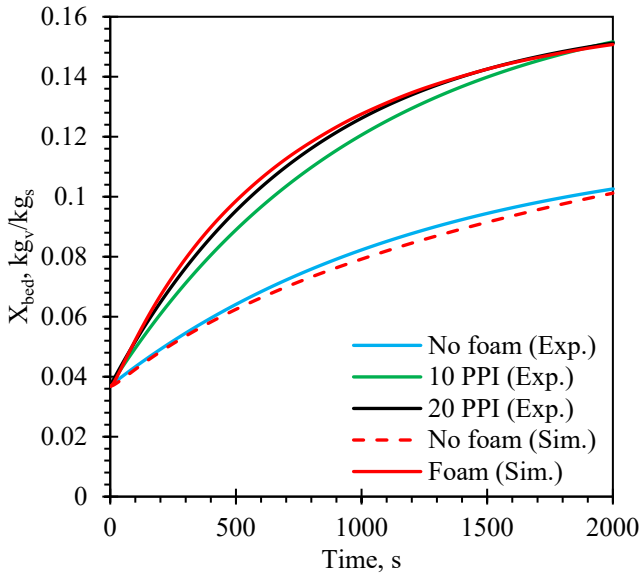

Figure 8-10 Temporal variation of the average beds uptake with and without foam

8.6.2 Effect of particle size

Experimental measurements and numerical studies are performed for the smaller silica gel particle size of 0.35 mm and the results are compared to those of 0.7 mm to investigate the importance of the flow resistance and the intra-particle mass transfer resistance on the bed performance. Generally, decreasing the particle diameter has two opposing influences: (i) increasing the adsorption rate (see Eq. 60) that results in an enhancement of adsorption phenomenon (ii) decreasing the permeability of the porous bed that leads to an increase in the flow resistance (see Eqs. 63 and 64). Moreover, decreasing the particle size increases the rate of heat generated during the adsorption period. As a result, a bed with low thermal resistance is required to transfer this heat to the cooling fluid. Figure 8-11 illustrates the percentage of the pressure drop across the bed for different particle sizes. A bed with 0.35 mm particle size has the higher pressure drop. In particular, AL foam filled with small particle size produces a considerable pressure drop at the beginning of the adsorption due to the high adsorption rate. On the other hand, the variation of pressure drop for 0.70 mm particle size bed is less significant when compared to 0.35 mm.

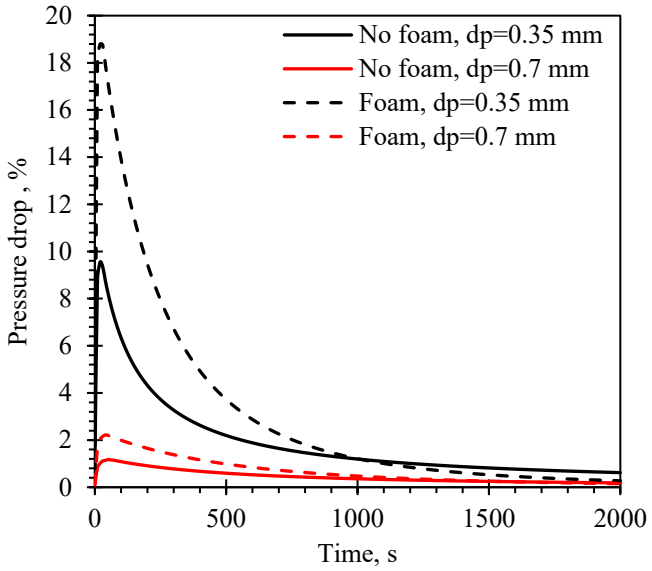

Figure 8-11 Percentage of the pressure drop across the beds for different particle sizes

Temporal temperature variations of the silica gel/20 PPI AL foam bed and a layer of silica gel at different particle sizes are compared and exhibited in Fig. 8-12. Generally, the average bed temperature declines significantly when using the AL foam. It is also found that the temperature curve of AL foam filled with 0.7 mm silica gel is steeper than that filled with 0.35 mm silica gel at the beginning of the adsorption process. This is attributed to the higher heat of adsorption released due to the faster mass diffusion in the smaller particles size. However, the maximum difference between the two curves of AL foam bed temperature is less than 2.5ºC. Accordingly, the thermal conductivity of the AL foam is high enough to conduct the heat released during the adsorption process to the heat transfer fluid and hence cool down the bed. There is also a small difference between the temperature profiles of silica gel bed without AL foam for different particles sizes. This is attributed to the slightly higher thermal resistance of the silica gel layer when the smaller particle size is used.

The enhancement of the thermal behavior of the silica gel/AL foam bed directly affects the average bed uptake as depicted in Fig. 8-13. It is evident from the figure that the 0.35 mm silica

gel/AL foam bed outperforms the other studied beds in term of the average bed uptake and adsorption rate. This is attributed to the low thermal resistance of the bed and the low intra-particle mass diffusion resistance. On the other hand, the average uptakes of silica gel layers are nearly the same regardless of the particle size because the performance of the two silica gel layers is mainly controlled by the high thermal resistance of the beds. Thus, it can be concluded that the adsorption dynamics of AL foam bed using 0.35 mm particle size is limited by the low surface diffusion of vapor into silica gel, whereas the thermal diffusion through the bed governs the adsorption dynamics for the case of a silica gel layer. Analysis of this figure shows that the SCP increased by a factor of 2.6 using AL foam after 600 s of adsorption time.

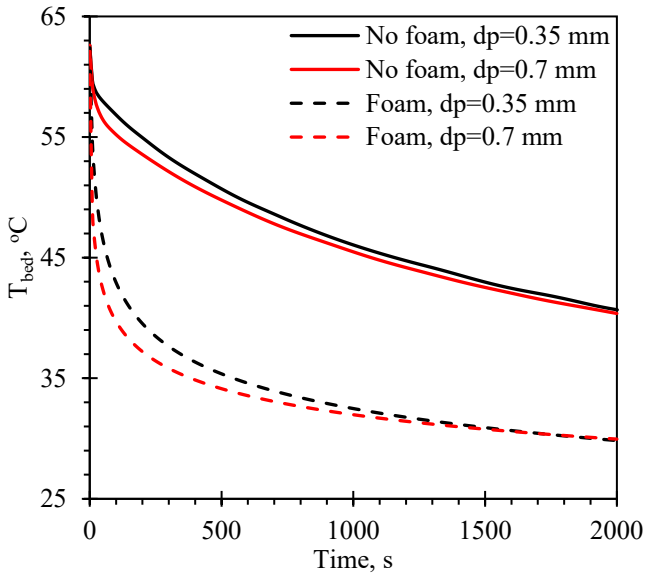

Figure 8-12 Average bed temperature for different particle sizes

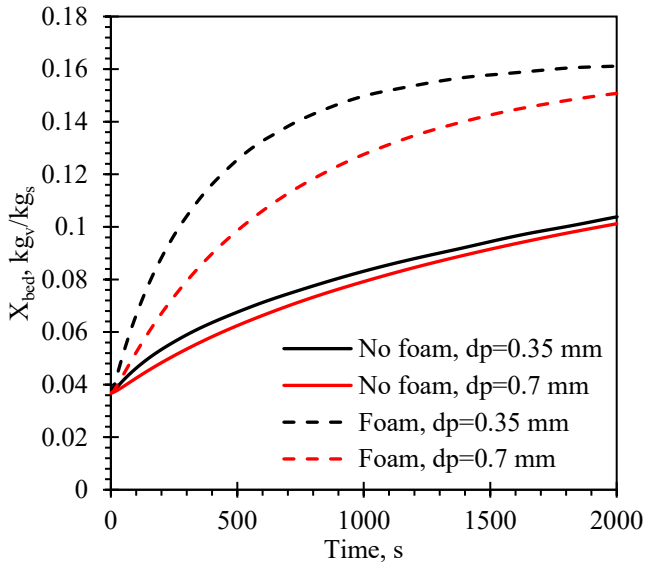

Figure 8-13 Average bed uptake for 0.35 mm and 0.70 mm particle sizes

8.6.3 Effect of bed height

AL foams with various heights are filled with silica gel particles of 0.35 mm to evaluate the effect of the bed conductive thermal resistance on the thermal response of the bed. Figure 8-14 presents the average bed temperature at various heights. It is shown that the temperatures curves become much steeper as AL foam bed height decreases. Silica gel/AL foam bed with 10 mm and 20 mm height reaches the equilibrium condition (i.e., T~30ºC) after an adsorption time of 700 s and 1600 s, respectively. On the other hand, a silica gel layer of 10 mm and 20 mm height reaches an average temperature of 35ºC and 45ºC, respectively after an adsorption time of 2000 s. Figure 8-15 depicts the temporal variation of volume-averaged uptake for different bed heights using a particle size of 0.35 mm. It is apparent from the figure that beds with faster cooling curve show faster adsorption dynamics. For bed height of 10 mm, using AL foam increases the water vapor uptake by 65% after an adsorption time of 600 s compared to a silica gel layer with the same height. The AL foam bed with a height of 20 mm shows slower adsorption kinetics compared to 10 mm because of the higher inter-particle permeation resistance. The water vapor uptake for the

AL foam bed with a 10 mm height increases as the adsorption time increases and level off after 1000 s. Accordingly, increasing the adsorption time more than 1000 s decreases the cooling power produced by this bed. It can be concluded that 20 PPI AL foam bed with a height of 10 mm filled with 0.35 mm particles sizes outperforms all the studied cases.

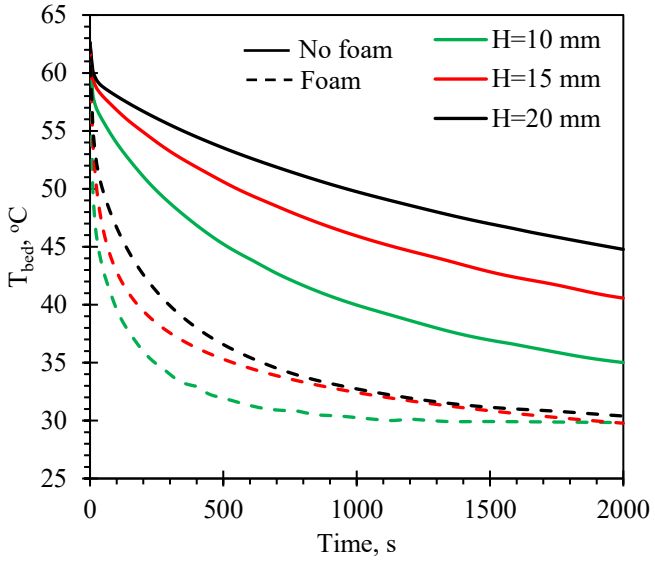

Figure 8-14 Temporal average temperature of beds with different heights using 0.35 mm particle size

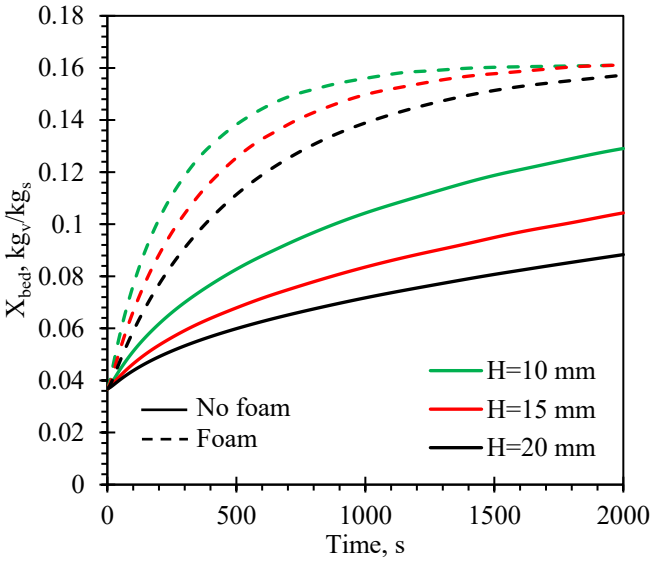

Figure 8-15 Temporal average uptake of beds with different heights using 0.35 mm particle size

8.6.4 Effect of silica gel/water adsorption isotherm

As the efficacy of adsorption cooling cycles depends on the adsorption isotherm of the working pair, various types of silica-gel are investigated. The coefficients of the adsorption isotherm equation (Eq. 62) of the tested silica gel types are shown in Table 8-3. Also, the adsorption isotherm of each silica-gel is plotted in Fig. 8-16. It is shown that silica-gel RD has the highest equilibrium uptake at the end of the adsorption process.

Table 8-3 Coefficients of adsorption isotherm equation (Eq. 4) for different silica-gels

Silica-gel type	X_∞	k	n
Fuji silica gel	0.31	16	1.2
Silica gel RD-2060 [41]	0.37	14	1.15
Silica gel RD [72]	0.48	20	1.2

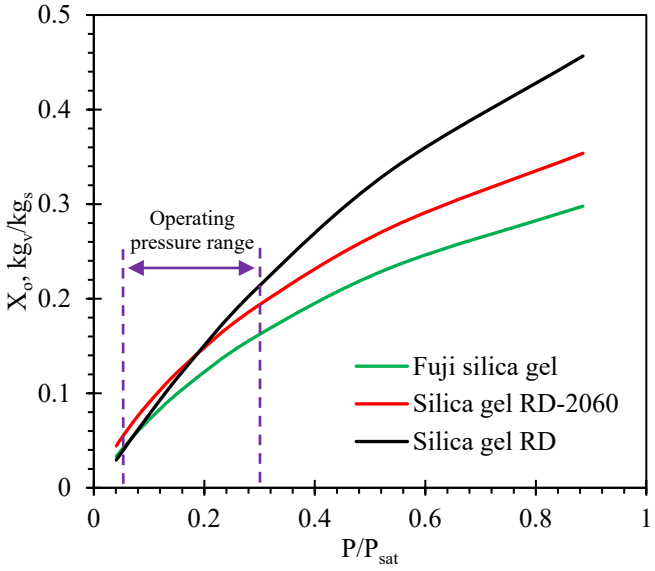

Figure 8-16 Adsorption isotherm of various silica gel types

Figure 8-17 compares the temporal average temperature profiles of 20 PPI AL foam bed and a layer of silica gel. It is clear that there is no significant difference between the temperature profiles of 20 PPI AL foam filled with different types of silica gel. Although the equilibrium uptake of silica gel RD shown in Fig. 8-18 is the highest, AL foam is able to conduct the heat generated

during the adsorption process to the heat transfer fluid efficiently. The time constant for the temperature profile of AL foam curves is about 100 s compared to 1000 s for a layer of Fuji silica-gel. This significant enhancement in the thermal response of the foam bed is due to its low thermal resistance and large surface area. Figure 8-18 also depicts that the adsorption dynamics AL foam beds is generally faster than a layer of silica gel owing to the faster thermal response of the AL foam beds. It is also shown that the AL foam beds reach to the equilibrium uptake, while a layer of silica gel RD reaches to only 70% of the equilibrium uptake after 2000 s of adsorption time. The time constant for adsorption kinetics curve of the AL foam filled with Fuji silica-gel, silica-gel RD, and silica-gel RD-2060 is about 310, 400 s and 360 s, respectively. Moreover, the adsorption kinetics curves for silica gel layers are nearly the same regardless of the different adsorption isotherms. Therefore, it is apparent that the conductive thermal resistance of the silica gel layers has a significant influence on the adsorption dynamics of adsorption packed bed. As a result, 20 PPI AL foam with a height of 10 mm filled with 0.35 mm silica gel RD is recommended for adsorption cooling applications, which is the same conclusion reached earlier.

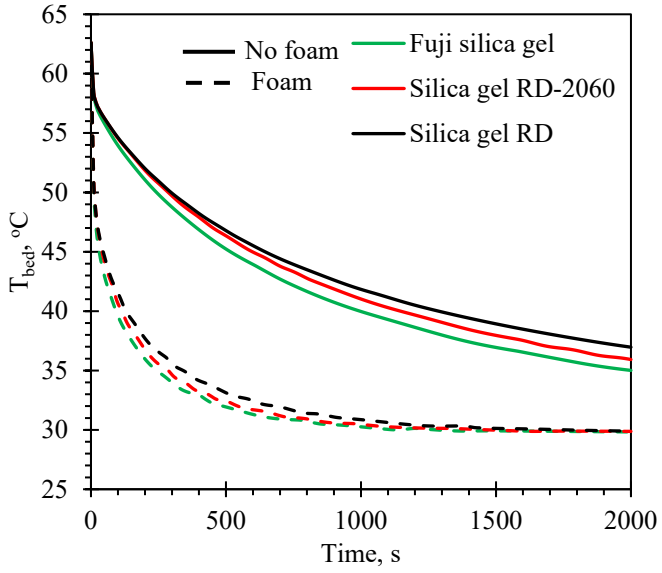

Figure 8-17 Temporal temperature of beds using various silica gel types

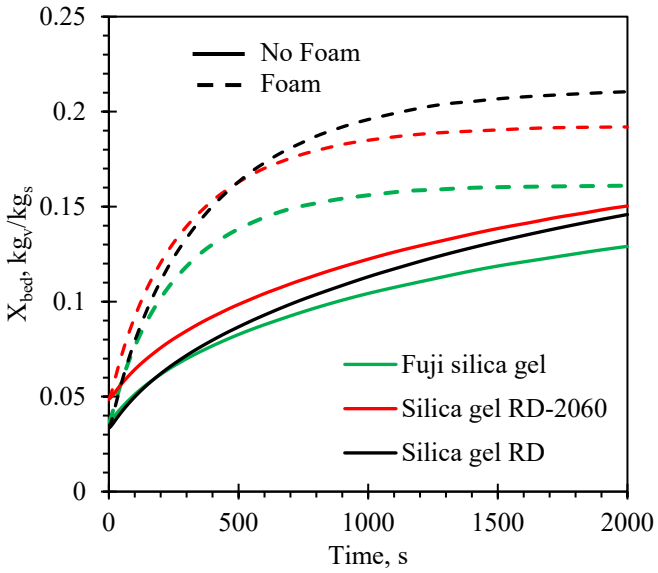

Figure 8-18 Dynamic adsorption characteristics for various silica gel

8.6.5 Bed performance

SCP, CP_v and COP of AC cycle using the investigated beds are predicted based on their adsorption/desorption dynamics using Eqs. 67-70. Table 8-4 illustrates the SCP, CP_v and COP of beds with a height of 10 mm using various types of silica gel with a particle size of 0.35 mm. Silica gel RD shows the best performance owing to its highest maximum uptake. It is found that the SCP produced by silica-gel RD/AL foam bed is 2.6 times higher than that delivered by silica gel bed through 300 s of adsorption process. Compared with previous studies, SCP and COP of silica gel RD/AL foam bed produced after 300 s of adsorption time is found to be 4.2 and 2.0 times, respectively higher than that delivered by the finned-tube adsorption bed [145, 146]. This pronounced enhancement in the bed performance is due to the low conductive thermal resistance of the silica-gel/AL foam bed and using a small particle size. The cooling capacity of silica gel RD/AL foam bed after 600 s of adsorption process is about 30% less than that after only 300 s. Accordingly, specifying the duration of the adsorption period has a significant effect on the SCP. Similar statements can be made for the cooling power per unit volume.

Table 8-4 SCP and COP for beds with a height of 10 mm using 0.35 mm silica gel at T_e=10°C, T_c=30°C and T_d=85°C

Bed	$t_a = t_d$	300 s			600 s		
	Silica gel type	SCP (W/kg)	CP_v (kW/m^3)	COP	SCP (W/kg)	CP_v (kW/m^3)	COP
Silica gel/20 PPI AL foam	Silica gel RD	827	517	0.75	577	361	0.79
	Silica gel RD-2060	752	470	0.72	502	314	0.78
	Fuji silica gel	676	423	0.73	444	278	0.79
Silica gel layer	Silica gel RD	317	218	0.69	246	169	0.71
	Silica gel RD-2060	298	205	0.66	230	158	0.67
	Fuji silica gel	275	189	0.68	211	145	0.68

8.7 Conclusion

In this study, open-celled aluminum foam filled with silica gel beads is proposed to be used as an adsorber bed for adsorption cooling applications. The bed porosity is measured to be in the range of 0.41-0.44 depending on the particle diameter of silica gel and the pore size of the AL foam. An experimental setup and a CFD model are implemented to examine the heat and mass transfer processes inside AL foam filled with three different types of silica gel. Experimental measurements reveal that 20 PPI AL foam bed outperforms 10 PPI AL foam bed due to its higher surface area and smaller cell size. Thus, the 20 PPI AL foam is preferred to be used in adsorption cooling applications. Results show that the 0.35 mm silica gel/AL foam bed outperforms the 0.7 mm silica gel/AL foam bed in terms of the average bed temperature and adsorption rate. This is attributed to the low thermal resistance of the bed and the low intra-particle mass diffusion resistance. For the 0.35 silica gel/AL foam bed, the time constant for the temperature profile is 90 s, 180 s and 290 s for a height of 10 mm, 15 mm and 20 mm, respectively. It is also found that AL foam bed performance with a height of 20 mm is controlled by the inter-particle permeation resistance. Among the three investigated silica gel types, silica gel RD exhibits the highest SCP of

827 W/kg due to its highest adsorption uptake capacity. Results show that the COP of the cycle is 0.75 and increases as the cycle time increases. Comparing to a 10 mm height of silica gel RD bed, the SCP of 0.35 mm silica gel/AL foam bed is 260% higher for adsorption time of 300 s. Accordingly, using AL foam reduces the conductive thermal resistance of the bed significantly. Overall, more efficient and more compact AC systems can be designed using AL foam.

CHAPTER 9 SUMMARY AND FUTURE WORK

9.1 Summary and Conclusions

In the development of any adsorption system design, it is essential to study the characteristics of adsorption isotherm and kinetics of the adsorbate/adsorbent pair. Based on the gravimetric approach, an experimental test rig is designed and built to monitor the adsorption rate at a desired pressure and temperature. It also can be used to investigate the performance of adsorption beds with different structures and various working pairs. Experimental measurements show that the maximum uptakes of silica gel RD-2060 and Type-RD are 0.38 kg/kg and 0.48 kg/kg, respectively. Apparent capillary condensation is observed at a relative pressure of 0.4 and 0.35 for silica-gel RD and RD-2060, respectively. Also, it is found that the D-A model can fit the adsorption isotherms of silica-gels appropriately for the entire range of relative pressure when the characteristic energy is set as a function of relative pressure instead of assuming constant values. Based on the adsorption rate and the adsorbent temperature measured simultaneously, a new approach is proposed to measure the surface diffusivity in the temperature and pressure ranges typical of those during the operating conditions of adsorption cooling systems. Analysis of the results indicates that the surface diffusivity follows the Arrhenius-form equation. The calculated activation energy at different adsorption conditions varies from 40.0 to 41.2 kJ/mol and the pre-exponential factor varies from 2.5×10^{-4} to 2.8×10^{-4} m^2/s. These values are close to those previously reported in the literature. Thus, the proposed approach can be used to measure the surface diffusivity in porous materials.

A scaling analysis of heat and mass transfer processes in an adsorption packed bed is presented. New scaling parameters that characterize the performance of the adsorption cooling bed are derived and their importance are discussed. It is found that the presence of heat of adsorption

makes the apparent heat capacity of an adsorption bed much larger than the heat capacity of the adsorbent material itself. The present results indicate that the heat diffusion and vapor penetration depths can be used to specify the desired working pair properties and the adsorbent layer thickness for producing the maximum cooling power. From the results of scaling analysis, it can be concluded that the inter-particle permeation resistance has a considerable effect on the performance of an adsorption silica gel bed when the particle diameter to adsorbent layer thickness ratio is less than 0.1. It can also be concluded that performance of a silica gel packed bed is controlled by the conductive thermal resistance when the Fourier number of the adsorbent-adsorbate layer (F_o) is less than 1.0. The convective resistance (i.e., external resistance) dominates the bed performance when the dimensionless temperature ratio (Θ) of adsorption silica gel packed bed is more than 0.2.

A lab-scale adsorption unit is designed and constructed to investigate its efficacy under typical operating conditions of a practical adsorption cooling system. A detailed coupled heat and mass transfer (CHMT) model and a lumped parameter (LP) model are implemented to estimate the Specific Cooling Power (SCP) of an adsorption cooling system using silica gel/water as the working pair. It is found that the optimal cycle time can be predicted by using the LP model. Results show that the SCP obtained from the CHMT model is always higher than that measured from the experiment because the dynamic effect of the evaporator is not considered. The LP model, with its input parameters estimated by the CHMT, actually produces reliable estimates of the SCP because the evaporator dynamic effect is considered. The difference between the two models is higher at shorter cycle times because the evaporator pressure drop is very high at the beginning of the adsorption process. Without considering this pressure drop, the CHMT yields a higher SCP compared to that calculated from the LP model. In view of the evaporator pressure

variation during the adsorption process, a modified CHMT model that considers the evaporator dynamic behavior is developed. It is shown that the modified CHMT model can be used to evaluate the performance of an adsorption bed and to estimate the SCP accurately.

The main objective of this research work is to design an efficient adsorption cooling system. the effective thermal conductivity of a silica gel/water adsorption packed bed is significantly enhanced by placing the silica gel particles in a high-porosity aluminum (AL) foam. The enhancement leads to several folds increase in the specific cooling power (SCP), cooling capacity per unit volume (CP_v) and coefficient of performance (COP) of an adsorption cooling (AC) chiller. The thermal response and adsorption kinetics of various silica-gel/AL foam beds under typical operating conditions are investigated experimentally and numerically. The effect of pores per inch (PPI) of the foam, silica-gel particle size, bed height and adsorption isotherm of different types of silica gel on the bed performance are investigated. The results reveal that the AL foam with 20 PPI is preferred in adsorption cooling applications due to its high surface area and small cell size. It is found that the adsorption kinetics is faster when 0.35 mm silica-gel particles are used. A taller bed shows relatively lower adsorption dynamics due to the higher inter-particle permeation resistance. Among the three types of silica gel investigated, silica-gel RD exhibits the highest equilibrium uptake at the end of the adsorption process. The present results demonstrate that the 20 PPI AL foam with a height of 10 mm filled with 0.35 mm silica-gel RD can deliver a SCP of 827 W/kg, a CP_v of 517 W/m^3 and a COP of 0.75 at evaporator temperature of 10^{o}C, condenser temperature of 30^{o}C, desorption temperature of 85^{o}C and adsorption/desorption time of 300 s. Compared with previous studies, SCP and COP of silica gel RD/AL foam bed produced after 300 s of adsorption time is found to be 4.2 and 2.0 times, respectively higher than that delivered by the finned-tube adsorption bed [145, 146]. Accordingly, using AL foam reduces the

conductive thermal resistance of the bed significantly. Overall, more efficient and more compact AC systems can be designed using AL foam.

9.2 Future Work

The modular bed design proposed and evaluated in this study can lead to lower manufacture cost and scalability to AC systems for different heat loads. However, further studies such as a prototype system demonstration should be conducted to investigate the practicality of employing this novel bed in an AC unit. The overall dynamic performance of the AC systems should also be evaluated. In addition, further studies are recommended to evaluate the performance of the new adsorption bed for hybrid adsorption cooling and desalination applications. A new evaporator design should be proposed for adsorption cooling systems. Moreover, more studies should focus on enhancement of the vapor diffusion onto nanoporous materials to be able to achieve several folds increase in the SCP of AC systems. For instance, it would be highly beneficial to produce a new version of nonporous silica gel with a narrow pore size distribution around 2 nm. This allows the filling up of the pores to be mainly controlled by capillary condensation rather than surface diffusivity.

LIST OF REFERENCES

1. Chihara, K. and M. Suzuki, *Air drying by pressure swing adsorption.* Journal of chemical engineering of Japan, 1983. **16**(4): p. 293-299.
2. Xia, Z.Z., et al., *Adsorption equilibrium of water on silica gel.* Journal of Chemical & Engineering Data, 2008. **53**(10): p. 2462-2465.
3. Qasem, N., *Thermodynamic analysis and modeling study of an intermittent solar adsorption refrigeration system*. 2013, King Fahd University of Petroleum and Minerals (Saudi Arabia).
4. Oh, S.T., *Silica gel/Water Based Adsorption Cooling System Employing Compact Fin-Tube Heat Exchanger*. 2013, Kyushu University.
5. Mohammed, R.H., et al., *Novel compact bed design for adsorption cooling systems: parametric numerical study.* International Journal of Refrigeration, 2017. **80**: p. 238-251.
6. Ruthven, D.M., *Principles of adsorption and adsorption processes*. 1984: John Wiley & Sons.
7. Choi, J.-G., D. Do, and H. Do, *Surface diffusion of adsorbed molecules in porous media: Monolayer, multilayer, and capillary condensation regimes.* Industrial & engineering chemistry research, 2001. **40**(19): p. 4005-4031.
8. Do, D.D., *Adsorption Analysis: Equilibria and Kinetics:(With CD Containing Computer Matlab Programs)*. Vol. 2. 1998: World Scientific.
9. Gilliland, E., R. Baddour, and J. Russell, *Rates of flow through microporous solids.* AIChE Journal, 1958. **4**(1): p. 90-96.
10. Sladek, K.J., E.R. Gilliland, and R.F. Baddour, *Diffusion on surfaces. II. Correlation of diffusivities of physically and chemically adsorbed species.* Industrial & Engineering Chemistry fundamentals, 1974. **13**(2): p. 100-105.
11. Sakoda, A. and M. Suzuki, *Fundamental study on solar powered adsorption cooling system.* Journal of chemical engineering of Japan, 1984. **17**(1): p. 52-57.
12. Sapienza, A., et al., *Dynamic study of adsorbers by a new gravimetric version of the Large Temperature Jump method.* Applied Energy, 2014. **113**: p. 1244-1251.
13. Strauss, R., K. Schallenberg, and K. Knocke, *Measurement of the kinetics of water vapor adsorption into solid zeolite layers.* Sci Tech Froid, 1992. **1**: p. 246-250.
14. Jaroniec, M., *Adsorption on heterogeneous surfaces: The exponential equation for the overall adsorption isotherm.* Surface Science, 1975. **50**(2): p. 553-564.
15. Langmuir, I., *The adsorption of gases on plane surfaces of glass, mica and platinum.* Journal of the American Chemical society, 1918. **40**(9): p. 1361-1403.
16. Ruthven, D.M., *Fundamentals of adsorption equilibrium and kinetics in microporous solids*, in *Adsorption and Diffusion*. 2006, Springer. p. 1-43.
17. Cevallos, O.R., *Adsorption Characteristics of Water and Silica Gel System for Desalination Cycle*. 2012.
18. Saha, B.B., E.C. Boelman, and T. Kashiwagi, *Computer simulation of a silica gel-water adsorption refrigeration cycle--the influence of operating conditions on cooling output and COP*. 1995, American Society of Heating, Refrigerating and Air-Conditioning Engineers, Inc., Atlanta, GA (United States).
19. Pan, B. and H. Zhang, *A modified Polanyi-based model for mechanistic understanding of adsorption of phenolic compounds onto polymeric adsorbents.* Environmental science & technology, 2012. **46**(12): p. 6806-6814.
20. Dubinin, M. and V. Astakhov, *Description of adsorption equilibria of vapors on zeolites over wide ranges of temperature and pressure*. 1971, ACS Publications.
21. Talu, O. and A.L. Myers, *Rigorous thermodynamic treatment of gas adsorption.* AIChE journal, 1988. **34**(11): p. 1887-1893.

22. Tamainot-Telto, Z. and R. Critoph, *Advanced solid sorption air conditioning modules using monolithic carbon–ammonia pair.* Applied Thermal Engineering, 2003. **23**(6): p. 659-674.

23. Zhao, Y., E. Hu, and A. Blazewicz, *A non-uniform pressure and transient boundary condition based dynamic modeling of the adsorption process of an adsorption refrigeration tube.* Applied energy, 2012. **90**(1): p. 280-287.

24. Critoph, R., *Performance limitations of adsorption cycles for solar cooling.* Solar energy, 1988. **41**(1): p. 21-31.

25. Tóth, J., *Uniform interpretation of gas/solid adsorption.* Advances in colloid and interface science, 1995. **55**: p. 1-239.

26. Tóth, J., *A uniform interpretation of gas/solid adsorption.* Journal of Colloid and Interface Science, 1981. **79**(1): p. 85-95.

27. Thu, K., et al., *Operational strategy of adsorption desalination systems.* International Journal of Heat and Mass Transfer, 2009. **52**(7): p. 1811-1816.

28. Mitra, S., et al., *Modeling study of two-stage, multi-bed air cooled silica gel+ water adsorption cooling cum desalination system.* Applied Thermal Engineering, 2017. **114**: p. 704-712.

29. Wu, J.W., L. Chen, and E.J. Hu, *Performance estimation of adsorption cooling cycle with sorption hysteresis.* Applied Thermal Engineering, 2016. **105**: p. 159-162.

30. Kapilan, N., *TECHNICAL ASPECTS OF ADSORPTION COOLING SYSTEM.* Acta Technica Corviniensis-Bulletin of Engineering, 2016. **9**(3): p. 103.

31. Al-Mousawi, F.N., R. Al-Dadah, and S. Mahmoud, *Novel system for cooling and electricity: Four different integrated adsorption-ORC configurations with two expanders.* Energy Conversion and Management, 2017. **152**: p. 72-87.

32. Palomba, V., et al., *Increasing the share of renewables through adsorption solar cooling: A validated case study.* Renewable Energy, 2017. **110**: p. 126-140.

33. Labban, O., et al., *Next-generation HVAC: Prospects for and limitations of desiccant and membrane-based dehumidification and cooling.* Applied Energy, 2017. **200**: p. 330-346.

34. Sah, R.P., B. Choudhury, and R.K. Das, *A review on low grade heat powered adsorption cooling systems for ice production.* Renewable and Sustainable Energy Reviews, 2016. **62**: p. 109-120.

35. Sah, R.P., B. Choudhury, and R.K. Das, *A review on adsorption cooling systems with silica gel and carbon as adsorbents.* Renewable and Sustainable Energy Reviews, 2015. **45**: p. 123-134.

36. Thu, K., et al., *Thermo-physical properties of silica gel for adsorption desalination cycle.* Applied Thermal Engineering, 2013. **50**(2): p. 1596-1602.

37. Freni, A., et al., *Thermal conductivity of selective water sorbents under the working conditions of a sorption chiller.* Applied thermal engineering, 2002. **22**(14): p. 1631-1642.

38. Wang, L., R. Wang, and R. Oliveira, *A review on adsorption working pairs for refrigeration.* Renewable and Sustainable Energy Reviews, 2009. **13**(3): p. 518-534.

39. Allouhi, A., et al., *Optimal working pairs for solar adsorption cooling applications.* Energy, 2015. **79**: p. 235-247.

40. Sharafian, A. and M. Bahrami, *Adsorbate uptake and mass diffusivity of working pairs in adsorption cooling systems.* International Journal of Heat and Mass Transfer, 2013. **59**: p. 262-271.

41. Mohammed, R.H., et al., *Revisiting the adsorption equilibrium equations of silica gel/water for adsorption cooling applications.* International Journal of Refrigeration, 2018. **86**: p. 40-47.

42. Aristov, Y.I., I.S. Glaznev, and I.S. Girnik, *Optimization of adsorption dynamics in adsorptive chillers: loose grains configuration.* Energy, 2012. **46**(1): p. 484-492.

43. Aristov, Y.I., et al., *Kinetics of water sorption on SWS-1L (calcium chloride confined to mesoporous silica gel): influence of grain size and temperature.* Chemical engineering science, 2006. **61**(5): p. 1453-1458.

44. Freni, A., et al., *Simulation of water sorption dynamics in adsorption chillers: One, two and four layers of loose silica grains.* Applied Thermal Engineering, 2012. **44**: p. 69-77.

45. Solmuş, İ., et al., *A two-energy equation model for dynamic heat and mass transfer in an adsorbent bed using silica gel/water pair.* International Journal of Heat and Mass Transfer, 2012. **55**(19): p. 5275-5288.

46. Girnik, I., et al., *Dynamic optimization of adsorptive chillers: Compact layer vs. bed of loose grains.* Applied Thermal Engineering, 2017. **125**: p. 823-829.

47. Restuccia, G., A. Freni, and G. Maggio, *A zeolite-coated bed for air conditioning adsorption systems: parametric study of heat and mass transfer by dynamic simulation.* Applied thermal engineering, 2002. **22**(6): p. 619-630.

48. Wang, X. and H. Chua, *Two bed silica gel–water adsorption chillers: an effectual lumped parameter model.* International Journal of Refrigeration, 2007. **30**(8): p. 1417-1426.

49. San, J.-Y. and F.-K. Tsai, *Testing of a lab-scale four-bed adsorption heat pump.* Applied Thermal Engineering, 2014. **70**(1): p. 274-281.

50. Thu, K., et al., *Performance investigation of a waste heat-driven 3-bed 2-evaporator adsorption cycle for cooling and desalination.* International Journal of Heat and Mass Transfer, 2016. **101**: p. 1111-1122.

51. Al-Mousawi, F.N., R. Al-Dadah, and S. Mahmoud, *Different bed configurations and time ratios: Performance analysis of low-grade heat driven adsorption system for cooling and electricity.* Energy Conversion and Management, 2017. **148**: p. 1028-1040.

52. Maxwell, J.C., *A treatise on electricity and magnetism*. Vol. 1. 1881: Clarendon press.

53. Wang, R., L. Wang, and J. Wu, *Adsorption refrigeration technology: theory and application*. 2014: John Wiley & Sons.

54. El-Sharkawy, I., et al., *Experimental investigation of activated carbon fibers/ethanol pairs for adsorption cooling system application.* Applied Thermal Engineering, 2006. **26**(8): p. 859-865.

55. Saha, B.B., et al., *Accurate adsorption isotherms of R134a onto activated carbons for cooling and freezing applications.* international journal of refrigeration, 2012. **35**(3): p. 499-505.

56. San, J.-Y. and W.-M. Lin, *Comparison among three adsorption pairs for using as the working substances in a multi-bed adsorption heat pump.* Applied Thermal Engineering, 2008. **28**(8): p. 988-997.

57. Askalany, A.A., et al., *A review on adsorption cooling systems with adsorbent carbon.* Renewable and Sustainable Energy Reviews, 2012. **16**(1): p. 493-500.

58. Askalany, A.A., et al., *High potential of employing bentonite in adsorption cooling systems driven by low grade heat source temperatures.* Energy, 2017.

59. Ghazy, M., et al., *Adsorption isotherms and kinetics of activated carbon/Difluoroethane adsorption pair: Theory and experiments.* International Journal of Refrigeration, 2016. **70**: p. 196-205.

60. Ghazy, M., et al., *Adsorption isotherms and kinetics of HFC-404A onto bituminous based granular activated carbon for storage and cooling applications.* Applied Thermal Engineering, 2016. **105**: p. 639-645.

61. Wang, J., R. Wang, and L. Wang, *Water vapor sorption performance of ACF-CaCl 2 and silica gel-CaCl 2 composite adsorbents.* Applied Thermal Engineering, 2016. **100**: p. 893-901.

62. Zheng, X., et al., *Thermal conductivity, pore structure and adsorption performance of compact composite silica gel.* International Journal of Heat and Mass Transfer, 2014. **68**: p. 435-443.

63. Aristov, Y.I., et al., *A family of new working materials for solid sorption air conditioning systems.* Applied Thermal Engineering, 2002. **22**(2): p. 191-204.

64. Tokarev, M., et al., *New composite sorbent CaCl 2 in mesopores for sorption cooling/heating.* International Journal of Thermal Sciences, 2002. **41**(5): p. 470-474.

65. Restuccia, G., et al., *Selective water sorbent for solid sorption chiller: experimental results and modelling.* International Journal of Refrigeration, 2004. **27**(3): p. 284-293.

66. Cacciola, G., G. Restuccia, and L. Mercadante, *Composites of activated carbon for refrigeration adsorption machines.* Carbon, 1995. **33**(9): p. 1205-1210.

67. Zhequan, J., et al., *Comparison on thermal conductivity and permeability of granular and consolidated activated carbon for refrigeration.* Chinese Journal of Chemical Engineering, 2013. **21**(6): p. 676-682.

68. Tamainot-Telto, Z. and R. Critoph, *Monolithic carbon for sorption refrigeration and heat pump applications.* Applied thermal engineering, 2001. **21**(1): p. 37-52.

69. Wang, L., et al., *Study of thermal conductivity, permeability, and adsorption performance of consolidated composite activated carbon adsorbent for refrigeration.* Renewable energy, 2011. **36**(8): p. 2062-2066.

70. Wang, L., et al., *Development of thermal conductive consolidated activated carbon for adsorption refrigeration.* Carbon, 2012. **50**(3): p. 977-986.

71. El-Sharkawy, I.I., et al., *A study on consolidated composite adsorbents for cooling application.* Applied Thermal Engineering, 2016. **98**: p. 1214-1220.

72. Wang, X., et al., *Investigation on the isotherm of silica gel+ water systems.* Journal of thermal analysis and calorimetry, 2004. **76**(2): p. 659-669.

73. Sayılgan, Ş.Ç., M. Mobedi, and S. Ülkü, *Effect of regeneration temperature on adsorption equilibria and mass diffusivity of zeolite 13x-water pair.* Microporous and Mesoporous Materials, 2016. **224**: p. 9-16.

74. Teo, H.W.B., A. Chakraborty, and B. Han, *Water adsorption on CHA and AFI types zeolites: Modelling and investigation of adsorption chiller under static and dynamic conditions.* Applied Thermal Engineering, 2017. **127**: p. 35-45.

75. Gordeeva, L. and Y. Aristov, *Dynamic study of methanol adsorption on activated carbon ACM-35.4 for enhancing the specific cooling power of adsorptive chillers.* Applied Energy, 2014. **117**: p. 127-133.

76. Shmroukh, A.N., A.H.H. Ali, and S. Ookawara, *Adsorption working pairs for adsorption cooling chillers: A review based on adsorption capacity and environmental impact.* Renewable and Sustainable Energy Reviews, 2015. **50**: p. 445-456.

77. Zheng, W., et al., *Activated carbon fiber composites for gas phase ammonia adsorption.* Microporous and Mesoporous Materials, 2016. **234**: p. 146-154.

78. El-Sharkawy, I.I., et al., *Adsorption of ethanol onto parent and surface treated activated carbon powders.* International Journal of Heat and Mass Transfer, 2014. **73**: p. 445-455.

79. El-Sharkawy, I.I., et al., *Adsorption of ethanol onto phenol resin based adsorbents for developing next generation cooling systems.* International Journal of Heat and Mass Transfer, 2015. **81**: p. 171-178.

80. Glueckauf, E., *Theory of chromatography. Part 10.—Formulæ for diffusion into spheres and their application to chromatography.* Transactions of the Faraday Society, 1955. **51**: p. 1540-1551.

81. Li, Z. and R.T. Yang, *Concentration profile for linear driving force model for diffusion in a particle.* AIChE journal, 1999. **45**(1): p. 196-200.

82. El-Sharkawy, I.I., et al., *A study on the kinetics of ethanol-activated carbon fiber: theory and experiments.* International journal of heat and mass transfer, 2006. **49**(17): p. 3104-3110.

83. El-Sharkawy, I.I., *On the linear driving force approximation for adsorption cooling applications.* international journal of refrigeration, 2011. **34**(3): p. 667-673.

84. Raymond, A. and S. Garimella, *Intraparticle mass transfer in adsorption heat pumps: limitations of the linear driving force approximation.* Journal of Heat Transfer, 2011. **133**(4): p. 042001.

85. Sun, B. and A. Chakraborty, *Thermodynamic frameworks of adsorption kinetics modeling: dynamic water uptakes on silica gel for adsorption cooling applications.* Energy, 2015. **84**: p. 296-302.

86. Sapienza, A., et al., *"Water-Silica Siogel" working pair for adsorption chillers: Adsorption equilibrium and dynamics.* Renewable Energy, 2017. **110**: p. 40-46.

87. Teo, H.W.B., et al., *Experimental study of isotherms and kinetics for adsorption of water on Aluminium Fumarate.* International Journal of Heat and Mass Transfer, 2017. **114**: p. 621-627.

88. Poyelle, F., J.-J. Guilleminot, and F. Meunier, *Experimental tests and predictive model of an adsorptive air conditioning unit.* Industrial & Eng. Chem. Res, 1999. **38**: p. 298.

89. Sharafian, A., et al., *Thermal conductivity and contact resistance of mesoporous silica gel adsorbents bound with polyvinylpyrrolidone in contact with a metallic substrate for adsorption cooling system applications.* Int. J. Heat & Mass Transfer, 2014. **79**: p. 64.

90. Demir, H., M. Mobedi, and S. Ülkü, *The use of metal piece additives to enhance heat transfer rate through an unconsolidated adsorbent bed.* international journal of refrigeration, 2010. **33**(4): p. 714-720.

91. Rezk, A., et al., *Effects of contact resistance and metal additives in finned-tube adsorbent beds on the performance of silica gel/water adsorption chiller.* Applied Thermal Engineering, 2013. **53**(2): p. 278-284.

92. Askalany, A.A., et al., *Effect of improving thermal conductivity of the adsorbent on performance of adsorption cooling system.* Applied Thermal Engineering, 2017. **110**: p. 695-702.

93. Fayazmanesh, K., S. Salari, and M. Bahrami, *Effective thermal conductivity modeling of consolidated sorption composites containing graphite flakes.* International Journal of Heat and Mass Transfer, 2017. **115**: p. 73-79.

94. Chan, K.C., et al., *Enhancing the Performance of a Zeolite 13X/CaCl 2–Water Adsorption Cooling System by Improving Adsorber Design and Operation Sequence.* Energy and Buildings, 2018. **158**: p. 1368-1378.

95. Tatlier, M., *Performances of MOF vs. zeolite coatings in adsorption cooling applications.* Applied Thermal Engineering, 2017. **113**: p. 290-297.

96. Saha, B., et al., *Performance evaluation of a low-temperature waste heat driven multi-bed adsorption chiller.* International Journal of Multiphase Flow, 2003. **29**(8): p. 1249-1263.

97. Saha, B., et al., *Waste heat driven dual-mode, multi-stage, multi-bed regenerative adsorption system.* International Journal of Refrigeration, 2003. **26**(7): p. 749-757.

98. Wang, D., Z. Xia, and J. Wu, *Design and performance prediction of a novel zeolite–water adsorption air conditioner.* Energy conversion and management, 2006. **47**(5): p. 590-610.

99. Deshmukh, H., M. Maiya, and S.S. Murthy, *Continuous vapour adsorption cooling system with three adsorber beds.* Applied Thermal Engineering, 2015. **82**: p. 380-389.

100. Mitra, S., et al., *Performance evaluation and determination of minimum desorption temperature of a two-stage air cooled silica gel/water adsorption system.* Applied Energy, 2017. **206**: p. 507-518.

101. Wang, Y., et al., *Experimental investigation of a solar-powered adsorption refrigeration system with the enhancing desorption.* Energy Conversion and Management, 2018. **155**: p. 253-261.

102. Ng, K.C., et al., *Adsorption desalination: an emerging low-cost thermal desalination method.* Desalination, 2013. **308**: p. 161-179.

103. Shahzad, M.W., et al., *An experimental investigation on MEDAD hybrid desalination cycle.* Applied energy, 2015. **148**: p. 273-281.

104. Elsayed, M.L., et al. *Effect of changes in input parameters on the operation of a MED-TVC plant*. in *ASTFE Digital Library*. 2018. Begel House Inc.

105. Elsayed, M.L., et al., *Effect of input parameters intensity and duration on dynamic performance of MED-TVC plant.* Applied Thermal Engineering, 2018. **137**: p. 475-486.

106. Elsayed, M.L., et al., *Transient performance of MED processes with different feed configurations.* Desalination, 2018. **438**: p. 37-53.

107. Elsayed, M.L., et al., *Effect of disturbances on MED-TVC plant characteristics: Dynamic modeling and simulation.* Desalination, 2018. **443**: p. 99-109.

108. Elsayed, M.L., et al., *Exergy and thermo-economic analysis for MED-TVC desalination systems.* Desalination, 2018. **447**: p. 29-42.

109. Elsayed, M.L., et al., *Transient and thermo-economic analysis of MED-MVC desalination system.* Energy, 2019. **167**: p. 283-296.

110. Elsayed, M.L., et al., *Performance modeling of MED-MVC systems: Exergy-economic analysis.* Energy, 2019. **166**: p. 552-568.

111. Aristov, Y.I., et al., *A new methodology of studying the dynamics of water sorption/desorption under real operating conditions of adsorption heat pumps: experiment.* International Journal of Heat and Mass Transfer, 2008. **51**(19): p. 4966-4972.

112. Mohammed, R.H., *A simplified method for modeling of round and square ceiling diffusers.* Energy and Buildings, 2013. **64**: p. 473-482.

113. Aziz, M.A., et al., *Experimental and numerical study of influence of air ceiling diffusers on room air flow characteristics.* Energy and Buildings, 2012. **55**: p. 738-746.

114. Tran, H.N., et al., *Mistakes and inconsistencies regarding adsorption of contaminants from aqueous solutions: A critical review.* Water Research, 2017.

115. Solmuş, İ., et al., *Transient behavior of a cylindrical adsorbent bed during the adsorption process.* Applied Energy, 2015. **142**: p. 115-124.

116. Solmuş, İ., et al., *Numerical investigation of coupled heat and mass transfer inside the adsorbent bed of an adsorption cooling unit.* Int. J. Refrigeration, 2012. **35**: p. 652.

117. Di, J., et al., *Theoretical and experimental study on characteristics of a novel silica gel–water chiller under the conditions of variable heat source temperature.* International Journal of Refrigeration, 2007. **30**(3): p. 515-526.

118. Aristov, Y.I., et al., *Kinetics of water adsorption on silica Fuji Davison RD.* Microporous and Mesoporous Materials, 2006. **96**(1): p. 65-71.

119. Dervin, S., et al., *Graphene oxide reinforced high surface area silica aerogels.* Journal of Non-Crystalline Solids, 2017. **465**: p. 31-38.

120. Sato, T. and K. Nakatani, *Analysis of Distribution and Intraparticle Diffusion of a Fluorescent Dye in Mesoporous Silica Gel by Confocal Fluorescence Microspectroscopy.* Analytical Sciences, 2017. **33**(2): p. 179-183.

121. von der Lehr, M., et al., *Mesopore etching under supercritical conditions–A shortcut to hierarchically porous silica monoliths.* Microporous and Mesoporous Materials, 2017. **243**: p. 247-253.

122. Rezk, A., et al., *Experimental investigation of metal organic frameworks characteristics for water adsorption chillers.* Proceedings of the Institution of Mechanical Engineers, Part C: Journal of Mechanical Engineering Science, 2013. **227**(5): p. 992-1005.

123. Wang, X., H. Chua, and L. Gao, *A thermogravimetric analyzer for condensable gas adsorption under subatmospheric conditions.* Journal of thermal analysis and calorimetry, 2007. **90**(3): p. 935-940.

124. Chua, H.T., et al., *Adsorption characteristics of silica gel+ water systems.* Journal of Chemical & Engineering Data, 2002. **47**(5): p. 1177-1181.

125. Saliba, S., et al., *Combined influence of pore size distribution and surface hydrophilicity on the water adsorption characteristics of micro-and mesoporous silica.* Microporous and Mesoporous Materials, 2016. **226**: p. 221-228.

126. Huang, H., et al., *Development research on composite adsorbents applied in adsorption heat pump.* Applied Thermal Engineering, 2010. **30**(10): p. 1193-1198.

127. Alcaniz-Monge, J., M. Pérez-Cadenas, and D. Lozano-Castelló, *Influence of pore size distribution on water adsorption on silica gels.* Journal of Porous Materials, 2010. **17**(4): p. 409-416.

128. Ali, E.S., et al., *Weather effect on a solar powered hybrid adsorption desalination-cooling system: A Case Study of Egypt's Climate.* Applied Thermal Engineering, 2017.

129. Alsaman, A.S., et al., *Performance evaluation of a solar-driven adsorption desalination-cooling system.* Energy, 2017. **128**: p. 196-207.

130. Mohammed, R.H., et al., *Performance evaluation of a new modular packed bed for adsorption cooling systems.* Applied Thermal Engineering, 2018. **136**: p. 293-300.

131. Mohammed, R.H., et al., *Physical properties and adsorption kinetics of silica-gel/water for adsorption chillers.* Applied Thermal Engineering, 2018. **137**: p. 368-376.

132. Mohammed, R.H., et al., *Scaling analysis of heat and mass transfer processes in an adsorption packed bed.* International Journal of Thermal Sciences, 2018. **133**: p. 82-89.

133. Cheng, D., E.F. Peters, and J.H. Kuipers, *Performance study of heat and mass transfer in an adsorption process by numerical simulation.* Chemical Engineering Science, 2017. **160**: p. 335-345.

134. Mohammed, R.H., *Numerical investigation of displacement ventilation effectiveness.* Int. J. Mech. Aero. Ind. Mech. Eng, 2014. **8**.

135. Nield, D.A. and A. Bejan, *Convection in porous media*. 2006: Springer Science & Business Media.

136. Li, A., et al., *A heat transfer correlation for transient vapor uptake of powdered adsorbent embedded onto the fins of heat exchangers.* App. Therm. Eng., 2016. **93**: p. 668-677.

137. Ramji, H.R., S.L. Leo, and M.O. Abdullah, *Parametric study and simulation of a heat-driven adsorber for air conditioning system employing activated carbon–methanol working pair.* Applied energy, 2014. **113**: p. 324-333.

138. Wang, L., et al., *Study of the performance of activated carbon–methanol adsorption systems concerning heat and mass transfer.* Applied Thermal Engineering, 2003. **23**(13): p. 1605-1617.

139. Mohammed, R.H., et al., *Assessment of numerical models in the evaluation of adsorption cooling system performance.* International Journal of Refrigeration, 2019. **99**: p. 166-175.

140. Hahn, D.W. and M.N. Özişik, *Heat conduction*. 2012: John Wiley & Sons.

141. ; Available from: https://ergaerospace.com/materials/duocel-aluminum-foam/.

142. Mohammed, R.H., et al., *Experimental and numerical investigation of a new silica-gel/water packed bed for adsorption cooling applications*, in *3rd Thermal and Fluids Engineering Conference (TFEC)*. 2018, ASTFE: Fort Lauderdale, FL, USA.

143. Demir, H., M. Mobedi, and S. Ülkü, *Effects of porosity on heat and mass transfer in a granular adsorbent bed.* International Communications in Heat and Mass Transfer, 2009. **36**(4): p. 372-377.

144. Mitra, S., et al., *Study on the influence of adsorbent particle size and heat exchanger aspect ratio on dynamic adsorption characteristics.* Applied Thermal Engineering, 2018.

145. Wang, D., et al., *Experimental research on novel adsorption chiller driven by low grade heat source.* Energy conversion and management, 2007. **48**(8): p. 2375-2381.

146. Ng, K.C., et al., *Solar-assisted dual-effect adsorption cycle for the production of cooling effect and potable water.* International Journal of Low-Carbon Technologies, 2009. **4**(2): p. 61-67.